공 학 박 사 학 위 논 문

Development of Novel Hybrid Adsorbents of Strong Base Anion Exchange Resin and Inorganic Nanoparticles for Selective Removal of Phosphate and Arsenic from Water

인산과 비소의 선택적 흡착을 위한 새로운 강염기 음이온 교환수지와 무기 나노 입자 복합 흡착제 개발

2018년 2월

서울대학교 대학원

화학생물공학부

부이후트렁

Development of Novel Hybrid Adsorbents of Strong Base Anion Exchange Resin and Inorganic Nanoparticles for Selective Removal of Phosphate and Arsenic from Water

by

Bui Huu Trung

under the supervision of

Professor Jeyong Yoon, Ph. D.

A dissertation submitted in partial fulfillment of the requirements for the Degree of

Doctor of Philosophy

FEBRUARY 2018

SCHOOL OF CHEMICAL AND BIOLOGICAL NGINEERING

SEOUL NATIONAL UNIVERSITY

Abstract

Development of selective adsorbents with an enhanced removal efficiency for the removal of phosphate and arsenic from water/wastewater is urgently needed to obtain safe water. Firstly, a hybrid adsorbent of nanoscale zirconium molybdate embedded within a macroporous anion exchange resin (ZMAE) was fabricated for selective removal of phosphate and arsenate. The ZMAE was characterized with low agglomeration of zirconium molybdate (ZM) NPs dispersed within the structure of the anion exchange resin (AE). As major results, the adsorption capacity of ZMAE for both phosphate and arsenate (26.1 mg-P/g and 46.7 mg-As/g, respectively) in the presence of excessive sulfate (5 mM) showed much superior to that of the pristine AE (1.8 mg-P/g and 6.9 mg-As/g, respectively) although their capacities were similar in the absence of sulfate. This selective performance of the ZMAE for both phosphate and arsenate in the presence of excess sulfate ion is attributed by the role of loaded ZM NPs which contributed to be more than 90% of the selective capacities of the ZMAE. Furthermore, the selective phosphate and arsenate of the ZMAE was confirmed by not only the batch experiment with synthetic model water/wastewater but also the column test.

Secondly, this study proposed a new and effective method for fabricating a hydrated zirconium oxide NPs embedded anion exchange resin (ZAE) in purpose of development a robust and high selective adsorbent for phosphate removal. This proposed method achieved much more effective loading Zr within the resin than the

conventional method. A series of the ZAE adsorbents with different Zr contents were fabricated and examined the selective adsorption of phosphate. As major results, the HZO NPs contributed to enhance both adsorption efficiency and selectivity of the anion exchange resin (AE). The selective adsorption of the ZAE for phosphate ion relied on the loaded HZO NPs and was in a function of the Zr content. Indeed, linear equation with high coefficient R^2 value ($R^2 \sim 1.00$) well described for the correlation between the Zr content and the maximum capacity of effective phosphate adsorption for either batch or column adsorption. These results allow to understand the selective insights of the ZAE toward phosphate ion.

In overall, both hybrids ZMAE and ZAE promise a great potential for effective removal of phosphate and arsenic in real water/wastewater treatment. These could allow to explore a new route for synthesis of low cost and novel hybrid adsorbents for phosphate and arsenic.

Key words: Selective adsorption; zirconium molybdate; hydrated zirconium oxide; phosphate removal; arsenic removal; anion exchange resin; hybrid adsorbent.

Student number: 2014-30864.

Contents

List of Figures

List of Tables

1. Introduction

1.1. Research background

Water pollution, especially arsenic (As) contamination in water and groundwater is a worldwide concern. It has been reported that many countries have been seriously concerned with arsenic pollution in water resource such as, Bangladesh, India, Chile, Argentina, South East Asia, China, Mongolia and the United State. Long-term exposure to arsenic can cause many dangerous diseases to human including cancers (skin lung, liver and bladder and kidney) and other non-caner effects (muscular weakness, loss of appetite and nausea) [1-4]. Due to its harmful properties, the US Environmental Protection Agency (US EPA) has established the guideline for arsenic concentration permitted in drinking water to be lower than 0.01 mg/L [5-7]. In order to obtain safe water, which meets the arsenic standard in local communities, it is required to develop relatively simple, inexpensive and effective arsenic removal technologies [8].

Unlike arsenic, phosphorous (known in phosphate) is a necessary macronutrient that takes an important role for the growth and development of biological organisms in most of the ecosystems. However, the excessive phosphate concentration is regarded as one of the main sources causing eutrophication of lakes, rivers, and coastal regions. Eutrophication becomes the widespread problem deteriorating water quality which leads to accumulation of organic maters (plants and algae) and

development of color and odor in water as well [9, 10]. In recent decades, reducing phosphate discharged from wastewater have been considered as one of the key issues of regulating eutrophication. The Water Framework Directive of EU suggests the phosphate concentration in the wastewater discharge to be in the range between 0.1–0.5 mg-P/L [11]. The US EPA has recommended that the maximum level of phosphorus in water should not exceed 0.05 mg-P/L [12]. Therefore, the development of effective technologies for phosphate removal in wastewater going into the lakes, rivers and reservoirs is required in order to become an effective way to control the eutrophication problem in water.

So far, adsorption is a relatively simple technology commonly used in water treatment system with low cost and effective removal of trace amount of contaminants leading to better conduct in regions/countries concerning of electricity and economy [13, 14]. Phosphorous and arsenic belong to the same group in the periodic chart and their oxidation state +5 of phosphate and arsenate have very similar ionic form and pK_a values [3, 15]. Thus, phosphate and arsenate have a similar chemical properties. Indeed, an effective arsenic adsorbent is expected to effectively remove phosphate ion from water and vice versa. Be usually occurring in trace level compared with other coexisting ions in water and groundwater, the removal of arsenic requires selective adsorbents which should have a much greater affinity toward arsenic species than other ions. Although the regulation of phosphate does not strictly require at trace level like the case of arsenic, the removal of phosphate from high matrix ions of discharged wastewater or polluted water may be

suffered greatly. Therefore, development of novel adsorbents for selective removal of arsenic and phosphate from water/wastewater is urgently required.

In last decade, hybrid adsorbents of inorganic NPs impregnated a macro-porous structure of high mechanical crosslinking anion exchange resin have developed and extensively studied for effective removal of both phosphate and arsenic from water. These hybrid adsorbents can combine a selective properties of embedded NPs toward target anions and a high mechanic properties of the polymeric host hard problems of nanoparticles (NPs) for overcoming the hard problems of nanoparticles (NPs). In addition, the use of anion exchange resin (AE) as a host can utilize advantages of Donnan membrane effect from the high density of quaternary ammonium functional groups, which greatly enhanced the adsorption capacity and efficiency of target ions [16, 17]. In fact, Sengupta group developed novel hybrid adsorbent of hydrated iron oxide (HFO) impregnated porous AE for effective removal of arsenic showing important role of Donnan membrane effect for the enhancement of arsenate removal [16]. In similar way, Pan et al. has developed a hybrid of hydrated zirconium oxide (HZO) impregnated AE (D201), named HZO-201, for arsenic and phosphate removal with a great performance [18]. In addition, the hybrid HZO-201 has exhibited its excellent stability against with acid/base and organic substances compared with that of HFO-201.

Although these types of hybrid adsorbents have shown a great potential for effective removal in real water application, the diversity of inorganic NPs dispersed

within the AE was limited, leading to a lack of comparative information between materials as well as the choice of suitable materials for specific water system of application. This could be due to the major challenge of dispersing metal ions into the polymeric phase because of the Donnan exclusion between the fixed positively charged ammonium functional grooups of the resin and the cationic form of metal ion [19]. Furthermore, although the loaded inorganic NPs was thought to have an important role for the selective adsorption of phosphate using this type of hybrid adsorbent, no systematic investigation how effect of loaded metal content to the adsorption performance and selectivity have been reported. This leads to lack of understanding the adsorption selectivity and capacity insights these hybrid adsorbents.

1.2. Objectives

In this dissertation, novel hybrids (nano-composites) of inorganic NPs embedded a commercial macroporous anion exchange resin were developed for removal of arsenic/phosphate from water/wastewater in respect of selective adsorption. These adsorbents were not only be fabricated by effective methods in purpose of reducing cost, time and chemicals as well but also exhibit their great performance of selective adsorption. For this purpose, the extensive study of following topics was conducted.

(1) To develop a nano-scale zirconium molybdate embedded anion exchange resin (ZMAE) for selective removal of phosphate and arsenic. For this, the ZMAE was fabricated by in-situ precipitation of molybdate oxoanion with zirconium ion within the structure of the anion exchange resin with a single cycle of synthesis process. Surface characteristics of the ZMAE were examined by a SEM, HR-TEM, XRD, FTIR, BET surface area and XPS analysis. In addition, the potential of ZMAE for selective removal of phosphate and arsenic were conducted and evaluated in presence of competing ions for both batch and column adsorption tests.

(2) To propose a new and effective method for fabrication of the hybrid of HFO (without molybdate) embedded a macroporous anion exchange resin (ZAE), called molybdate-intermediate method, in purpose of reducing time, cost and used chemicals of the synthesis procedure for selective removal of

phosphate. A series of hybrid ZAE adsorbents with different zirconium contents were fabricated and examined for the phosphate adsorption performance and selectivity in this study. In addition, the correlation between zirconium content and the selective performance of ZAE toward phosphate ion was conducted using both batch and fixed-bed column experiments in presence of competing ions. The results would provide a new insight of the hybrid ZAE for development of a large-scale synthesis of the hybrid ZAE.

2. Literature Review

2.1. Arsenic and phosphate problems

2.1.1. Arsenic and its contamination in water

Arsenic (As) is a well-known dangerous and carcinogenic metalloid with atomic number 33, atomic mass 74.92 and electronic configuration $4s^2 3d^{10} 4p^3$ found as a trace element in the earth's crust. Arsenic exists mainly in four oxidation states in environment: arsenate (As(V)), arsenite (As(III)), arsenic (As(0) and arsine (As(-III)). Among them, As(V) is the most stable form. Besides, arsenic can be found in a variety of organic form in environment, such as monomethylarsonic acid [MMA, $CH_3AsO(OH)_2$], dimethylarsinic acid [DMA, $(CH_3)_2AsOOH$], trimethylarsine oxide [TMAO, $(CH_3)_3AsO$], arsenobetaine [AsB, $(CH_3)_3As\beta\text{-}CH_2COOH$], arsenocholine [AsC], arsenosugars [AsS] [13]. In general, inorganic arsenic is more toxic than organic ones and inorganic As(III) is much more toxic than inorganic As(V).

The Eh-pH diagram provides a view of arsenic forms and its possibility of mobilization in water environment depending on the solution pH and oxidation potential Eh values [3, 13]. Positive Eh indicates oxidative condition, whereas negative Eh represents reducing condition. In natural water with pH often from 6 to 9, arsenic is almost predominated in two inorganic forms: arsenate (As(V)) and arsenite (As(III)) under several forms (such as $H_2AsO_4^-$, $HAsO_4^{2-}$ and H_3AsO_3). Generally, As(III) mainly occur under anaerobic conditions (e.g. groundwater),

whereas As(V) is the major specie under aerobic conditions (e.g. surface water) [20]. Comparing to As(V), As(III) seem to be more difficult to remove from the water sources [3, 21, 22]. As(III) generally has a weaker physiochemical affinity towards most absorbents. Therefore, a pretreatment process is usually introduced for As(III) oxidation, then As(V) formation are selectively absorbed on to the surface of solid materials [5, 23-25].

Arsenic concentration in water varies from one water body to another water body. In groundwater, arsenic concentration can vary in a large range from 0.5 to 5000 μg/L with naturally releasing from the aquifers containing arsenic being weathered. Thus, the arsenic concentration in groundwater is greatly affected by the mineralogical characteristics of the aquifer and the physicochemical properties of the groundwater [26]. Natural reactions including weathering reactions, biological activity, geochemical reactions, volcanic emissions are considered as the main factors causing the mobilization of arsenic from aquifers/soils to water systems causing its contamination. In addition, anthropology activities such as mining, combustion of fossil fuels and uses of chemical for crops and industries also contribute to the source of polluted arsenic. Arsenic in fresh water and river water are often found in lower concentration than groundwater, which have been reported in the range of 0.15 – 0.45 μg/L depending on the source, availability, and geochemistry of the catchments. Arsenic contamination in marine water is often low concentration [13].

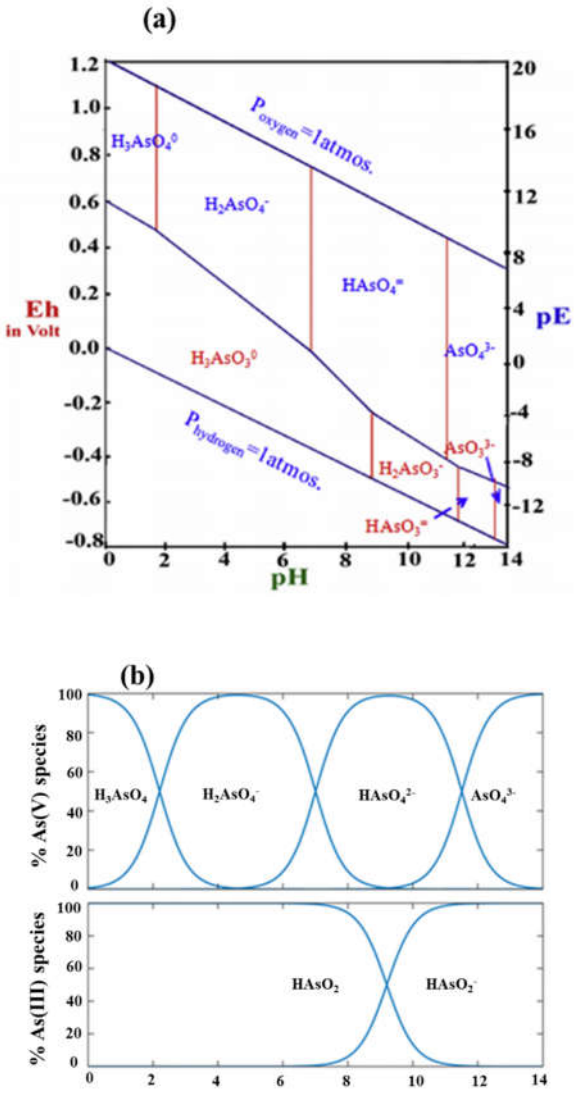

Fig. 2-1. (a) Eh-pH diagram for dissolved arsenic species in water at 25 ^{o}C and 1 atmospheric pressure and (b) Distribution of arsenic species versus pH in water.

2.1.2. Eutrophication and its relationship with phosphate

Eutrophication is the process of nutrients enrichment of water which results in inducing overgrowth of phytoplankton and thus deteriorating water quality, depopulating of aquatic biodiversity and species distribution and depletion of dissolved oxygen [27]. Eutrophication problem has become a strategy problem in many coastal regions in UK, China and other industrial countries concerning with the increase of phosphate concentration. For example, the cost of eutrophication to the UK industry water are estimated at > £15 M annually [28]. Nitrogen and phosphorous are considered as the main sources of nutrients in water. Extensive study reported that phosphorous is the key nutrient regulating eutrophication in lakes and reservoirs but not nitrogen because of the difficulty in controlling the exchange of nitrogen between atmosphere and water and the fixation of atmospheric nitrogen [29, 30]. According to the Water Framework Directive of EU, phosphorous is likely to be required in discharge levels ranging between 0.1–0.5 mg-P/L. The US EPA has recommended that the maximum level of phosphorus in water should not exceed 0.05 mg P/L. The recommended total P concentration by The Australian and New Zealand water quality guidelines in lakes and reservoirs < 0.01 – 0.025 mg-P/L [12].

Human activities including industries and agriculture with overuse of phosphorous are unavoidable causing a tremendous phosphate in discharging wastewater, which could be uncontrollably released into an aquatic system [31, 32]. Discharged wastewater usually containing orthophosphate and phosphorous

compounds forms such as condensed phosphates (pyrophosphate or tripolyphosphate) and organic phosphate. These polyphosphates could be hydrolyzed to be orthophosphate in water [33]. Among phosphorous forms, orthophosphate (or phosphate) is the only phosphorous form can be directly absorbed by most plants including algae. Phosphate can be occurred under soluble forms in water or can be adsorbed by mineral or sediment in water [12]. The presence of phosphate in water can be influenced by the pH of water because pH can affect to surface charges of both mineral/sediments and the form of phosphate (phosphoric acid has three pKa values ($pKa_1 = 2.15$, $pKa_2 = 7.20$, $pKa_3 = 12.33$ [15])).

Removal of phosphate from discharged wastewater going into received waters (such as lakes and reservoirs) becomes a critical issue to control eutrophication problem in water. As the eutrophication occurs, the recovery of water properties by reducing phosphate concentration is difficult because the phosphate trapped by sediments and minerals in water were not effectively removed, which could slowly be released back into the water.

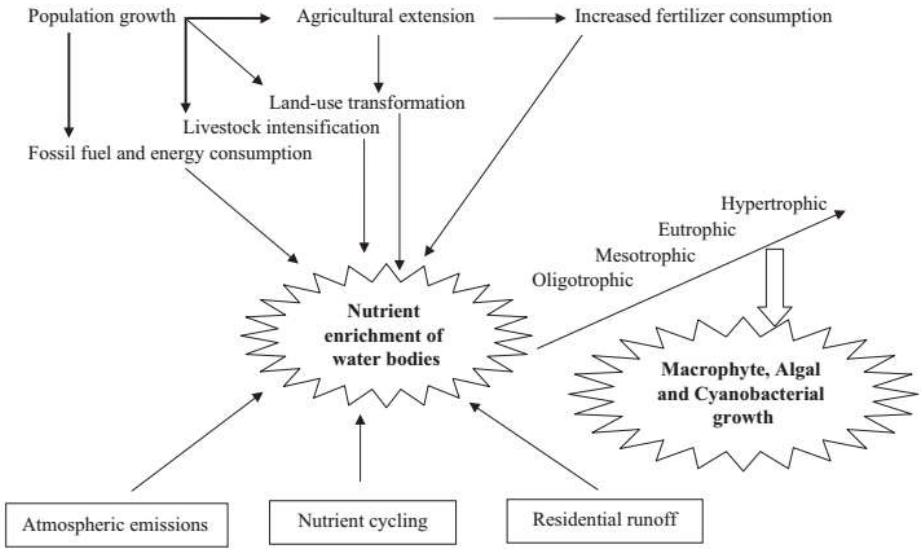

Fig. 2-2. Simplified illustration of direct and indirect sources driving eutrophication in water [34].

2.2. Adsorption technology for arsenic and phosphate removal

2.2.1. Overview

Many treatments and processes have been employed for removal of arsenic and phosphate from water and wastewater mainly classified as coagulation or co-precipitation, ion exchange, membrane and adsorption technologies. The efficiency of these technologies were summarized and compared in Table 2.1 [35]. Sometimes, the ion exchange is usually classified into the adsorption process [3]. Recently, the adsorption process has become the most promising method for removal of both arsenic and phosphate from water because of it is low cost, energy-efficient, removal- effective and operation-easy leading to suitably conduct in worldwide, especially in countries/regions concerning of electricity and economy [36-39].

A variety of adsorbents have been synthesized, studied and commercialized for phosphate and arsenic removal over decades [3]. They could be organic materials (carbon, chitosan, polymeric resin, etc.), inorganic materials (iron/iron oxide, zirconium oxide, titan oxide, iron-manganese mixed oxide, iron-ziconium mixed oxide, etc.) and hybrid materials (organic-inorganic composites such as, metal oxide loaded activated carbon, metal oxide impregnated ion exchange resin or chitosan, etc.) depending on the purpose of study. As principle, phosphate or arsenic species could be removed from water by interaction-attached on the surface/pore surface of adsorbents. Solid-liquid equilibrium established between the electrolyte solution and

a solid adsorbent is quite complicated depending on many factors such as pH of water, number of active adsorption sites, single or multi ions system, affinity of adsorption sites towards target ion compared with other ions. Most studies of the adsorption process were conducted with single ion prepared in DI water while the multi-ions system was less considered [3]. However, arsenic usually exists in trace level in water/groundwater containing many coexisting ions such as, chloride, nitrate, sulfate, bicarbonate [40]. Also, phosphate in discharged wastewater even accompanied with complicated matrix of ions. Thus, the removal of arsenic or phosphate in certain contaminated water could greatly suffered from coexisting ions from water. For examples, the uptake of arsenic on Fe^0 was decreased in the presence of sulfate ion and the effect was stronger at low pH value [41, 42]. Novillo et al. reported that the phosphate adsorption on Mg/Al layered double hydroxides (LDH) was affected by competing other anions in water (SO_4^{2-}, HCO_3^-, NO_3^- and Cl^-) and the adsorption decreased in order $NO_3^- > HCO_3^- > Cl^- > SO_4^{2-}$ due to the affinity of the LDH toward divalent anions [43]. Organic substances in water such as humic acid could suppress the adsorption of phosphate (or arsenic) on adsorbents or could delay the adsorption equilibrium which could lead to re-assessment and establishment of proper system designs [44, 45].

Along with adsorption capacity, desorption and regeneration of adsorbents have recently been considered as critical issues in contribution to reduce process cost and recover of elements/adsorbents. It requires adsorbents should be retained their original adsorption behaviors after regeneration process. For inorganic anion

adsorption like arsenic or phosphate, the common desorption method is based on chemical process. Recent studies on metal oxides or their composites demonstrated that both arsenic and phosphate were almost completely desorbed by solution of NaOH (or NaOH–NaCl) [46-49]. As pH increases by loading solution of NaOH, the surface hydroxyl groups of metal oxides are deprotonated and become negatively charged which leads to desorb arsenic or phosphate species [50].

Table 2-1. Comparison of arsenic removal among technologies.

Technology	Chemical reagent	As(III) removal (%)	As(V) removal (%)
Coagulation- filtration precipitation (including lime softening)	Ferric chloride	< 30	90 – 95
	Sulfates (Al, Cu, NH_3)	< 30	80 – 90
Adsorption	Activated carbon or activated alumina	30 – 60	> 95
	Fe hydroxide (granular)	30 – 60	>95
Ion exchange	Anion exchange resins	< 30	80 – 95
Membrane filtration (nanofiltration and reverse osmosis)	–	60 – 90	> 95
		80 - 95	> 95

2.2.2. Ion exchangers for anion removal

2.2.2.1. Introduction

Ion exchange is one of the most popular method employed for removal of ions from solution in many last decades due to its simplicity, effectiveness, recovery and low cost. To be considered as adsorption process, ion exchange is defined as a heterogeneous process where interchange takes place between a counter ion on a solid phase of ion exchanger and counter ions in electrolyte solution [51, 52]. Historically, ion exchange was discovered from H. S. Thomson and J. T. Way in the middle of the 19th century, which described the percolation of ammonium sulfate through the tube filled with soil into the calcium surface. In 1935, Adams and Holmes synthesized the first organic-based (polymeric) cation and anion exchangers by polycondensation of phenol with formaldehyde and a polyamine, respectively. In 1944, D' Alelio prepared and patented a sulfonated crosslinked polystyrene anion exchange resin [53]. These inventors were considered as fundaments for the diverse development of new ion exchangers which were diversely and powerfully applied in biotechnology, agriculture, pharmaceuticals, pure chemicals, microelectronics and etc. [54]. Nowadays, ion exchangers are synthesized by a three-dimensional cross-linked polymer constituting a separate insoluble phase, usually a polystyrene crosslinked with 3 to 8% divinylbenzene (DVB). The functional groups (fixed co-ions) was covalently attached on the polymeric phase, which permeated and electrically balanced by an exchangeable counter-ion [53, 54]. In general, ion

exchangers can be classified into four main groups based on their functional groups including: strong acid cation (SAC) exchanger (e.g., sulfonate, $-SO_3^-$); weak acid cation (WAC) exchanger (e.g., carboxylate, $-COO^-$); strong base anion (SBA) exchanger (e.g., quaternary amine, $-N^+(CH_3)_3$) and weak base anion (WBA) exchanger (e.g., tertiary amine, $-N(CH_3)_2$). Besides, there are also some special types of ion exchangers fabricated for specific purposes.

For anion exchangers, cross-linked polystyrene covalently attached amine functional group was commonly commercialized. Depending on the order of basicity of amine functional group, anion exchanger can be classified into strong to weak base and arranged as follows [53]:

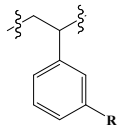

where R can be:

$CH_2N^+(CH_3)_3Cl^-$: Type 1 strong base resin (e.g. Amberlite IRA402)

$CH_2N^+(CH_3)_2CH_2CH_2OHCl^-$: Type 2 strong base resin (e.g. Amberlite IRA410)

$CH_2N^+(CH_3)_2$: Weak base resin (e.g. Amberlite IRA96)

Resin with quaternary ammonium functional groups (benzyltrimethylammonium) are strongly basic and known as type 1. This type of resin can remove a wide range of anions including hard anions (from strong acids, such as Cl^-, SO_4^{2-}) and soft anions (from weak acids, such as $HSiO_3^-$, SiO_3^{2-}). The type 1 anion exchange resin are

widely used in water treatment. This process used for removal of phosphate (or arsenate) ion is shown in follow equations:

$$\overline{R_4N^+}Cl^- + H_2PO_4^- \Leftrightarrow \overline{(R_4N^+)_2}H_2PO_4^- + Cl^- \quad (2\text{-}1)$$

$$2\overline{R_4N^+}Cl^- + HPO_4^{2-} \Leftrightarrow \overline{(R_4N^+)_2}HPO_4^{2-} + 2Cl^- \quad (2\text{-}2)$$

$$3\overline{R_4N^+}Cl^- + PO_4^{3-} \Leftrightarrow \overline{(R_4N^+)_2}PO_4^{3-} + 3Cl^- \quad (2\text{-}3)$$

Resin with benzyldimethylethanolammonium groups are known as type 2 and are less slightly basic. This type of resin is also basic enough to remove anions; however, they showed less chemical stability than the type 1. The weak base anion exchange resin was known with the primary amine functional group and rarely used in water treatment.

2.2.2.2. Mechanism and non-selectivity of anion exchangers

Ion exchange describes a stoichiometric interchange between chemically equivalent number of counter anion on the surface ion exchanger and another counter ion in electrolyte solution. This interaction process is governed by columbic or electrostatic force and is a reversible process. Thus, the adsorption is prior to counter ions with higher valence and smaller hydrated radius [12]. Besides, the Bronsted and Lewis acid-base interaction were also pronounced for the case of weak base AE [53].

The selectivity of anion exchangers toward ion B over ion A can be expressed by the selectivity coefficient ($S_{B/A}$) (simply for a monovalent anion):

$$\overline{R_4N^+}A^- + B^- \Leftrightarrow \overline{R_4N^+}B^- + A^- \qquad (2\text{-}4)$$

At equilibrium, $S_{B/A} = \frac{[B^-]_R[A^-]}{[A^-]_R[B^-]}$

where, $[A^-]_R$and $[B^-]_R$ are the equilibrium concentration of A^- and B^- on the resin; $[A^-]$ and $[B^-]$ are the equilibrium concentrations of A^- and B^- in solution. Assuming activities of ions are constant.

Fig. 2-3 shows the arsenate removal from tap water by the strong base AE Relite A-490. As the result, the efficiency of arsenate removal was sharply decreased in the presence of competing anion (Cl^- or SO_4^{2-} ion) [55]. Awual et al. investigated the effect of common anions in natural water (Cl^-, NO_3^- and SO_4^{2-}) to the phosphate adsorption with varying pH value in comparison between the weak base AE Diaion WA20 and the strong base AE Diaion SA10A [56]. As shown, the phosphate

adsorption to both resin types were strongly affected by the competing anions. In addition, the weak base AE prefers phosphate to these univalent ion, while the strong base AE prefer less hydrated anions to highly hydrated ones.

Table 2-2. The relative selectivity of a type 1 and the type 2 strong base anion exchange resin for monovalent anions in respect to OH^- ion.

Anion	**Resin**	
	Type 1	**Type 2**
OH^-*	1.0	1.0
F-	1.6	0.3
Cl^-	22	0.5
Br^-	50	6
CH_3COO^-	3.2	0.5
HCO_3^-	6.0	1.2
NO_2^-	24	3
NO_3^-	65	8
CN^-	28	3
HSO_4^-	85	15

*Reference value

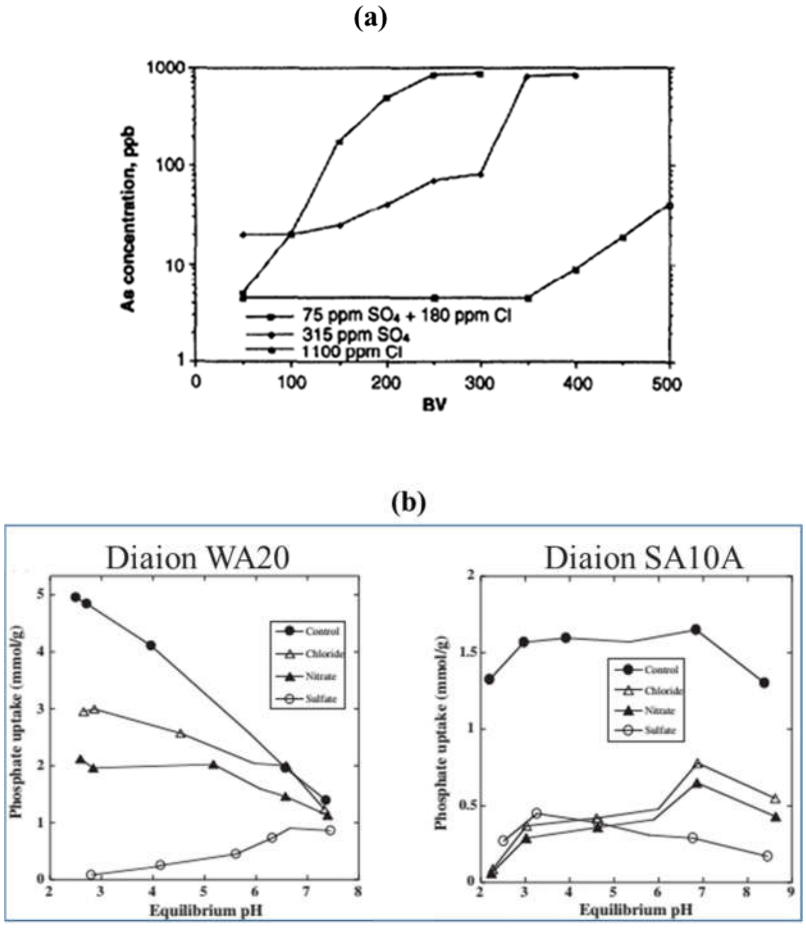

Fig. 2-3. (a) Effluent arsenic concentration vs. bed volumes for different water concentration using strong base AE Relite A-490 ([As(V) = 820 μg/L, flow rate 20 BV/h); (b) Equilibrium phosphate concentration as a function of equilibrium pH in the presence and absence of competing ions in comparison between the Dianion WA20 and Dianion SA10A ([PO_4] = 0.01M, [Adsorbent] = 50 mg/50 mL, [Cl] = [NO_3] = [SO_4] = 0.01M, 30°C, 24 h).

2.2.3. Adsorption by metal oxides and their limitations

Recently, a variety of polyvalent metal oxides NPs have been extensively employed for removal of arsenic or phosphate species due to their large surface area and specific functionalities [18, 57], which could be single oxides (such as, Al oxide/hydroxide [58, 59], Fe oxide [6, 60], Zr oxide [9, 61], Cu oxide[62], Mn oxide [63], Ti oxide [64], Sn oxide [65]) and binary oxides (such as, Fe-Mn [31, 66], Fe(III)-Zr(IV) [67, 68], Fe(III)-Cu(II) [10, 69], Fe-Ti [70, 71], Al-Mn [72] and Ce-Zr oxide [73]). Among them, iron oxides have been mostly used because it is abundant, inexpensive and innocuous source. Many forms of iron oxide have been considered as promising adsorbents for arsenic and phosphate removal, including hydrous ferric oxide (FeOOH) [6, 60], goethite (α-FeOOH) [74, 75] and hematite (α-Fe_2O_3) [76], magnetite (Fe_3O_4) [77, 78]. In particular, the use of magnetite iron oxide or zero valent iron could allow magnetic separation of adsorbents, which bring advantages in technical design of filtration process [79]. Nevertheless, iron oxides can be dissolved in acidic condition and in contact with organic substances. In addition, the reduction of Fe(III) to Fe(II) by reducing agents can increase their dissolution, which could increase risk of arsenic release from the arsenic-laden to landfill conditions [11, 50]. To compare with iron oxides, zirconium oxide has been recently reported with high stability against with pH ranges, organic substances and oxidants [18, 80]. An increasing study of zirconium oxide and its binary oxide has

extensively introduced for high efficient removal of phosphate and arsenic removal from water [9, 81, 82].

Unlike anion exchanger, metal oxides are able to selectively adsorb arsenic and phosphate species on their surface functional groups in the presence of high concentrations of competing anions such as sulfate, nitrate, chloride, and bicarbonate. Interaction of hydrated metal oxide with arsenic or phosphate in electrolyte solution is mainly taken placed on their surface functional groups, –OH groups [83]. The hydrated metal oxides can be viewed as diprotic weak acids that can deprotonate as follows [84]:

$$\overline{MOH_2^+} \quad \overline{MOH} + H^+ \qquad (2\text{-}5)$$

$$\overline{MOH} \quad \overline{MO^-} + H^+ \qquad (2\text{-}6)$$

Surface charge of metal oxides could be positive ($\overline{MOH_2^+}$), neutral ($\overline{MOH}$) or negative ($\overline{MO^-}$) depending on the solution pH. When the pH < pH_{pzc} of the oxides, the protonated form ($\overline{MOH_2^+}$) will be favorable for phosphate or arsenate ion. Arsenic/phosphate was effectively adsorbed on hydrated surface of metal oxides through their inner-sphere complexation between arsenic/phosphate and surface hydroxyl groups [85, 86] (Fig. 2-4). However, when pH > pH_{pzc}, the deprotonated form ($\overline{MO^-}$) of metal oxide surface was created, resulting in decreasing the removal efficiency due to the electrostatic repulsion [49].

Besides chemical bonding with surface hydroxyl groups, surface precipitation and co-precipitation process were also reported for the case of nano zero-valent iron (nZVI) in removal of arsenic and phosphate [87, 88]. The outstanding arsenic adsorption property of nZVI is explained by the role of its reactive corroded products (Fe species) [88-90].

However, be present as fine particles, the use of NPs can deal with hard problems including difficult manipulation and separation, high pressure drop during operation, which could lead to limitation of their application for water treatment. In addition, risk of leaking of NPs to environment causes another environmental concern [50, 91]. Recently, embedding metal/metal oxide NPs within a large-sized or porous support has been recently studied for overcoming technical problems of NPs. Various materials have been used as supports including activated carbon/graphite [92-94], cellulose [32], chitosan[95, 96], zeolites [97, 98], or functional polymers [99-102].

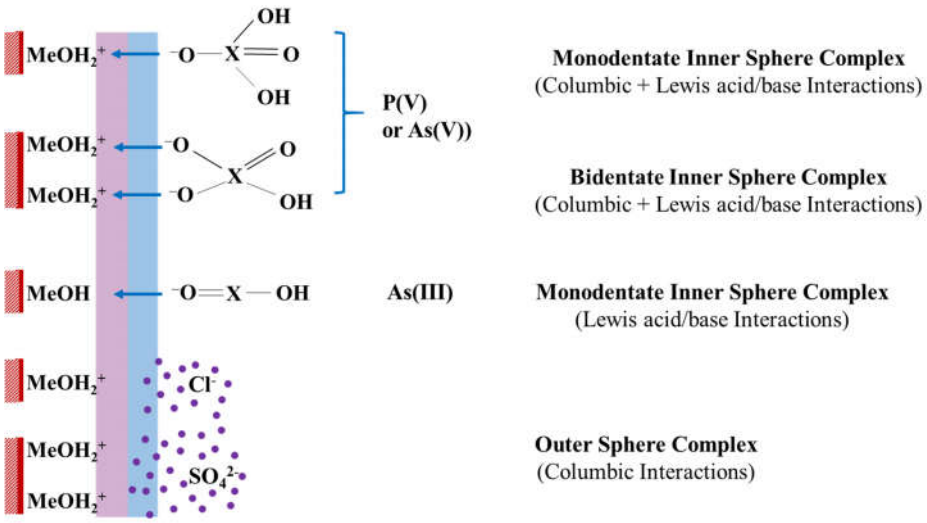

Fig. 2-4. Schematic illustrates the interaction mechanism between metal oxide surface and common anions in water.

2.2.4. Adsorption by molybdate-based materials

Molybdate oxoanion is well-known as a selective agent which reacts with phosphate to form molybdophosphate complex applied for trace analysis of phosphate in water [103, 104]. Similar behavior of molybdate was reported for the case of arsenate where the molyboarsenate complex was form [104, 105]. The reaction between molybdate and phosphate (or arsenate) prefers in acidic solution [106]. Zhao et al. reported a flotation method to effectively separate the phosphate and arsenic from other co-existing anions in aqueous solution of molybdate ion by optimizing the pH, collector (dodecylamine) and co-precipitant (Fe^{3+}) concentrations [107]. In the last decade, a couple of studies about molybdate impregnated chitosan beads (MICB) were introduced for efficient adsorption of arsenic. Dambies et al. showed a great capacity of MICB toward As(V) about 230 mg-As/g-Mo at pH ~3 [108]. Another studies of MICB showed high potential of column design of MICB for effective removal of arsenic from wastewater without any pretreatment process [109]. However, although MICB exhibited a promising efficiency of arsenic removal, the strong release of molybdenum during the arsenic adsorption was considered due to the natural properties of molybdate component. It could be reason in limitation of number of study on molybdate-based adsorbents for arsenate and phosphate removal in literature.

2.2.5. Hybrid Inorganic NPs embedded anion exchanger

Impregnating oxides/hydroxides NPs into a porous structure of a crosslinking anion exchange resin is one of the effective ways to overcome hard problem of NPs. In addition, this type of hybrid exhibited excellent performance of arsenic (or phosphate) removal from water sources because it can not only inherit the selective property of embedded NPs for arsenic (or phosphate), but also utilize the advantage of Donnan membrane effect from high density of quaternary ammonium positive charges of the supported resin for enhancing adsorption capacity and efficiency as shown in Fig. 2-5 [16, 17]. Sengupta group has shown the superior efficiency of arsenate removal HFO impregnated AE compared with HFO impregnated cation exchange resin [16]. Indeed, the HFO impregnated AE enhanced permeation of arsenate oxyanions inside the anion exchanger, and subsequently selectively bind onto dispersed HFO nanoparticles, while the Donnan exclusion of the HFO impregnated cation exchanger leading to significantly decrease adsorption efficiency. Qiong et al. compared the arsenic adsorption between two host polymers of different surface functional groups on the same cross-linked polystyrene matrix (quaternary ammonium functional groups and chloride groups) embedded nZVI. It is noticed that the arsenate adsorption on the hybrid of quaternary ammonium functional group was better than that of the hybrid of the chloride functional group due to the Donnan membrane effect [110]. For better understanding, the following parts discuss about the role of Donnan equilibrium established between a strong base anion exchanger

and arsenate (or phosphate) anion compared with sodium cation. In addition, the synthesis for anion exchanger embedded with metal oxide will be also discussed.

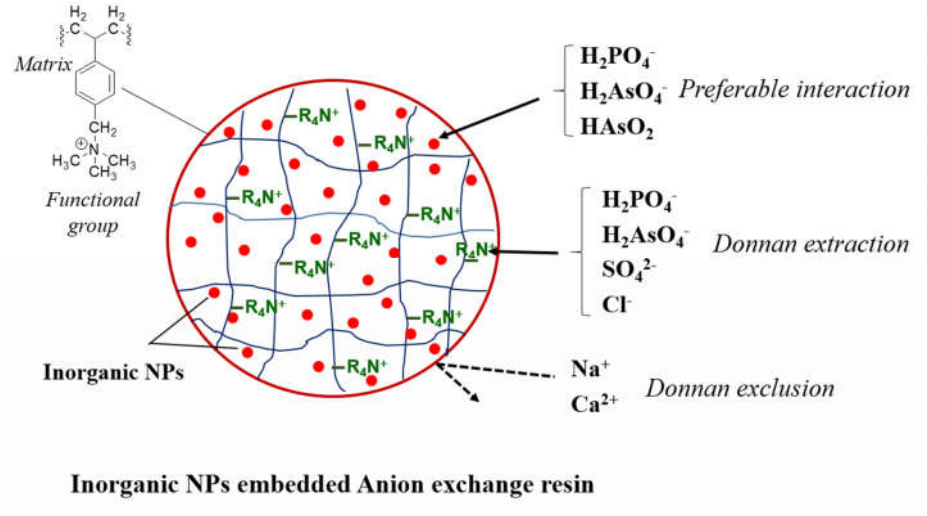

Fig. 2-5. Diagram of inorganic nanoparticles embedded within an anion exchange resin.

2.2.5.1. Principle of Donnan membrane equilibrium of anion exchanger

Donnan membrane equilibrium (usually referred as Donnan membrane effect or Gibbs-Donnan membrane equilibrium) describes a thermodynamic equilibrium of two aqueous compartments separated by a permeable membrane, where water and a certain charged components (ions) can allow to permeate through the membrane but others cannot [111, 112]. Such equilibrium is important to the observation of heterogeneous adsorption systems between ion exchanger and electrolyte solution. Fig. 2-6a demonstrates clearly different general mechanism of ion permeability through the anion exchanger and cation exchanger. As shown, ion exchangers have a tendency to attract counter ions and exclude other co-ions from electrolyte solution. For instance, anion exchangers allow anion B^- to migrate through the membrane but do not allow cation A^+ and versa.

In order to evaluate the equilibrium established for an adsorption system of phosphate (or arsenate) ion interacting with anion exchange beads, let's consider the heterogeneous solution of $\overline{R}Cl$ (the anion exchanger form) and mono sodium phosphate (or arsenate) (NaX). The dissociation of $\overline{R}Cl$ and NaX salts are expressed as follows:

$$NaX \rightarrow Na^+ + X^- \qquad (2\text{-}7)$$ (X^- is $H_2PO_4^-$ or $H_2AsO_4^-$)

$$\overline{R}Cl \rightarrow \overline{R^+} + Cl^- \qquad (2\text{-}8)$$

Fig. 2-6b illustrates the initial and equilibrium states established between two sides of the membrane (symbolized by a vertical line). As shown in Fig. 2-6b, assuming at initial state, the solution of $\overline{R}Cl$ and NaX are placed in both sides of the membrane, where the salt of $\overline{R}Cl$ is placed on the left-hand side (L) of the membrane and NaCl salt is in the other side (R). The ion Cl^-, Na^+ and X^- are then migrated to other sides of the membrane and reached equilibrium while the cation $\overline{R^+}$ is an impermeable ion. At equilibrium, the isothermal reversible change of these ions is balanced and the Donnan membrane equilibrium provides the following equation:

$$\frac{[Na^+]_R}{[Na^+]_L} = \frac{[Cl^-]_L}{[Cl^-]_R} = \frac{[X^-]_L}{[X^-]_R} \qquad (2 \quad 9)$$

Expressing Eq. (2-9) for equilibrium concentration of ions permeability through the membrane as follow:

$$\begin{cases} \frac{c_2 \quad y}{y} = \frac{c_1 \quad z}{z} = \frac{x}{c_2 \quad x} & (2 \quad 11) \\ z = x \quad y & (2 \quad 12) \end{cases}$$

Substitution of (2-12) to (2-11) results in:

$$x = \frac{(c_1 + c_2)c_2}{c_1 + 2c_2} \qquad (2 \quad 13)$$

$$y = \frac{c_2^2}{c_1 + 2c_2} \qquad (2 \quad 14)$$

Combing value of x and y in (2-13) & (2-14), the equilibrium equation (2-9) can be derived:

$$\frac{[Na^+]_R}{[Na^+]_L} = \frac{[Cl^-]_L}{[Cl^-]_R} = \frac{[X^-]_L}{[X^-]_R} = \frac{x}{c_2 \quad x} = \frac{c_1 + c_2}{c_2} = constant \qquad (2 \quad 15)$$

From Eq. (2-15), the percent of X^- and Na^+ migrated from the left-hand side (L) to the right-hand side (R) and their distributions between those sides in specific values of c_1/c_2 were calculated and summarized in Table 2.3. As the results, the ion $[X^-]$ (phosphate or arsenate ion) in the left-hand side is much greater than the right-hand side and their difference is significantly increasing at high ratio of c_1/c_2. For example, at $c_1/c_2 = 100$, $[X^-]_L$ is about two orders of magnitude greater than $[X^-]_R$, which indicates about 99% of ion X^- migrated into the polymeric phase of the resin. In contrast to the case of ion X^-, the migration of ion Na^+ from the left-hand side to the right-hand side is remarkably suppressed (lower 1% of Na^+ migrated at $c_1/c_2 = 100$), which is related to the Donnan exclusion phenomenon.

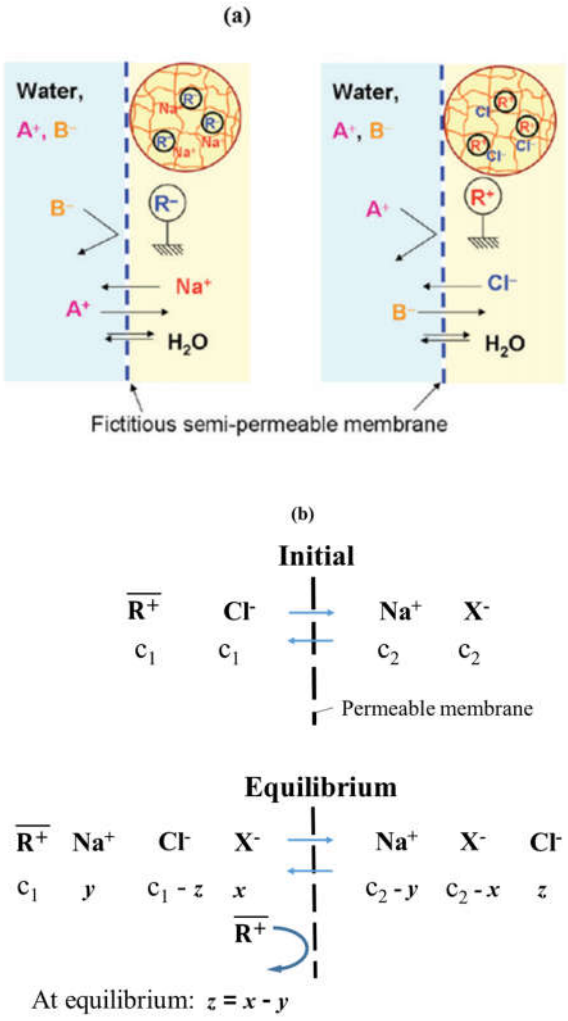

Fig. 2-6. (a) Diagram of Donnan membrane equilibrium in comparison between a cation exchanger and anion exchanger; (b) Equilibrium established between two sides of the membrane (symbolized by a vertical line) of an anion exchanger.

Table 2-3. Distribution of ion X^- ($H_2PO_4^-$ or $H_2AsO_4^-$) and ion Na^+ into polymeric phase of anion exchange resin with difference of initial ratio [$\overline{R}$Cl]/[NaX].

Initial ratio of [$\overline{R}$Cl]/[NaX]	**%X^- migrated from L to R**	**Distribution of X^- between L and R**	**%Na^+ migrated from L to R**	**Distribution of Na^+ between L and R**
$\frac{c_1}{c_2}$	$\frac{x}{c_2}100$	$\frac{[X^-]_L}{[X^-]_R}=\frac{x}{c_2-x}$	$\frac{y}{c_2}100$	$\frac{[Na^+]_L}{[Na^+]_R}=\frac{y}{c_2-y}$
1	66.7	2	33.3	1/2
10	91.7	11	8.3	1/11
100	99.0	101	0.98	1/101
1000	99.9	1001	0.1	1/1001

2.2.5.2. Synthesis of inorganic NPs embedded anion exchanger

A variety of techniques have been reported for synthesis of hybrid inorganic NPs embedded polymer (hybrid polymer-NPs) in general and hybrid inorganic NPs embedded anion exchanger in particularly. Based on the process of formation of hybrids, the synthesis can be classified into two major routes, which are *ex situ* (or direct compounding) and *in situ* synthesis.

- *Ex situ synthesis*

This route of synthesis has been extensively used for fabrication of hybrid polymer-NPs because this method was not picky to any NPs. In this method, the pre-made NPs was dispersing in a solution of polymer or monomer which was then polymerized to produce a nano-composite. The synthetic principle of *ex situ* route can be expressed in Fig. 2-7a.

As shown in Fig. 2-7a, the nano-particles was separately prepared, isolated and purified before introducing to compound. Thus, the desired properties of NPs such as size, crystalline, functionalities could be well controlled, leading to be suitable for large-scale production. However, NPs are known to be aggregated during the mixing due to the high surface energy of NPs. This results in a significant difficulty from controlling the dispersion of NPs in/on the polymeric structure. Sometimes, appropriate stabilizers or dispersants could be added for improving the homogeneous mixing of NPs and polymer solution.

If the supported polymer was prepared separately before compounding with NPs, the process is called blending method or direct compounding, whereas the *in situ* polymerization was described for the simultaneous of polymerization and compounding [113-115]. The blending method is a simplest method for preparation of nano-composite which can be achieved by either solution or melt blending. Melt blending can be proceeded in a minimal solvent for mixing and then thermal evaporation. This process is high efficiency; however, the obtained nano-composite is usually un-controlled agglomeration of dispersed NPs. The solution blending was shown with easier way to prepare of nano-composite which is usually followed with casting or centrifuging and solvent evaporation [113]. This process requires soluble polymers or co-polymers. On the other hand, impregnating inorganic NPs with solution of monomer or organic precursor followed by *in situ* polymerization is more popular than the direct method for preparing nano-composites because the strong interaction between NPs and support and performance of hybrids could be enhanced [116, 117]. For example, Wu et al. reported the comparison of polyimide/multiwalled carbon nanotube (PI/MWCNT) synthesized by the *in situ* polymerization and blending methods [118]. The results indicated that *in situ* polymerization provided better dispersion of MWCNT in polyimide matrix. In addition, thermal and mechanical properties of composites were improved owing to hydrogen bonding interaction. Table 2.4 summarizes several hybrid materials of NPs embedded anion exchanger prepared by the *ex situ* route including direct compounding and *in situ* polymerization.

Table 2-4. Summary of some typical hybrids of inorganic NPs embedded anion exchangers prepared by *ex situ* method.

NPs	Supported polymer	Name of hybrid	Synthesis method	Ref.
Fe_2O_3-SO_4^{2-}	Sulfonated poly (2,6-dimethyl-1,4-phenylene oxide)	sPPO-Fe_2O_3-SO_4^{2-}	Direct compounding	[114]
AgCl/$AgVO_3$	Fe: 10.2polyvinyl pyrrolidone	ACV	Direct compounding	[115]
SiO_2 and Fe_3O_4	Polyethylenimine	PEI-grafted magnetic porous adsorbent	Direct compounding	[119]
$(Al(OH)_3$	Polyacrylonitrile	PAN–$Al(OH)_3$	Direct compounding	[120]
Sn(IV)tungstophosphate	Polyaniline	Polyaniline-Sn(IV)tungstophosphate	Direct compounding	[121]
TiO_2	Quaternary polysulfone	QPSf/TiO_2	Direct compounding	[122]
Mg/Al mixed oxide	Polycinnamamide	Polycinnamamide Mg/Al mixed oxide nanocomposite	Direct compounding	[123]
y-Fe_2O_3	Polyaniline	PANI/c-Fe_2O_3 MNCs	In situ polymerization	[124]
TiO_2	Polyaniline	Polyaniline-modified TiO_2	In situ polymerization	[125]
Al_2O_3	4-Aminoantipyren	Hybrid inorganic/organic adsorbents	In situ polymerization	[126]

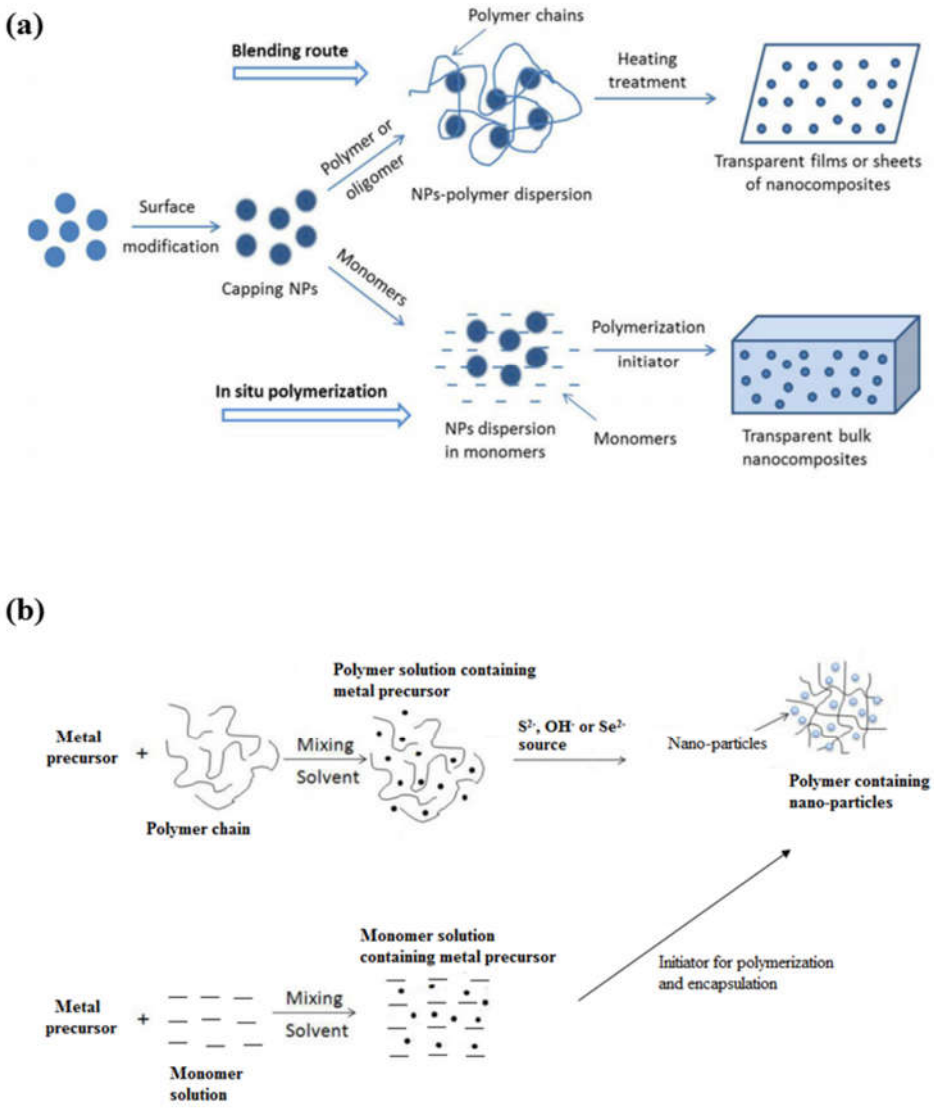

Fig. 2-7. *Ex situ* route (a) and *in situ* (b) for synthesis of hybrid inorganic nano-particles embedded anion exchanger.

❖ *In situ synthesis*

The principle of *in situ* synthesis was in contrast with the *ex situ* method, where in organic NPs (metal oxides, metal salts) was prepared within the matrix of polymer. With this method, the NPs are expected to be uniformly distributed within the matrix of polymer because the precursor metal ion is supposed to contact with polymer/monomer matrix. Thus, the formed NPs can be stabilized and isolated by units of polymer (served as nano-reactors), which allow to prevent the agglomeration of NPs [127]. Recently, most of the hybrid adsorbents of NPs embedded anion exchanger in literature have been fabricated by the *in situ* method. There are two ways of preparing hybrid of inorganic NPs embedded anion exchanger (Fig. 2-7b). As shown in Fig. 2-7b, the supported anion exchanger could be premade or simultaneously compounded with NPs.

(1) Metal ions are firstly loaded onto the pore surface of anion exchanger as a precursor of NPs, where metal ions are supposed to distribute uniformly. The, the precursor of NPs are exposed to contact with solution/gas of containing S^{2-}, OH^-, or Se^{2-} for in situ precipitate the target NPs inside the polymeric matrix [17, 48, 128, 129]. Many applications of hybrids NPs embedded AE was synthesized by this route for arsenic and phosphate application (Table 2-5). For example, Kociolek-Balawejder et al. prepared hybrid AE-CuO from the heterogeneous mixing of $CuCl_2$ solution and the Amberlite IRA 900Cl resin. The *in situ* precipitation of $Cu(OH)_2$ within the supported AE

was controlled by solution of NaOH, which was further dried to form CuO NPs. The instrumental characteristics of the hybrid showed that CuO NPs was successfully deposited in a macroporous pore of the resin while the contribution to the mesoporous pore of the resin was negligible [130].

(2) Another approach is performed by simultaneously blending the precursor of NPs and the monomer of polymer in with an initiator in proper solvent [131-133]. Singh et al. reported the sol-gel method for preparation of an anion-exchange silica precursor -poly(vinyl alcohol) in acidic medium followed by chemical crosslinking of –OH groups via formal reaction [132].

❖ *Popular Hybrid of inorganic NPs embedded anion exchanger*

This part focuses on some hybrid adsorbents of inorganic NPs embedded within a macroporous/gel anion exchange resin, which was extensively studied for arsenic and phosphate removal by the *in situ* route. The synthesis of following hybrids were described in principle of overcoming the Donnan exclusion of dispersing metal ion within the resin as well as the *in situ* precipitation of NPs.

- *Metal NPs*

Iron metal NPs or nano zero valent iron (nZVI) has been widely studied for adsorption removal of contaminants from water including arsenic and phosphate [89]. The hybrid nZVI embedded anion exchange resin (AE) was fabricated by sorption

followed *in situ* redox reaction [110, 134, 135]. Firstly, the nZVI precursor, anionic $FeCl_4$, was introduced to the AE resin and anion exchanged with counter ion Cl of the AE (Eq. (2-16)). The AE beads were then added to the $NaBH_4$ solution for reducing $FeCl_4$ in to nZVI, which was *in situ* precipitated within AE structure (Eq. (2-17)). The anionic $FeCl_4$ was used instead of Fe^{3+} ion for utilizing the Donnan principle of fixed positively charged quaternary ammonium functional group of the resin. Jiang et al. reported that the concentration of $NaBH_4$ affected directly to the reduction of iron ion and the stability of the formed nZVI, which required at least Na BH_4 3.6% in mass [135]. This type of hybrid can inherit the oxidizing property of nZVI for oxidation of As(III), leading the much enhancement of As(III) adsorption capacity and efficiency of the hybrid [110].

$$\overline{R_4N^+}Cl^- + FeCl_4^- \rightarrow \overline{R_4N^+}FeCl_4^- + Cl^- \quad (2\text{-}16)$$

$$\overline{R_4N^+}FeCl_4^- + 2BH_4^- + 6H_2O \rightarrow \overline{R_4N^+}Fe^0 + 2H(OH)_3 + H_{2\uparrow} \quad (2\text{-}17)$$

- *Metal oxide NPs*

Several metal oxides have been dispersed within a macroporous/gel strong base AE resin, including titanium oxide, iron oxide, zirconium oxide, copper oxide or iron-manganses oxide as shown in Table 2-5. Among them, hydrated iron oxide NPs embedded AE (FAE) is the most popular hybrid has been recently studied. There were two typical techniques for fabrication of the FAE reported elsewhere [48, 129].

The first method for synthesis of the FAE consists of four steps as follows [129]:

- Firstly, the AE resin was introduced to contact with solution of potassium permanganate to form the permanganate-loaded resin:

$$\overline{R_4N^+}Cl^- + MnO_4^- \rightarrow \overline{R_4N^+}MnO_4^- + Cl^- \quad (2\text{-}18)$$

- Secondly, the permanganate-loaded resin was allowed to contact with solution of $FeSO_4$, where the simultaneous desorption and oxidation processes were occurred. The MnO_4^- ion replaced by SO_4^{2-} ion oxidized Fe^{2+} to Fe^{3+}.

$$2\,\overline{R_4N^+}Cl^- + SO_4^{2-} \rightarrow \overline{(R_4N^+)_2}SO_4^{2-} + 2MnO_4^{2-} \quad (2\text{-}19)$$

$$MnO_4^{2-} + 4H^+ + 3Fe^{2+} \rightarrow MnO_{2\downarrow} + 4Fe^{3+} + 2H_2O \quad (2\text{-}20)$$

- The third step was followed by loading NaOH solution for precipitation of $Fe(OH)_3$ within the resin

$$Fe^{3+} + 3OH^- \rightarrow Fe(OH)_{3\downarrow} \quad (2\text{-}21)$$

- Finally, the resultant beads were washed (water and acetone) and dried. This technique could allow to fabricate magnetic iron oxide embedded AE with carefully controlled at the second step of the procedure.

Another technique for synthesis of FAE was reported using a binary $FeCl_3$–HCl solution as a NPs precursor [48], which included three steps of process. In first step, the AE was loaded with solution of binary $FeCl_3$–HCl (containing 30 – 50% ethanol),

where the resulting $FeCl_4^-$ ion in solution was preferably ion exchanged onto the AE, which is similar to the case of nZVI (Eq. (2-16). The second and third steps of this method were similar to the above procedure, where the AE beads were followed contacting with NaOH solution (Eq. (2-21)) and washed and air dried after that.

Recently, hydrated zirconium oxide NPs embedded AE (ZAE) has exhibited its excellent stability against with acid/base and organic substances compared with that of HFO NPs while both hybrids showed compatibility of adsorption capacity and efficiency [18]. For synthesis of the ZAE, the dispersing of zirconium onto AE seemed to be more difficult than ferric ion because zirconium does not produce an anion complex form with chloride ion nor participate in oxidation reaction with permanganate like the case of Fe^{3+} ion. In 2013, Pan et al. introduced the method for dispersing by mixing of high amount of $ZrOCl_2 \cdot 8H_2O$ in acidic solution containing 30% ethanol (zirconium ion was in form of $[Zr_4(OH)_8(OH_2)_{16}]^{8+}$) [17]. The resin-zirconium beads were followed by contacting with solution of NaOH the procedure for the synthesis of HFO embedded AE. In similar way, Sengupta group proposed and patented the method of loading zirconium oxide within AE in 2015 [19]. From this patent, zirconium solution prepared by dissolving zirconium oxide into a solution comprising an organic solvent and an acid was brought to contact with AE to form zirconium-loaded resin. The zirconium-loaded resin was followed to contact with solution of NaOH for the *in situ* precipitation of HFO NPs within the resin structure. However, for achieving the desired content of Zr in ZAE (about 10% in mass), at least three repetitive cycles of the synthetic process were carried out.

- *Binary oxide NPs*

Recent studies showed that the binary metal oxide adsorbents could better adsorption performance than single oxide adsorbents. For example, Zhang et al. developed an Fe-Mn binary oxide which exhibited high capacity towards both As(V) and As(III) (0.93 mmol/g and 1.77 mmol/g, respectively) due to not only the synergetic effect between two metal oxides for additional active sites for the adsorption but also high capability of oxidation of As(III) to As(V) for enhancing the adsorption [5]. Based on this principle, Li et al. development of Fe-Mn binary oxide embedded AE D201 (D201-Fe/Mn) for efficient removal of As(III) from water [136]. The D201-Fe/Mn was synthesized as follow. Firstly, the hybrid HFO embedded D201 (D201-HFO) was prepared as the second technique of the FAE described above. The D201-HFO was then exposed to contact with $KMnO_4$ solution. Similar to $FeCl_4^-$, MnO_4^- was also exchanged onto D201. Finally, the MnO_4^- preloaded D201-HFO was deoxidized to MnO_2 by 50% (v/v) ethanol solution. The resultant hybrid D201-Fe/Mn was characterized with well dispersed Fe and Mn within the resin. Sengupta et al. was also reported the synthesis of the hybrid adsorbent of binary Fe-Cu oxide embedded AE DOWEX M4195 (DOW-HFO-Cu) for selective removal of phosphate [137]. The synthetic procedure of the DOW-HFO-Cu was similar to the D201-Fe/Mn, where the DOW-HFO was firstly prepared and then exposed to load copper oxide for producing hybrid DOW-HFO-Cu.

Table 2-5. Summary of Inorganic NPs embedded anion exchange resin reported in literature for removal of target pollutants from water.

Nano-particles	Metal content (wt%)	Supported resin	Target pollutant	Ref.
HFO	Fe: 10.2	D201 (PS–DVB matrix, quaternary ammonium functional group)	Phosphate	[48]
HFO	Fe: 6	Purolite C-100 (PS–DVB matrix, quaternary ammonium functional group)	Arsenic(V)	[16]
HFO	–	Amberlite IRA-900 (PS–DVB matrix, quaternary ammonium functional group)	Phosphate	[100]
HFO	Fe: 6	Synthetic fiber AE (acrylic matrix and -N- $(CH_3)_2$ secondary amine groups)	Phosphate	[101]
HFO	9.6	NDA802 (PS–DVB matrix and amine groups -$N(CH_3)_2$	Phenol and Phosphate	[138]
HFO	Fe: 18–23	Lewatit FO36 (PS–DVB matrix and Tertiary amine groups P-CH_2-N-CH_2-$CH_3)_2$ functional group	Phosphate	[139]
HFO	–	PhosXnp or LayneRT (PS–DVB matrix, quaternary ammonium functional group)	Diclofenac and Phosphate	[140]

HFO	Fe: 8.6	D201 (PS–DVB matrix, quaternary ammonium functional group)	Chromate(VI)	[141]
Fe-Mn oxide	Mn: 9.4 Fe: 5.4	D201 (PS–DVB matrix, quaternary ammonium functional group)	Arsenic(III)	[136]
HZO	Zr: 11–13	Purolite A502P (PS–DVB matrix, quaternary ammonium functional group)	Arsenic(III&V)	[50]
HZO	15.2	D201 (PS–DVB matrix, quaternary ammonium functional group)	Phosphate and Fluoride	[11, 17]
HFO, HZO and CuO	Fe: 7.6 Zr: 6.7 Cu: 4.8	IRA-400 PS–(DVB matrix, quaternary ammonium functional group)	Phosphate	[142]
HFO and HFO–CuO	Fe: 4.5–6 Cu: –	Dow (PS–DVB matrix, Bis–picolylamine functional group)	Phosphate	[137]
HFO and HFO–Calcite sand	Fe: 16 Fe: 19.5	D201 (PS–DVB matrix, quaternary ammonium functional group)	Antimony(V)	[143]
nZVI	Fe: 13.5–14.3	D201 (PS–DVB matrix, quaternary ammonium functional group)	Nitrate	[135]
CuO	Cu: 11.9	Amberlite IRA-900 (PS–DVB matrix, quaternary ammonium functional group)	–	[130]

3. Development of nano-scale zirconium molybdate embedded anion exchange resin (ZMAE) for selective removal of phosphate an arsenic

3.1. Synthesis of the ZMAE

3.1.1. Materials and methods

3.1.1.1. Chemicals

All chemicals used in this study were purchased from Sigma-Aldrich. For synthesis of the ZMAE and zirconium molybdate (ZM) NPs, ammonium heptamolybdate tetrahydrate ($(NH_4)_6Mo_7O_{24}\cdot 4H_2O$) and zirconium(IV) oxychloride octahydrate ($ZrOCl_2\cdot 8H_2O$) were used as reagents. The anion exchange resin used in this study was a macroporous strong base anion exchange resin with polystyrene-divinylbenzene matrix (a Dowex™ Marathon™ MSA, 640 ± 50 μm). Prior to use, the resin was washed with hydrochloric acid solution, replacing the anionic form with chloride ion and then rinsed with ethanol for 24 h and dried at room temperature.

3.1.1.2. Synthesis of the ZMAE adsorbent

In this study, the ZMAE was fabricated with zirconium oxide embedded the AE (ZAE) for the comparison. To fabricate the ZMAE, 10 g of AE was added into 0.05

M of $(NH_4)_6Mo_7O_{24}$ solution with shaking for 6 h. This treated AE was immersed in 0.2 M of $ZrOCl_2$ solution (containing 5% of sodium chloride) with shaking for 24 h, in order to precipitate ZM NPs inside of the AE. This AE containing ZM NPs was washed by deionized water and ethanol. Finally, ZMAE was obtained after drying at 50 – 55°C.

The ZAE adsorbent only containing zirconium oxide not molybdate was synthesized, following the method reported in the previous studies [16, 17, 144]. The synthetic procedure similarly with the synthetic procedure of the ZMAE. The difference is that the hydrated zirconium oxide was precipitated with 5% NaOH solution instead of the immersing process into $(NH_4)_6Mo_7O_{24}$ solution.

3.1.1.3. Analytical methods

The content of Zr and Mo loaded in hybrid adsorbents (ZMAE and ZAE) were determined with ICP-AES after digesting with mixed acids (HCl, H_2SO_4, and $HClO_4$).

The morphology and surface characteristics of the ZMAE were analyzed with a scanning electron microscope (SEM, JSM-6700F, Jeol, Japan), high resolution transmission electron microscope (HR-TEM, JEM 3010, Jeol, Japan), high resolution X-ray diffractometer (XRD, D8 Discover, Bruker, Germany), Fourier Transform Infrared Spectroscopy (FT-IR 200, Jasco, Japan) , and X-ray

photoelectron spectroscope (XPS, Sigma Probe, ThermoVG, U.K.). The specific surface area and pore volume of the materials were measured with a BET analyzer (ASAP 2000, Micromeritics, USA). The pH_{pzc} (point of zero charge) of the ZMAE was determined by the drift method [145].

3.1.2. Characterizations of the ZMAE

Fig. 3-1 and Table 3-1 show the characterization of the ZMAE (HR-TEM (Fig. 3-1a), FTIR spectra (Fig. 3-1b)). As shown in Fig. 3-1a and Table 3-1, the ZM NPs was successfully dispersing inside the structure of the AE with low agglomeration, and their size was estimated about 8.9±1.7 nm (N = 50 particles). The ZM NPs having a poor crystalline in nature and the higher BET surface area of the ZMAE than that of the pristine AE (Table 3-1) are presumed to be favorable to phosphate adsorption (Fig. S3-1a) [16, 99].

The FTIR spectra of the ZMAE in contrast with the pristine AE shows some specific peaks characterizing zirconium molybdate embedded inside the ZMAE (Fig. 3-1b). For example, the peaks at the region of 800 – 950 cm^{-1} indicate the presence of molybdate group of loaded NPs [144, 146].

Also, the FTIR spectrum of the ZMAE was distinguished from the pristine AE by the peaks in range of 450 – 550 cm^{-1} indicating the stretching vibration of metal–oxygen (Zr–O and Mo–O) [144, 147].

The inherent characteristic of the quaternary ammonium functional in the AE support resin was observed in the vibration of the merging stretching hydrogen bonded hydroxyl groups and hydroxyl groups of adsorbed water (~ 3500 – 3300 cm^{-1}), C–H peak (3,000 cm^{-1}), and C=C peak (1,650 cm^{-1}) [130, 148]. These results indicate that the ZMAE possesses not only the specific properties of the loaded ZM NPs but also the anion exchange properties of R_4N^+ functional groups in the AE.

Furthermore, the presence of zirconium and molybdenum in the ZMAE was confirmed by ICP-AES with their weight percent found to be 4.3 and 14.7%, respectively (Table 1) and by XPS spectra (Fig. S3-1b) with their oxidation states of Zr^{+4} and Mo^{+6}, respectively.

As shown in Fig. 3-1b, the structure of polymer matrix and functional group in the ZMAE appeared to be very similar with that of the pristine AE. However, the surface area of the ZMAE containing the ZM NPs inside of the AE was increased from 22.2 to 28.3 m^2/g, which is explained by poor crystalline of the ZM NPs (Table 3.1).

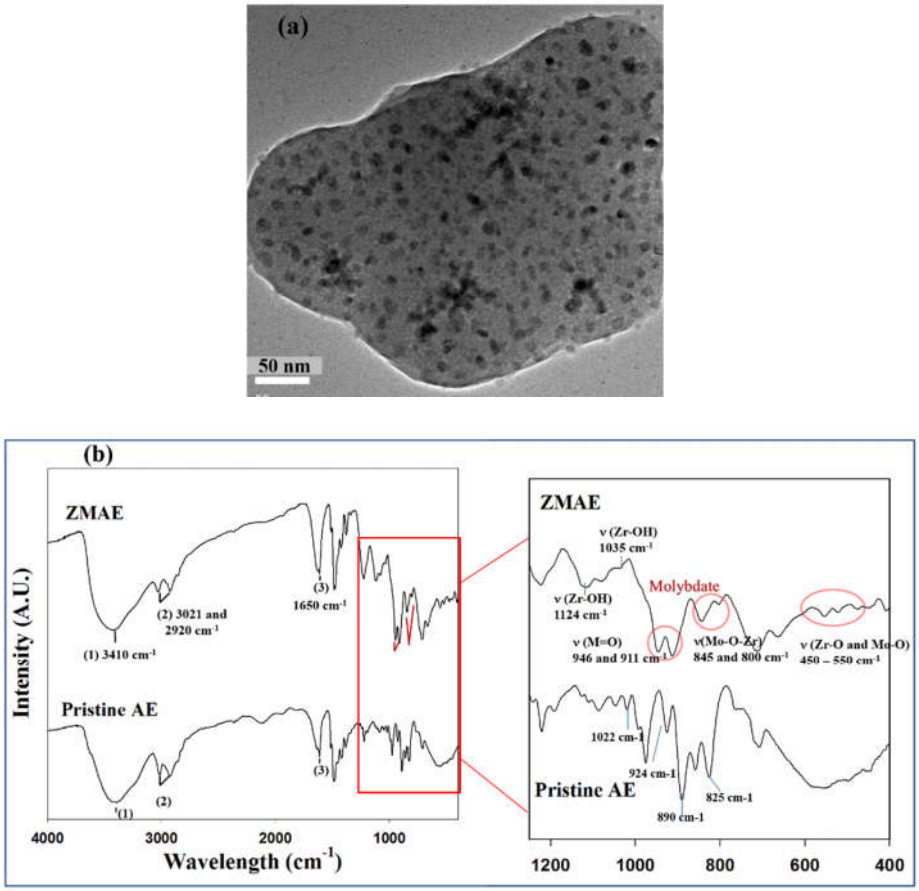

Fig. 3-1. Characteristics of the ZMAE: (a) HR-TEM image of the ZMAE showing zirconium molybdate nanoparticles (the ZM NPs, darker spots) dispersed in the AE support and (b) FTIR pattern of the ZMAE in comparison with the pristine AE.

Table 3-1. Summary of typical characteristics of the ZMAE in comparison with those of the pristine AE.

Adsorbent	ZMAE	Pristine AE
Matrix structure	Poly(styrene-divinylbenzene)	Poly(styrene-divinylbenzene)
Functional group	$R\text{-}N^{+}(CH_3)_3$	$R\text{-}N^{+}(CH_3)_3$
BET surface area (m^2/g)	28.3	22.2
Average pore diameter (nm)	30.2	32.5
Size of nanoparticle (nm)	8.9±1.7	
Metals content (% mass)	Zr: 4.3 Mo: 14.7	–
Mol ratio of Zr: Mo	1: 3.2	0

3.2. Study of selective phosphate adsorption on the ZMAE

3.2.1. Experiments and methods

3.2.1.1. Phosphate analysis

Phosphate concentration was analyzed by the molybdenum blue method with UV-Vis spectrometer (8453E UV/Vis, Agilent, USA) [149, 150]. The low concentration of phosphate was analyzed with an inductively coupled plasma – mass spectrometer (ICP-MS, Varian 820-MS, Varian, Australia).

3.2.1.2. Batch adsorption

Phosphate adsorption isotherm experiments with the ZMAE (0.5 g/L) were carried out in batch mode with shaking glass bottle (100 ml) containing 50 mL of phosphate solution (5 – 50 mg/L of $P\text{-}PO_4$) at initial pH 5.5 for 24 h (25^oC) and compared with the ZAE and the pristine AE. These experiments were conducted in the absence and presence of excess sulfate ion (5 mM).

Kinetic study with ZMAE (0.5 g/L) in the absence and presence of high sulfate (5 mM) was performed in phosphate solution (10 mg/L of $P\text{-}PO_4$ (0.31 mM), 200 mL) and compared with the pristine AE. At the predetermined time, 0.5 – 1.5 mL of this solution was withdrawn for measuring phosphate concentration.

To examine the pH effect for phosphate adsorption of the ZMAE, pH varied from 2 to 11. For maintaining pH, diluted solution of NaOH (or HCl) was added to batch at every 10-30 min.

3.2.1.3. Determination of selectivity coefficient of ZMAE

Selectivity of the ZMAE (0.5 g/L) toward phosphate ion relative to sulfate ion was examined in a mixed solutions of equal concentration of phosphate and sulfate ions at three different conditions (0.25, 0.75, and 2.0 mM) at pH 5 for 24 h (equilibrium condition) and compared with that of the pristine AE.

The selectivity coefficient ($S_{PO4/SO4}$) for either the ZMAE or the pristine AE was defined as a ratio of distribution coefficients of two respective ions between the solution and the adsorbent [151, 152].

$$S_{PO4/SO4} = \frac{D_{PO4}}{D_{SO4}}$$

where D_{PO4} or D_{SO4} (L of solution/g of adsorbent) is the distribution coefficient of phosphate or sulfate ion, respectively. The distribution coefficient (D) was defined as the following equation:

$$D_{PO4} = \frac{q_{e-PO4}}{C_{e-PO4}} \text{ or } D_{SO4} = \frac{q_{e-SO4}}{C_{e-SO4}}$$

where q_e (mmol/g) and C_e (mmol/L) are the adsorption capacity and concentration of phosphate or sulfate in the equilibrated solution, respectively.

3.2.1.4. Quantitative determination of the phosphate selectivity of the ZMAE

In order to evaluate the contribution of the ZM NPs to the selectivity of the ZMAE, the phosphate capacity of two different sites within the ZMAE ((i) the quaternary ammonium groups (R_4N^+) of the supported AE and (ii) the ZM NPs) were obtained in following ways separately with the assumption that the ZMAE have only these two different types of sites toward phosphate (TEM image in Fig. 3-1a).

Firstly, the ion exchange capacity (IEC, meq/g of dried resin) of the pristine AE and the supported AE in the ZMAE were measured by a conventional titration method under chloride from for the determining the number of R_4N^+ groups [153]. Assuming that the ion exchange behavior of the R_4N^+ of the AE resin inside the ZMAE is identical with that of the pristine AE resin, the fraction of the number of R_4N^+ functional groups of the AE inside the ZMAE over the pristine AE resin (*f*) (the mass fraction of the AE inside the ZMAE) was obtained from Equation (1). Note that the chloride adsorption on the ZM NPs was negligible (refer to Figure S3-2).

Secondly, the maximum phosphate capacity of the ZM NPs inside the ZMAE ($q_{m-NPs\ (\text{in ZMAE})}$) was estimated by subtracting the maximum phosphate capacity of the ZMAE ($q_{m-\text{ZMAE}}$) from the maximum phosphate capacity of the AE inside the ZMAE ($q_{m-AE\ (in\ \text{ZMAE})}$) in Equation (2). These values $q_{m-NPs\ (\text{in ZMAE})}$, $q_{m-\text{ZMAE}}$, and $q_{m-AE\ (in\ \text{ZMAE})}$ were obtained the values calculated from Langmuir isotherm model.

$$f = \frac{IEC\ of\ ZMAE}{IEC\ of\ pristine\ AE} \qquad (1)$$

$$q_{m-ZMAE} = q_{m-NPs\ (in\ ZMAE)} + q_{m-AE\ (in\ ZMAE)} \quad (2)$$

where,

- f: the fraction of the number of R_4N^+ functional groups of the ZMAE and the pristine AE
- IEC of the ZMAE: ion exchange capacity of ZMAE (meq/g)
- IEC of the pristine AE: ion exchange capacity of ZMAE (meq/g)
- $q_{m\text{-}ZMAE}$: the maximum phosphate capacity of the ZMAE $\left(\frac{\text{mg of P}}{\text{g of ZMAE}}\right)$
- $q_{m\text{-}NPs\ (in\ ZMAE)}$ and $q_{m\text{-}AE\ (in\ ZMAE)}$: the maximum phosphate capacity of the ZM NPs and supported AE in the ZMAE $\left(\frac{\text{mg of P}}{\text{g of ZMAE}}\right)$, respectively.

The $q_{m\text{-}NPs\ (in\ ZMAE)}$ can be obtained from Equation (2) since the $q_{m\text{-}ZMAE}$ can be determined experimentally.

On the other hand, in the presence of excess sulfate, their maximum phosphate capacity of the AE in ZMAE can be estimated from Equation (3).

$$q_{m-AE\ (in\ ZMAE)} = q_{m-ZMAE} - q_{m-NPs\ (in\ ZMAE)} \quad (3)$$

where, the additional "*" denotes (q_{m-ZMAE} , $q_{m-NPs\ (in\ ZMAE)}$ and $q_{m-AE\ (in\ ZMAE)}$) were defined for the condition of excessive SO_4, respectively. The value of $q^*_{m\text{-}ZMAE}$ (mg P/g ZMAE) was obtained by experiments.

3.2.1.5. Stability study of the ZMAE

In order to evaluate the stability of the ZMAE, concentrations of zirconium and molybdenum species which were leaked out from the ZMAE were measured in comparison with that of bare ZM NPs. For the stability test, the solution containing 1 g/L of the adsorbents was stirred for 48 h, varying pH range from 1 to 13. Then, the filtered supernatant solution was used for measuring zirconium and molybdenum concentration by ICP-AES. Note that the solution pH was maintained during the experiment.

3.2.1.6. Application of the ZMAE to Synthetic Water

To examine the feasibility of the ZMAE for practical application, the experiments of batch adsorption were conducted with two simulated acidic water (Mekong River) and wastewater (a typical effluent wastewater) with presence of phosphate and other coexisting ions, respectively.

The composition of Mekong River was as follows: 50 mg/L of Cl^-, 150 mg/L of CO_3^-, and 70 mg/L of SO_4^{2-} as competing ions, and 10 mg/L of P-PO_4 at pH 4.5 [40]. The typical effluent wastewater with excess presence of phosphate was as follows: 150 mg/L of Cl^-, 150 mg/L of CO_3^- and 200 mg/L of SO_4^{2-} with 10 mg/L of P-PO_4 at pH 4.5 [100].

In addition, fixed-bed column experiment was conducted with a glass column (12x50 mm in diameter and length) packed the ZMAE (5 mL) at constant temperature (25°C). The composition of feed water was as follows: phosphate (2.0 mg/L of $P\text{-}PO_4$) and other co-existing anions (110 mg/L of Cl^-, total carbonate 160 mg/L as $CaCO_3$, and 120 mg/L of SO_4^{2-} at pH 4.3 – 4.4) with the constant flow rate of 1.25 mL/mim (the empty bed contact time (EBCT) = 4 min).

3.2.2. Results and discussion

3.2.2.1. Selective phosphate adsorption of the ZMAE

Effective phosphate adsorption of the ZMAE

Fig. 3-2 shows the phosphate adsorption performance of the ZMAE in comparison with the pristine AE in terms of kinetic behavior (a), adsorption isotherm (b), and the effect of competing ion concentration (5 mM of sulfate) (c). As shown in Fig. 3-2a, in the absence of competing ion (sulfate ion), the difference of phosphate uptake between the ZMAE and the pristine AE is not much (64% removal for the ZMAE and 62% removal for the AE at 90 min). One difference is that the phosphate uptake of the ZMAE steadily occurred even up to 9 h, whereas the pristine AE was quickly reached to equilibrium. On the other hand, in the presence of excess sulfate ion (5 mM), the phosphate uptake of the pristine AE became negligible even after 9 h (3% removal), possibly due to the interfering effect from the presence of excess competing ion (sulfate ion, 5 mM) [138], whereas the ZMAE exhibited still much higher phosphate uptake capability (48% removal at 9 h). As a result, the ZMAE showed not only the higher phosphate removal efficiency in the absence of sulfate ion but also selective property in the presence of sulfate ion comparing with the performance of the AE.

Fig. 3-2b displays the phosphate adsorption isotherm of the ZMAE in comparison with the pristine AE. For whole range of phosphate concentration in Fig. 3-2b, the phosphate adsorption of the ZMAE was higher than that of the pristine AE regardless

of the presence of excess sulfate, as expected from the result of Fig. 3-2a. However, these difference between the ZMAE and the AE became more drastically in the presence of excess sulfate since phosphate adsorption of AE becomes negligible in the presence of sulfate. For example, the maximum adsorption capacity (q_m) values (obtained by Langmuir isotherm model) show that in case of the ZMAE, the q_m was decreased by 38%, (from 42.2 to 26.1 mg-P/g) in the presence of excess sulfate, however, the q_m of the pristine AE was significantly diminished by 96% (from 43.1 to 1.8 mg-P/g).

Fig. 3-2c shows the phosphate adsorption with respect to increasing sulfate concentration. A distinct phosphate uptake behavior between the ZMAE and pristine AE was observed with increasing concentration of sulfate. The ZMAE exhibited that its efficiency was decreased slowly with increasing sulfate concentration and maintained about 55% of removal even at extremely high concentration of sulfate. In contrast to the behavior of the ZMAE, the phosphate removal of the pristine AE was quickly dropped to almost zero.

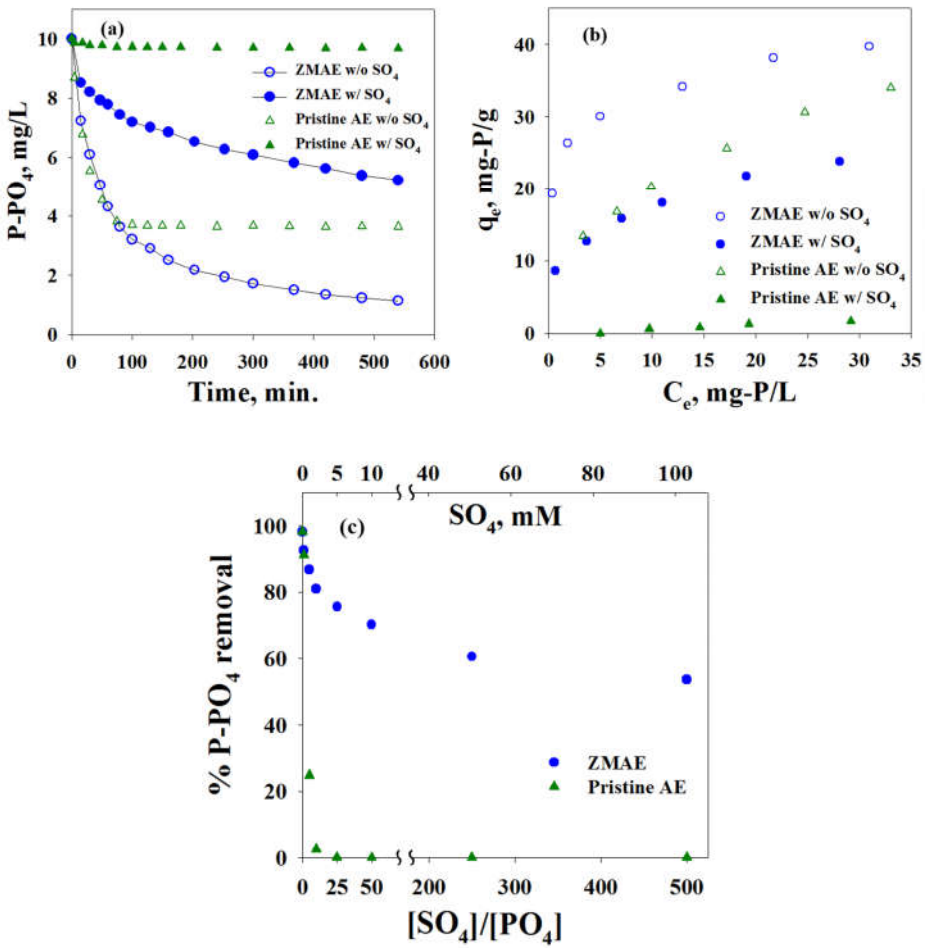

Fig. 3-2. Phosphate adsorption of the ZMAE compared with the pristine AE: (a) Phosphate uptake with time contact up to 9 h ([P-PO_4] = 10 mg/L, [adsorbent] = 0.5 g/L, [SO_4^{2-}] = 480 mg/L (5 mM), initial pH=5.5 at 25℃); (b) Equilibrium adsorption ([adsorbent] = 0.5 g/L, [SO_4^{2-}] = 480 mg/L (5 mM), initial pH=5.5 at 25℃, 24 h); and (c) Effect of sulfate concentration ([P-PO_4] = 6.2 mg/L (0.2 mM), initial pH=5.5 at 25℃, 24 h).

Selectivity coefficient of phosphate ion relative to sulfate ion

Table 3-2 shows the distribution coefficients of phosphate and sulfate (D_{PO4} and D_{SO4}) and the selectivity coefficients of the ZMAE for phosphate removal over sulfate ($S_{PO4/SO4}$) of ZMAE in comparison with the pristine AE, which were examined in the mixed solution of identical concentrations of phosphate and sulfate at pH 5 for 24 h (equilibrium condition). As shown in Table 3-2, D_{PO4} of the ZMAE was much higher than D_{SO4} regardless their initial concentrations, indicating that the phosphate adsorption of phosphate was much more favorable than sulfate adsorption. Furthermore, the difference between D_{SO4} and D_{PO4} was getting larger with increasing concentrations. Consequently, $S_{PO4/SO4}$ of the ZMAE was much higher than that of the pristine AE at three different conditions, which means the ZMAE had a selectivity for phosphate ion over sulfate ion. This implies that the ZMAE could be applied for separation and concentration of phosphate in sulfate mixed aqueous systems. Therefore, this result of selectivity compared between the ZMAE and pristine AE is experimentally explain the great performance of the ZMAE toward phosphate ion against with excessive sulfate ion as shown in Fig. 3-2.

Table 3-2. Selectivity coefficients (S) and distribution (D) of the ZMAE for phosphate adsorption over sulfate at equilibrium in comparison with the pristine AE.

Adsorbents	C_0 (mM)	$S_{PO4/SO4}$	D_{PO4} (L/g)	D_{SO4} (L/g)	$q_{e\text{-}SO4}$ (mmol/g)	$q_{e\text{-}PO4}$ (mmol/g)
ZMAE	0.25	**7.0**	10.9	1.56	0.219	0.425
	0.75	**4.7**	2.27	0.47	0.290	0.796
	2.0	**4.6**	0.91	0.19	0.358	1.248
Pristine AE	0.25	**0.086**	4.18	48.4	0.479	0.431
	0.75	**0.012**	0.17	14.1	1.314	0.120
	2.0	**0.038**	0.045	1.17	1.474	0.088

C_0: Initial concentration of phosphate and sulfate ion (mM)

$S_{PO4/SO4} = \frac{D_{PO4}}{D_{SO4}}$

Chemical characterization for selective phosphate adsorption of the ZMAE

Fig. 3-3 & 3-4 show the results of the XPS and FTIR analysis regarding the adsorption characteristics for selective phosphate removal, respectively. Fig. 3-3 presents the change of O1s and P2p XPS spectra of the ZMAE in terms of phosphate adsorption, showing a specific interaction between the loaded ZM NPs and phosphate ion.

As shown in Fig. 3-3a, the change in quantity of two overlapped peaks of the O1s XPS spectra at 531.9 and 530.5 eV corresponding to oxide oxygen (O^{2-}) and hydroxyl group (–OH) after the phosphate adsorption reveals a new bonding formation of the surface ZM NPs resulting from the interaction with phosphate species [9]. The initial content of –OH peak in O1s total peak was dropped after reacting with phosphate, corresponding to the relative increase of O^{2-} peak content. This change of O1s spectra means that the hydroxyl surface group of the ZM NPs in the hybrid is replaced by phosphate group during the adsorption process. On the other hand, the P2p XPS spectra of the ZMAE after the phosphate adsorption (Fig. 3-3b) appeared two main peaks at 133.8 and 132.8 eV corresponding to P^{5+} state, as a result of phosphate adsorption on the ZMAE which indicates that the specific interaction between phosphate and the surface of the ZM NPs [92, 154].

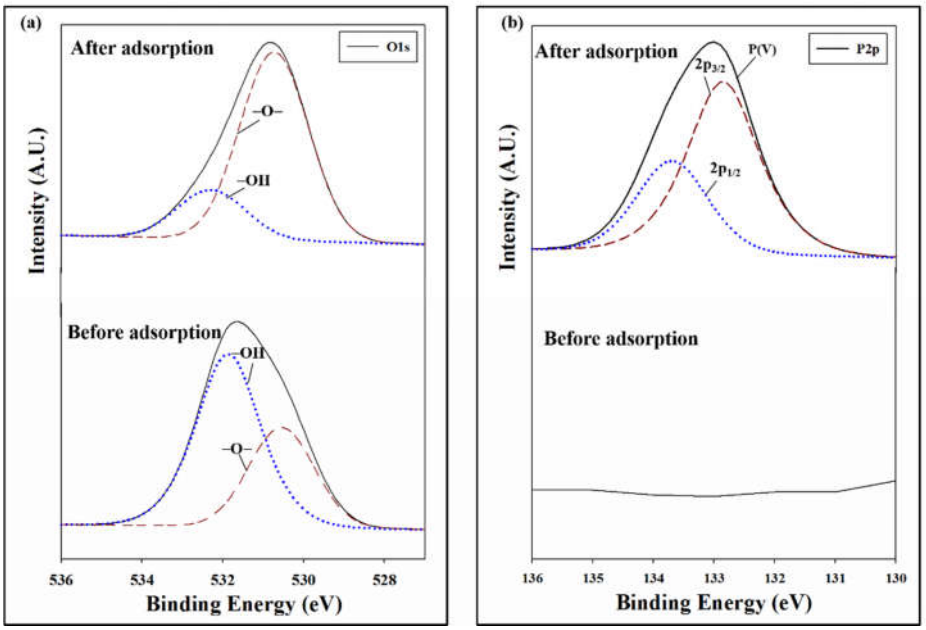

Fig. 3-3. O1s (a) and P2p (b) XPS spectra of the ZMAE in comparison between before and after phosphate adsorption.

Fig. 3-4 shows the FTIR spectra of the ZMAE in terms of phosphate adsorption. For example, as shown in Fig. 3-4, the adsorption of phosphate produces the slightly negative shift of stretching vibration of the molybdate component from the region of 800 – 946 cm^{-1} to 750 – 930 cm^{-1}, possibly resulting from a specific interaction between phosphate ion and molybdate component of the ZMAE forming a complex of phosphomolybdate [155, 156].

In addition, a new broad and intensive peak was observed at λ = 1052 cm^{-1}, indicating the asymmetry vibration of P–O bond of adsorbed phosphate after the phosphate adsorption [9]. The appearance of this peak confirms the certain surface adsorption of phosphate on the loaded NPs [9, 92] as demonstrated in the XPS analysis (Fig. 3-3).

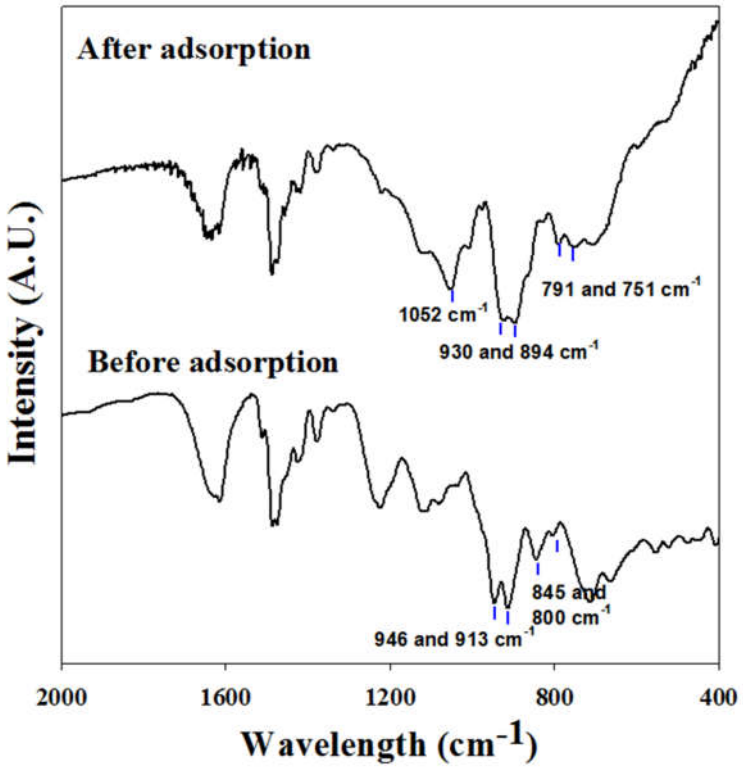

Fig. 3-4. FTIR spectra of the ZMAE in comparison between before and after the phosphate adsorption.

In addition to the specific interaction between phosphate and the ZM NPs of the ZMAE, the contribution of the ZM NPs to phosphate adsorption was observed also in aspect of kinetic (Fig. S3-3 and Table S3-1). Kinetic adsorption of phosphate on the ZMAE shows the diffusion mechanisms of phosphate consisting of two steps: (i) external surface diffusion (fast rate) where phosphate ion fast diffused and adsorbed to specific sites at the surface and (ii) intra-particle diffusion to the blocked space by NPs (low rate), supported by their diffusion rate (k_{1d} = 1.41 $mg.g^{-1}.min^{-1/2}$ and k_{2d} = 0.27 $mg.g^{-1}.min^{-1/2}$) (Fig. S3-3 and Table S3-1) [11, 17, 45]. In addition, the k_{2d} value of intra-particle diffusion seems to not be affected by the excess sulfate ion that was well consistent with the excellent selectivity loading NPs as of the discussed above.

3.2.2.2. Interpretation of the phosphate selectivity of the ZMAE

Fig. 3-5 shows the phosphate adsorption capacity distribution of the ZMAE compared with the pristine AE with or without the excessive sulfate. The maximum phosphate capacities of the pristine AE for each condition were already mentioned in Fig. 2 ($q_{m\text{-}AE}$ = 43.1 mg P/g and $q^*_{m\text{-}AE}$ = 1.8 mg P/g). As following the procedure described in the experimental section, the *f* value (Eq. (1)) was calculated as 0.56 ($q_{R4N+\ (in\ AE)}$ = 3.42 meq/g, $q_{R4N+\ (in\ ZMAE)}$ = 1.92 meq/g). From this, the supported AE of the ZMAE occupied around 56 wt% of the ZMAE, which has a phosphate capacity ($q_{m\text{-}AE\ (in\ ZMAE)}$) as 24.1 mg P/g. Therefore, the $q_{m\text{-}NPs\ (in\ ZMAE)}$ was estimated as 18.1 mg P/g which was 43% of $q_{m\text{-}ZMAE}$. In similar approach, the $q^*_{m\text{-}NPs\ (in\ ZMAE)}$ and $q^*_{m\text{-}AE\ (in\ ZMAE)}$ was calculated and found to be 25.1 and 1.0 mg P/g, respectively. Consequently, the ZM NPs can occupy about 96% of the selective adsorption capacity of the ZMAE.

It is interesting to note that the $q^*_{m\text{-}NPs\ (in\ ZMAE)}$ (25.1 mg P/g) in case of presence of sulfate ion was higher than the $q_{m\text{-}NPs\ (in\ ZMAE)}$ (25.1 mg P/g) in the absence of sulfate, even though the presence of sulfate ion was expected to reduce the adsorption efficiency of the ZMAE. This enhancement could be explained by that the excellent selectivity of the loaded ZM NPs toward phosphate ion (Fig. S3-4) could produce high density of phosphate surrounding which could permit the retention of phosphate ion in the supported AE inside the ZMAE by electrostatic interaction. This role of enhancement selectivity was consistent with the result in Fig. 3.2-c, where the role of supported AE to phosphate adsorption was slowly decreased

with further increasing sulfate concentration over the ratio $[SO_4]/[PO_4]$ of 10/1. The result infers the synergetic effect between the ZM NPs and the functional groups of the supported resin, resulting in the enhanced selective adsorption of phosphate although the further study will be required for exact explanation.

Furthermore, in the comparison between the ZMAE (4.3% Zr and 14.7% Mo) and ZAE (4.9 % of Zr and 0% of Mo), the ZMAE displayed much less decline of phosphate adsorption capacity under the presence of sulfate ion, which means the Mo species of ZM NPs showed high selective property rather than Zr species under the equilibrium phosphate adsorption condition (refer to Fig. S3-5).

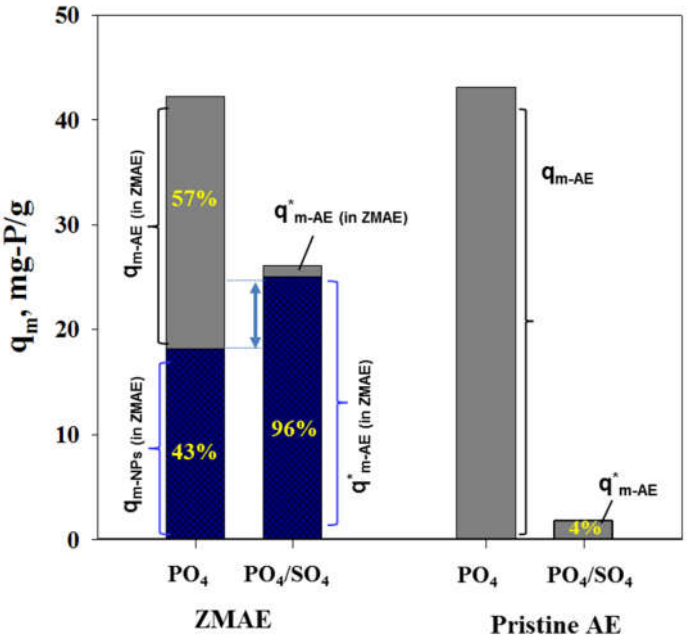

Fig. 3-5. The distributions of phosphate adsorption capacity for the ZMAE and the pristine AE with and without effect of sulfate (5 mM): The phosphate adsorption capacity of the ZM NPs (the zirconium molybdate nanoparticles, blue) and that of the quaternary ammonium functional group (R_4N^+) of polymer matrix (gray).

3.2.2.3. Effect of pH to the stability and phosphate adsorption of the ZMAE

Fig. 3-6 shows the pH effect on the stability and the phosphate adsorption of the ZMAE as the initial pH was maintained. As shown Fig. 3-6a, the release of Zr appeared to be negligible in a whole range of investigated pH, whereas the release of molybdenum became significant beyond pH 6, limiting the utilization of the ZMAE at higher pH more than 6. For example, the %release of molybdenum was found around 2.8% at pH 7 and 45.2% at pH 13, respectively. However, the release of Mo from the ZMAE at high pH was much lower than that of the ZM NPs (without supported resin) (Fig. S3-6). Therefore, the ZMAE should be proceeded at slightly acidic pH for the stability issue and also for achieving the maximum adsorption performance.

As the result of phosphate adsorption on the ZMAE (Fig. 3-6b), the phosphate adsorption capacity appears to be quite dependent upon pH conditions. The phosphate adsorption capacity is low at acidic condition of pH 2, whereas that maintained high around pH 3-5 and decrease again beyond pH 6. The specific reaction between phosphate and ZM NPs inside the ZMAE was playing a dominant role of a phosphate removal because phosphate ion has a neutral form at pH 2 (pk_{a1} = 2.15). The high capacity in the range of pH 3~5 is explained by that the increased number of monovalent phosphate anions, $H_2PO_4^-$, (pk_{a1} and pK_{a2} of phosphoric acid are 2.15 and 7.20, respectively [157]), leading to the enhanced electrostatic attraction between phosphate and R_4N^+ functional groups of the ZMAE with the favorable complexation of molybdate and phosphate at lower pH condition [107, 158]. Similar

effect of pH was also observed in previous studies for adsorption of phosphate on only zirconium oxide NPs [9, 157]. Meanwhile, phosphate capacity was decreased as pH increased over than 5 even though the amount of the negatively charged phosphate was increased due to unfavorable complexation reaction.

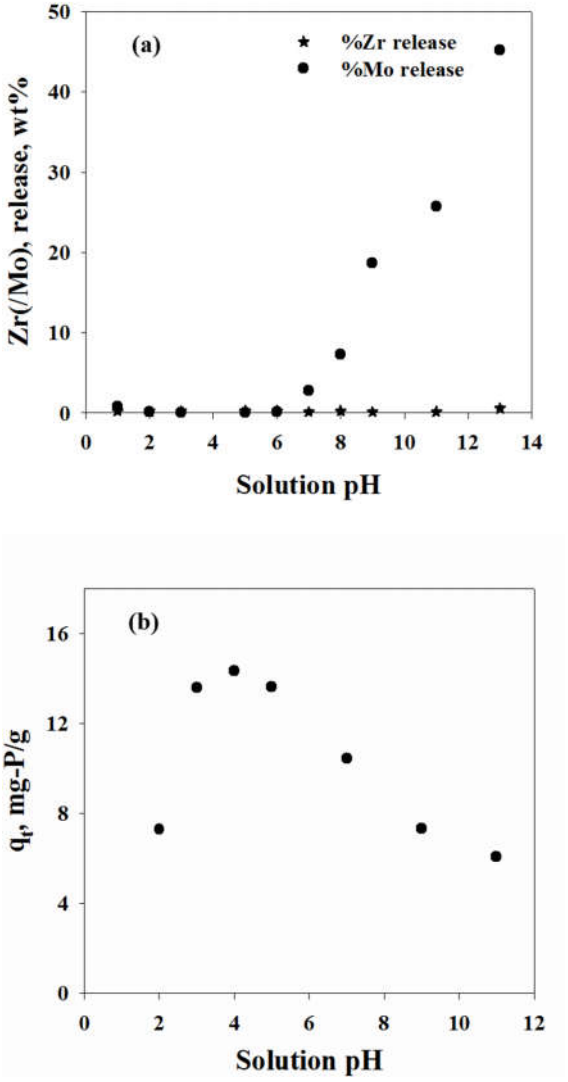

Fig. 3-6. Effect of pH to the phosphate adsorption and the stability of the ZMAE. For the phosphate adsorption: [P-PO_4] = 10 mg/L, [adsorbent] = 0.5 g/L, 4.5 h. For the stability test: [adsorbent] = 1 g/L, 24 h. Note that the solution pH was maintained during the reaction.

3.2.2.4. Application of the ZMAE for phosphate removal in synthetic water

The batch and column adsorption experiments in slightly acidic pH were carried out to examine the feasibility of the ZMAE for potential application, and presented in comparison with the pristine AE (Fig. 3-7).

As shown in Fig. 3-7a, the ZMAE exhibited the excellent effective removal of phosphate for all cases with maintaining phosphate adsorption performance in comparison with the pristine AE. The q_e values of the ZMAE were about 15 and 13 mg P/g for the synthetic Mekong river water and effluent wastewater, respectively; however, the pristine AE seem to be failed for removal of phosphate. If Fig. 3-2 shows the selectivity of the ZMAE toward phosphate ion with the effect of only sulfate ion, the Fig. 3-7a exhibits capability of potential application of the ZMAE in selective removal of phosphate in effect of multi-anions commonly occurring in water/wastewater.

The column run of the ZMAE by feeding a synthetic water was conducted and presented with the results of the pristine AE for the comparison in Fig. 3-7b. Obviously, ZMAE showed an extremely effective removal of phosphate compared with the pristine AE. For instance, ZMAE can achieved about 4400 BVs of total volume of effective treatment (below the allowance of phosphate concentration of discharging water (0.5 mg·P-PO_4/L)), whereas only about 70 BVs was achieved for the pristine AE.

These results promise a potential of the ZMAE for field application of selective treatment of phosphate from various waters.

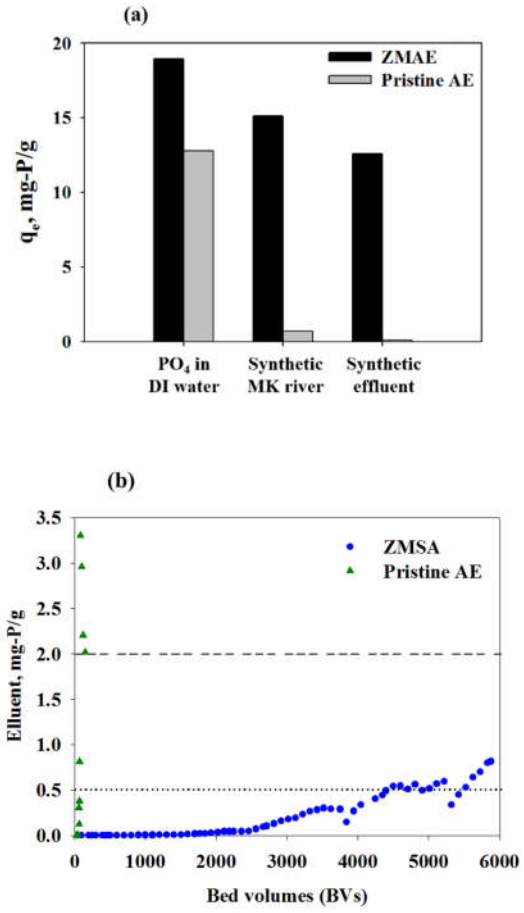

Fig. 3-7. Phosphate removal of ZMAE compared with pristine AE: (a) Batch experiment using synthetic water modelled to Mekong river water ($[Cl^-]$ = 50 mg/L, $[HCO_3^-]$ = 150 mg/L and $[SO_4^{2-}]$ = 70 mg/L) and effluent wastewater ($[Cl^-] = [HCO_3^-]$ = 150 mg/L and $[SO_4^{2-}]$ = 200 mg/L) at pH 4.5 ($[P\text{-}PO_4]$ = 10 mg/L, [adsorbent] = 0.5 g/L, 24 h); (b) Fixed bed column experiment using synthetic water (EBCT (empty bed contact time) 4 mL, $[P\text{-}PO_4]$ = 2.0 mg/L, $[SO_4^{2-}]$ = 120 mg/L, $[Cl^-]$ 110 mg/L, total carbonate 100 mg/L as $CaCO_3$, pH 4.3 – 4.4).

3.2.3. Conclusion

It was successfully fabricated a hybrid ZMAE, which is nanoscale zirconium molybdate embedded a commercial macroporous anion exchange resin. The ZMAE showed excellent selectivity toward phosphate, which much superior to that of the ZAE or pristine AE, supported by specific interaction of phosphate and molybdate component of the loaded ZM NPs. Although the pristine AE exhibited only 4% of for selective removal of phosphate in presence of excessive sulfate, the selective adsorption of phosphate on the ZMAE can achieved up to 62% of the capacity, which was supported with the selectivity coefficient of the ZMAE toward phosphate ion relative to sulfate ion about 100 times higher than the pristine AE. The ZM NPs played in a key role of determining the selectivity of the ZMAE (69–96% of selective capacity). Application of the ZMAE for removal of phosphate from synthetic water showed a great potential of treatment with over 4400 BVs of effective treatment capacity (from 2 mg/L $P\text{-}PO_4$ to below 0.5 mg/L $P\text{-}PO_4$), whereas that of the pristine AE was even lower than 70 BVs.

3.3. Study of selective arsenic adsorption on the ZMAE

3.3.1. Experiments and methods

3.3.1.1. Synthesis of the ZMAE adsorbent

The ZMAE was fabricated as the procedure described in the part 3.1.1.2. After the reaction with $ZrOCl_2$ solution step, the resultant resin was air dried instead of directly washed with water/ethanol as the procedure in part 3.1.1.2 in order to increase the loaded zirconium content. As the result, the weight percentage of Zr and Mo were found to be 7. 1 and 11.6 %, respectively. The characteristics of the ZMAE in this part showed the similar results with the part 3.1.2 (data not shown).

3.3.1.2. Analytical method

The arsenic concentration was determined by the molybdenum blue method measured by UV/Vis spectrometer (Agilent 8453, Agilent, America) [150]. Trace arsenic concentration was analyzed by an inductively coupled plasma – mass spectrometer (ICP-MS, Varian 820-MS, Varian, Australia). Other analysis for characterizing the ZMAE was described in part 3.1.3.

3.3.1.3. Batch adsorption experiments

Effect of pH to the arsenic adsorption of the ZMAE was conducted at the pH range of 3 and 11 in shaking 50 mL plastic tubes containing 40 mL solution of As(V) (10 mg/L) and adsorbent (0.5 g/L) (in NaCl 1 mM matrix) at 25^{o}C for about 6 h. The solution pH was adjusted using diluted solution of NaOH and HCl.

Arsenic adsorption isotherm of the ZMAE (0.5 mg/L) was carried out with varying the concentration of arsenic from 10 to 60 mg/L at initial pH about 6.0 for 24 h and compared with the ZAE and pristine AE. The experiments were performed in the absence and presence of excessive sulfate ion (5 mM).

Effect of coexisting ions concentration to the As(V) adsorption of the ZMAE compared with pristine AE were evaluated using two typical momo- and di-valent anions, nitrate and sulfate ions, at initial pH about 6.0. The concentration of nitrate and sulfate ions were increased from 0 to 100 mM.

For adsorption kinetic, every 0.5 – 1.5 mL of 200 mL adsorption solution (containing 10 mg/L of As(V) and 0.5 g/L adsorbent) in the absence and presence of high sulfate concentration were withdrawn at a selected interval of time for the analysis of adsorbed arsenic.

3.3.1.4. Interpretation procedure of the selective arsenic adsorption of the ZMAE

Following to the assumption and calculation in part 3.2.1.4, the maximum arsenic capacity of the ZM NPs ($q_{m-NPs\ (\text{in ZMAE})}$) and the supported AE($q_{m-AE\ (in\ \text{ZMAE})}$) in the ZMAE as well as their capacities in presence of excessive sulfate ion ($q_{m-NPs\ (in\ ZMAE)}$ and $q_{m-AE\ (in\ ZMAE)}$) were calculated as following equations:

$$f = \frac{IEC\ of\ ZMAE}{IEC\ of\ pristine\ AE} \quad (1)$$

$$q_{m-\text{ZMAE}} = q_{m-NPs\ (\text{in ZMAE})} + q_{m-AE\ (in\ \text{ZMAE})} \quad (2)$$

$$q_{m-AE\ (in\ ZMAE)} = q_{m-ZMAE} - q_{m-NPs\ (\text{in ZMAE})} \quad (3)$$

3.3.1.5. Fixed-bed column experiments

The column adsorption experiment was conducted in a glass column (10 mm x 150 mm) packed with 5 mL of ZMAE. The pristine AE was also involved for comparison. Synthetic water containing 0.1 mg/L of As(V) and other anions (120 mg/L of SO_4^{2-}, 120 mg/L of Cl^-, 150 mg/L of HCO_3^- and 12 mg/L of NO_3^-) was pumped down through the column with the constant flow rate of 1.25 mL/min (the empty bed contact time (EBCT) = 4 min) at 25ºC. The synthesis water was acidified to pH about 4.5 in order to satisfy the working pH of the ZMAE.

3.3.2. Results and discussion

3.3.2.1. Enhanced arsenic adsorption of the ZMAE

Selective adsorption of arsenic

The selective adsorption of arsenic on the ZMAE was examined in presence of two representative coexisting ions (mono- and di-valent anions) in water, nitrate ad sulfate ions. Fig. 3-8 shows the effect of increasing concentration of nitrate and sulfate to the As(V) adsorption on ZMAE compared with the pristine AE. As shown, the arsenic removal of ZMAE was slowly decreased as linearly increasing either nitrate or sulfate ion. Meanwhile, the arsenic adsorption of the pristine AE was quickly dropped to zero corresponding to the increase of the competing anions. For example, the efficiency of the ZMAE seems to be retained up to the ratio $[SO_4^{2-}]/[As]$ or $[NO_3^-]/[As]$ of 150/1, whereas that of the pristine AE was almost lost at the ratio $[SO_4^{2-}]/[As]$ of 15:1 and $[NO_3^-]/[As]$ of 150/1, respectively. It is clearly seen that the much larger effect of sulfate than nitrate to the As(V) adsorption on the pristine AE was almost compensated for the case of the ZMAE, which could be due to the ZM NPs attributing to the specific interaction toward arsenate ion but not nitrate nor sulfate. These results indicate the great enhancement of selective adsorption of the ZMAE toward arsenic compared with pristine AE.

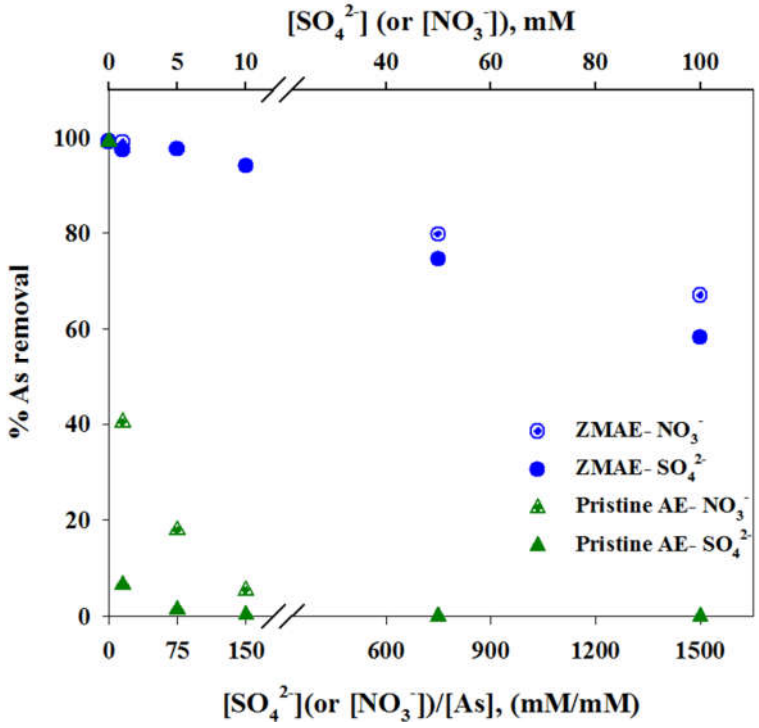

Fig. 3-8. Effect of competing ions to equilibrium As(V) adsorption on the ZMAE compared with pristine AE. [As(V)] 10 mg/L, adsorbent dose 0.5 g/L, pH 6.0, 25 ^{o}C, 24 h.

Equilibrium study: Role of loaded zirconium molybdate NPs

Fig. 3-9 shows the As(V) adsorption of the ZMAE at equilibrium condition (24 h) in comparison with the ZAE (8.2% Zr and 0% Mo) and pristine AE in absence and presence of excessive sulfate (5 mM), respectively. As the results, the ZMAE exhibited in similar adsorption capacity with the ZAE and pristine AE in the single arsenate solution. Nevertheless, in the presence of excessive sulfate ion, the distinct performance among the adsorbents became drastically due to the negligible adsorption of arsenic on AE. Indeed, the ZMAE exhibited much higher adsorption capacity than the ZAE in the whole range of investigated arsenic concentration.

The adsorption data of three adsorbents were examined to both Langmuir and Freundlich isotherm non-linear models and their parameters were summarized in Table 3-3. As the results, the Freundlich model well demonstrated the isotherm adsorption of arsenic on three adsorbents in the absence of sulfate ($R^2 > 0.99$), which was possible due to the heterogeneous property of the adsorbents. The larger affinity K_F value of both hybrid ZMAE and ZAE than pristine AE confirms the important role of loading NPs in enhanced specific affinity toward arsenic. On the other hand, in the presence of excessive sulfate ion, the Langmuir model ($R^2 \geq 0.99$) was better than Freundlich model ($R^2 < 0.99$) to demonstrate the adsorption of arsenic, which relies on the monolayer adsorption of arsenic on the loaded NPs due to the negligible adsorption of arsenic on the AE. In fact, the maximum capacity of selective arsenic adsorption calculated by the Langmuir equation for the ZMAE (47.6 mg/g) was more

than two times higher than the ZAE (20.1 mg/g), which means that the Mo species of ZM NPs showed high selective property rather than Zr species under the equilibrium arsenic adsorption condition. Thus, the role of Mo species of ZM NPs toward arsenic adsorption seems to be similar to the case of phosphate adsorption described in the part 3.2.

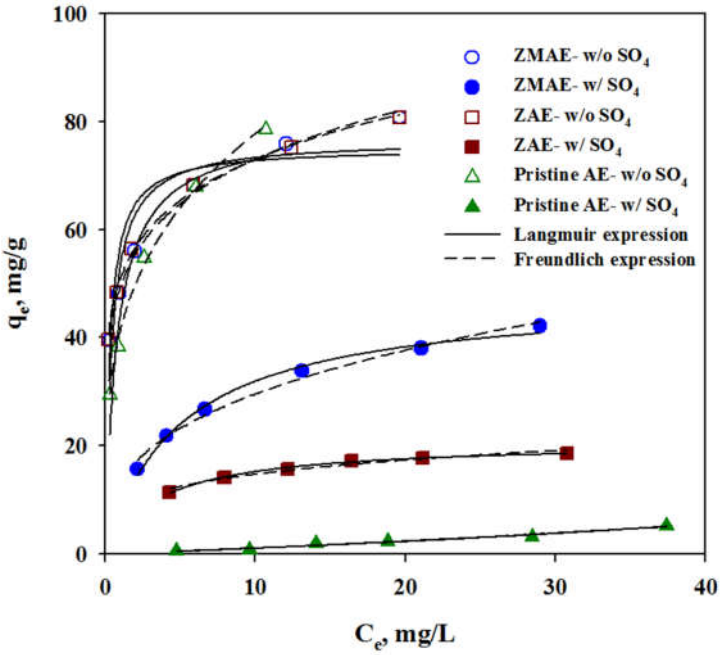

Fig. 3-9. Comparison of arsenic equilibrium adsorption among adsorbents ZMAE, ZAE and pristine AE) in absence and presence of sulfate ion. Adsorbent dose 0.5 g/L, [SO_4] 500 mg/L, pH 6, 25 ^oC, 24 h.

Table 3-3. Langmuir and Freundlich isotherm parameters for As(V) adsorption of nanoscale zirconium molybdate embedded anion exchange resin (ZMAE) compared with nanoscale zirconium oxide embedded anion exchange resin (ZAE) and pristine anion exchange resin (pristine AE).

	ZMAE		**ZAE**		**Pristine AE**	
	w/o SO_4	w/ SO_4	w/o SO_4	w/ SO_4	w/o SO_4	w/ SO_4
Langmuir						
q_m (mg/g)	76.6	47.6	75.1	20.7	78.8	6.96
K_L (L/mg)	2.27	0.20	3.09	0.278	1.24	0.012
R^2	0.880	0.990	0.855	0.996	0.926	0.966
Freundlich						
K_F (mg/g) $(mg/L)^{-1/n}$	49.2	13.2	50.7	8.53	40.9	0.033
1/n	0.172	0.348	0.158	0.236	0.279	1.42
R^2	0.996	0.988	0.997	0.960	0.998	0.996

Kinetic study

Fig. 3-10 shows the uptake of As(V) on the ZMAE versus contact time compared with the pristine AE in the absence and presence of excessive sulfate ion. Be consistent with the results in Fig. 3-9, the arsenic uptake of the ZMAE showed clearly the role of ZM NPs for selective removal of arsenic. For instance, the ZMAE still significantly adsorbed in the effect of sulfate ion, which was in contrast with the pristine AE where almost without arsenic was adsorbed (Fig. 3-10b) although the pristine AE was effectively adsorb arsenic in free sulfate effect even faster adsorption rate than the ZMAE (Fig. 3-10a).

The uptake of arsenic on the ZMAE compared with the pristine AE were examined to the first and second pseudo order models and their results were summarized in Table 3-4. As the results, both pseudo–first and pseudo–second order equations well expressed for the arsenic adsorption on both adsorbents, resulted by their high coefficient values ($R^2 \geq 0.99$) and the consistent values of adsorption capacity (q_e) between the theory and experiment. In details, the lower uptake of arsenic for ZMAE in generally was observed than for the pristine AE because the loaded NPs would inevitably prevent the diffusion of arsenic into the active pore-sites of the host (Table 3-1) [11]. In addition, arsenic may require longer time to form complexation with the loaded NPs than ion exchange with the host.

The diffusion of arsenic to ZMAE was found to be consisted of two steps of diffusion (Table 3-4): (i) the first step was proposed to the external surface

adsorption of arsenate ion that fast diffused to and adsorbed on the specific adsorption sites of the surface (k_{d1} = 1.66 mg/g.min$^{-1/2}$); (ii) the second step was in lower rate relating intra-particle diffusion of arsenate to inner space of loading NPs (k_{d1} = 0.52 mg/g.min$^{-1/2}$) [136]. Nevertheless, in the presence of sulfate ion, the diffusion of arsenic on the ZMAE seemed to be in one step of process, where the diffusion rate was equal to the second step of intra-particle diffusion rate in case of without effect of sulfate (0.51 and 0.52 mg/g.min$^{-1/2}$, respectively), because the surface functional group of the supported AE was covered by sulfate ion.

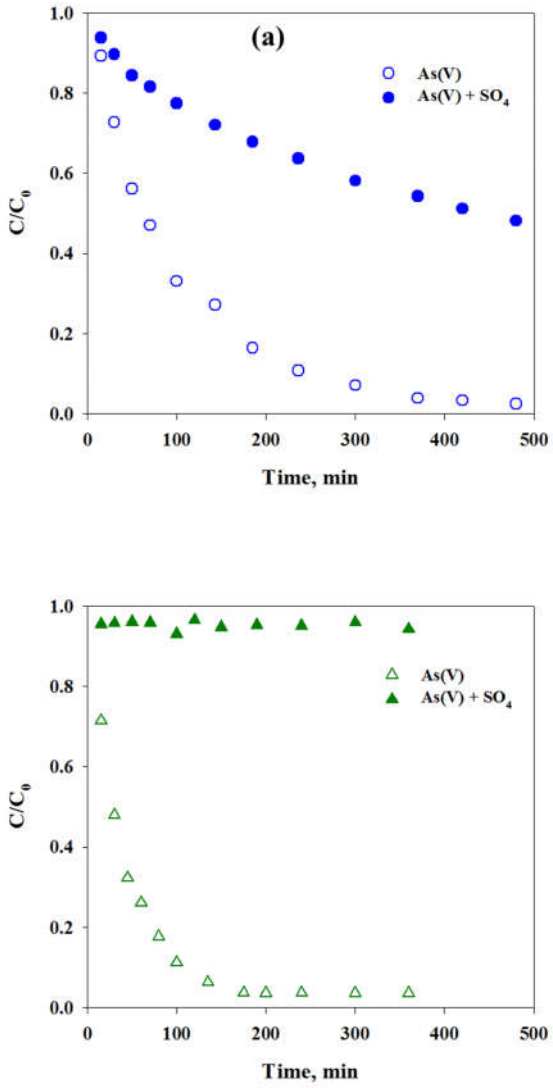

Fig. 3-10. Comparison of uptake of arsenic versus time contact in absence and presence of sulfate ion between: (a) ZMAE and (b) pristine AE. [As(V)] 10 mg/L, adsorbent dose 0.5 g/L, [SO_4] 5 mM (480 mg/L), pH 6, 25 ^oC, 24 h.

Table 3-4. Kinetic parameters of arsenic adsorption on nanoscale zirconium molybdate embedded anion exchange resin (ZMAE) compared with pristine anion exchange (AE) resin.

Adsorbents	q_e (mg/g) exp.	Pseudo-first-order			Pseudo-second-order			Intra-particle diffusion model			
		$k_1 x 10^2$ (min)	q_e (mg/g)	R^2	$k_2 x 10^3$ (min)	q_e (mg/g)	R^2	k_{1d} (mg/(g.min$^{1/2}$))	R_1^2	k_{2d} (mg/(g.min$^{1/2}$))	R_2^2
ZMAE[a]	19.9	0.90	17.5	0.996	0.51	23.3	0.997	1.66	0.996	0.52	0.894
ZMAE[b]	15.5	0.21	13.9	0.993	0.36	14.1	0.986	k_d = 0.51 and R^2 = 0.998			
Pristine AE[a]	19.9	2.59	19.9	0.996	1.03	24.2	0.997	–	–	–	–

[a]In the absence of sulfate

[b]In the presence of sulfate 5 mM

3.3.2.2. Interpretation of the arsenic selectivity of the ZMAE

Fig. 3-11 shows the distribution of arsenic adsorption capacities within the ZMAE evaluated in the absence and presence of excess competing ion (sulfate ion) in comparison with the pristine AE. Note, the adsorption capacities of the pristine AE were drawn from the results of isotherm part. As shown, the maximum adsorption capacity of the ZM NPs ($q_{m-NPs\,(in\,ZMAE)}$) and supported AE ($q_{m-AE\,(in\,ZMAE)}$) of the ZMAE were found to be 32.5 and 44.1 mg/g, respectively. Thus, the ZM NPs and supported AE contributed about 43% and 57% of arsenic capacity of the ZMAE in the absence of sulfate ion, respectively. On the other hand, in the presence of excessive sulfate ion, the values ($q_{\,m-NPs\,(in\,ZMAE)}$) and ($q_{\,m-AE\,(in\,ZMAE)}$) were found to be 43.8 and 3.8 mg/g, respectively. Consequently, the ZM NPs could contributed up to 92% of the selective capacity of the ZMAE.

In similar to the case of phosphate adsorption in part 3.2, the synergy between the ZM NPs and the supported AE in the ZMAE resulted in the enhancement of the selective adsorption of the ZM NPs (32.5 mg/g and 43.8 mg/g in the absence and presence of competing ion, respectively). Therefore, the ZM NPs not only exhibited itself excellent selectivity toward arsenic but also contributed to enhance the selective adsorption of the supported AE.

Overall, the ZM NPs played in a key role of selective adsorption of the ZMAE toward arsenic, where it could contributed up to 92% of the selective capacity of the ZMAE, although the further researches will be required for exact explanation.

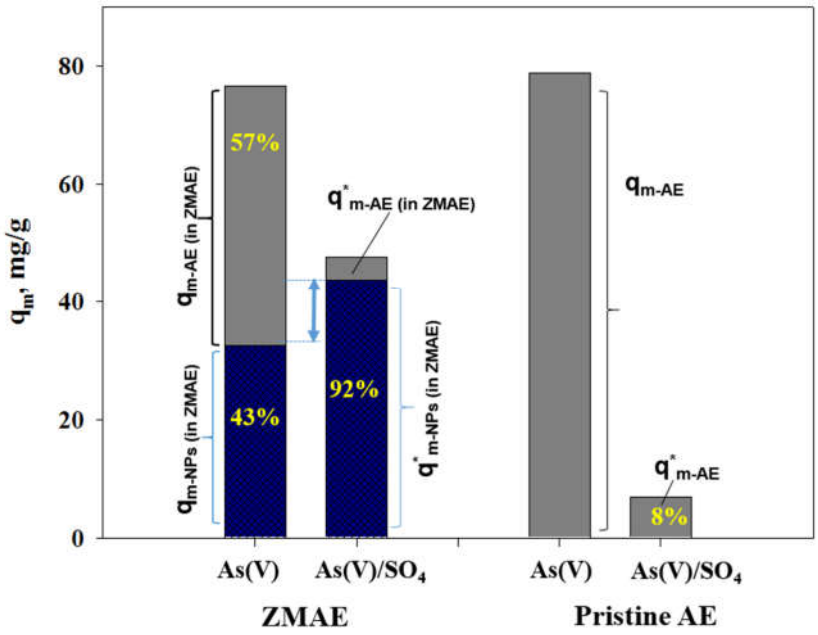

Fig. 3-11. Bar graph for schematizing the selective arsenic adsorption insights of the ZMAE compared with the pristine AE over excessive sulfate (5 mM).

3.3.2.3. Effect of pH to the arsenic adsorption

Fig. 3-12 shows the effect of solution pH to the As(V) adsorption on ZMAE was examined in presence of chloride ion (5 mM). As shown, arsenic removal by ZMAE was optimal and stable in a wide range of pH from 3 to 9 but then, reduced at pH 11. This result indicates that the adsorption of arsenic on the ZMAE was independent to the charged level of arsenate anionic forms (($H_2AsO_4^-$ and $HAsO_4^{2-}$). This pH dependence could be explained by that the specific reaction between arsenic and ZM NPs inside the ZMAE was playing a dominant role of a arsenic removal. Similar pH dependence was reported in separation of arsenic by flotation method using molybdate oxoanion [107].

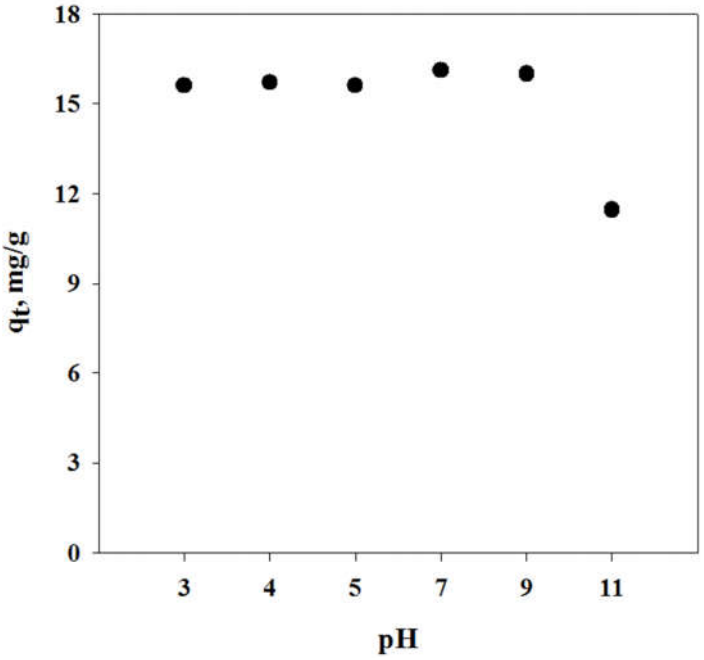

Fig. 3-12. Effect of solution pH to arsenate adsorption on ZMAE. [As(V)] 10 mg/L, adsorbent dose 0.5 g/L, [Cl^-] matrix 5 mM (178 mg/L), 5.5 h.

3.3.2.4. Fixed-bed column adsorption

To access the possibility of potential application of the ZMAE for arsenic removal from water and groundwater, the column run of the ZMAE with a synthetic solution containing arsenic and other competing ions (Cl^-, NO_3^-, SO_4^{2-}, HCO_3^-) was conducted. Fig. 3-13 presents the adsorption profile of column test for the ZMAE compared with the pristine AE. The results show that the effective volume treatment of the ZMAE could achieved about 9300 BVs as the arsenic was reduced from 0.1 mg/L to below 0.01 mg/L (the allowance of arsenic concentration in drinking water recommended by WHO), which was dramatically superior to that of the pristine AE (only about 300 BVs). The results promise potential application of the ZMAE for effective treatment of arsenic in polluted water.

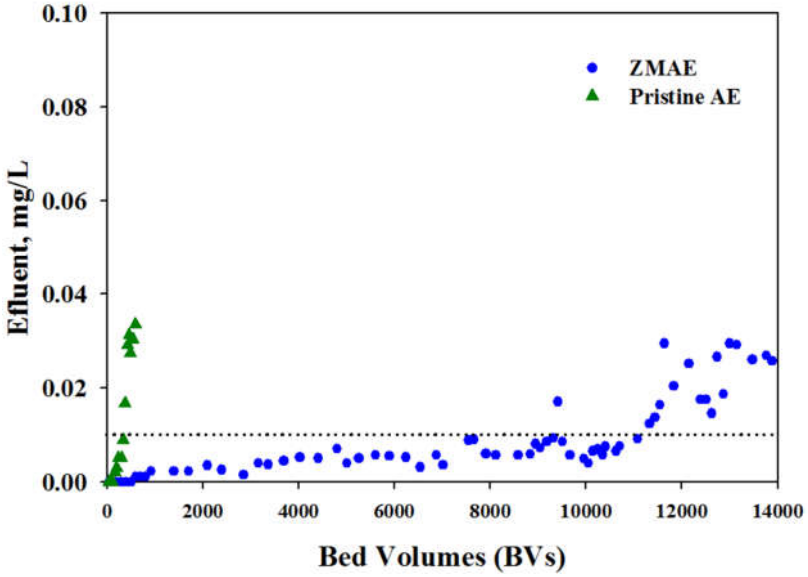

Fig. 3-13. Column adsorption of the ZMAE compared with pristine AE for arsenic removal from synthetic water (EBCT 4 min, As(V) 0.1 mg/L, SO_4^{2-} 120 mg/L, Cl^- 120 mg/L, NO_3^- 12 mg/L, total carbonate 140 mg/L as $CaCO_3$, pH ~ 4.5).

3.3.3. Conclusion

In this study, the ZMAE exhibited excellent selectivity toward arsenate ion in presence of competing anions (nitrate and sulfate), which superior to the ZAE or pristine AE. It was found that up to 62% capacity of the ZMAE served the selective adsorption of arsenate in presence of excessive sulfate ion which is attributed to the role of ZM NPs, whereas that of the pristine AE was only 8%. The selectivity insight of the ZMAE for arsenate ion was examined and schematized. The column adsorption of the ZMAE using synthetic water showed a great potential of the ZMAE for arsenic treatment in water and waste water, where the effective volume capacity can be achieved over 9000 BVs although the pristine AE showed only ~ 300 BVs of effective treatment.

4. Synthesis of Hydrated Zirconium Oxide Embedded Anion Exchange Resin for Selective Removal of Phosphate

4.1. Introduction

As the results in part 3, the ZMAE showed excellent performances toward both phosphate and arsenate adsorption. However, as shown in Fig. 3-6, there was only the problem of the Mo leaching as the pH increased over than 6. Thus, the ZMAE should be suitable to conduct to treat slightly acidic wastewater, whereas a pre-acidifying step is required for most of natural water/groundwater at neutral pH before the treatment [13]. It is, therefore, highly needed to develop a selective adsorbent for phosphate and arsenic removal which could be applied at neutral pH or higher.

Recently, the hybrid hydrated zirconium oxide (without molybdate) embedded AE (ZAE) has been reported with high stability against with acid/base and organic substances [18]. Also, the ZAE showed compatible phosphate (and arsenic) adsorption efficiency to others [50]. As shown in literature, most of current studies have fabricated the ZAE by directly dispersing of zirconium salt (such as $ZrOCl_2 \cdot 8H_2O$ in acidic solution containing ethanol) within the AE matrix and follow with *in situ* precipitating zirconium hydroxide within resin using a solution of NaOH. This procedure has major challenge of loading zirconium due to the Donnan

exclusion between the fixed positively charged of the resin and the cationic form of $[Zr_4(OH)_8(OH_2)_{16}]^{8+}$ [17, 18, 48, 159]. In order to achieve the ZAE with a desired Zr content, it is usually required multiple repetitive cycles of the synthesis procedure, which was well demonstrated in the US Patent 9120093 [19]. This certainly require time, cost and, consequently waste a lot of toxic chemicals.

Furthermore, although the loaded HZO NPs was thought to have an important role for the selective adsorption of phosphate using this type of hybrid adsorbent, no systematic investigation how effect of loaded metal content to the adsorption performance and selectivity have been reported. Most studies approached at a certain content of Zr obtained in randomly obtained from the synthesis, whereas the selective adsorption of varying content of Zr in presence of co-existing anions were not considered. This leads to insufficiently understanding the selective insights this type of hybrid adsorbent for the development of an effective and cost consuming adsorbent for phosphate removal.

Therefore, this study aims at introducing a new method for fabricating a similar hybrid ZAE with effectively dispersing zirconium ion into the AE matrix. A series of the ZAE adsorbents with different Zr content were fabricated and examined for the phosphate adsorption performance and selectivity. From this, the effect of Zr content to the selective adsorption of phosphate of the ZAE was examined using both batch and fixed-bed column experiments.

4.2. Experiments

4.2.1. Materials and Chemicals

Refer in part 3.1.1.1.

4.2.2. Preparation of ZAE

The method for fabrication of HZO embedded AE was well demonstrated in literature [17, 159]. However, based on this method, the precursor zirconium ion ($[Zr_4(OH)_8(OH_2)_{16}]^{8+}$) is hard to migrated into the AE because of the Donnan exclusion of fixed positively charged quaternary ammonium functional groups of the AE. Therefore, this part introduced a new approach for dispersing zirconium ion within the AE porous structure, which is a molybdate intermediate method (MIM).

The fabrication of ZAE by the MIM comprises of three steps of process as follow. Firstly, 10 g AE was added into 100 mL of solution ammonium heptamolybdate 0.1 M and continuously shaken for 4 h at 25^{o}C for producing AE-molybdate intermediate beads. Secondly, the intermediate beads were introduced into 100 mL (containing 50% ethanol) of zirconyl oxychloride (20 g) for simultaneous *in situ* precipitation of zirconium molybdate NPs onto the pore surface of the resin which was recognized by developing cyan color for the beads. Finally, the zirconium molybdate NPs embedded AE was decomposed and simultaneous precipitated under zirconium hydroxide by contacting solution of NaOH-NaOH (5% in mass of each)

and follow with DI water/ethanol washed and air dried to obtain hybrid ZAE. Note that this method does not mean with endorsement of MSA resin, other anion exchange resins can be used for preparing this type of hybrid.

In order to evaluate the molybdate intermediate method, the conventional method, called direct method (DM) (because the zirconium ion was directly loaded onto pore surface of the AE), was also involved for comparison [17]. This process of synthesis ZAE was similar with the above procedure but without the first step of loading molybdate oxoanion.

4.2.3. Analytical methods

Refer part 3.2.1.1 for the phosphate analysis and part 3.1.1.3 for other metals analysis as well as the characteristics analysis of the hybrid ZAE.

The point of zero charge (pH_{pzc}) of the ZAE was determined using the drift method [160].

4.2.4. Batch adsorption experiments

Effect of sulfate ion to phosphate adsorption on the ZAE was carried out in shaking plastic tubes (50 mL) containing 40 mL of P-PO_4 6.2 mg/L and ZAE (0.5

g/L) at pH about 7 for 24 h with varying the concentration of sulfate ion from 0–100 mM. In addition, the phosphate adsorption in presence of multi-anions modelled to Mekong river water (Cl^- 100 mg/L, NO_3^- 12 mg/L, HCO_3^- 120 mg/Land SO_4^{2-} 120 mg/L) was also examined [40]. The pristine AE was involved for comparison. Similar procedure was conducted for the isotherm study of phosphate adsorption on the ZAE compared with pristine AE with varying the amount of adsorbent added into solution in the absence and presence of excessive sulfate ion (5 mM).

Kinetic of phosphate adsorption on the ZAE was performed in a 500 mL glass bottle containing 250 mL of $P\text{-}PO_4$ 10 mg/L and adsorbent 0.5 g/L at pH 7 in the absence and presence of excessive sulfate ion (5 mM). At every determined time, an aliquot (0.5 – 1.5 mL) was withdrawn for analyzing phosphate concentration.

4.2.5. Fixed-Bed column experiments

A synthetic water containing phosphate (2 mg-P/L) and four regular anions (SO_4^{2-} 120 mg/L, Cl^- 100 mg/L, HCO_3^- 120 mg/L and NO_3^- 2 mg/L) was used as a feed solution for fixed-bed column test. The detail procedure was similar to the procedure described in part 3.2.1.6. After the adsorption, a binary solution NaOH–NaCl (5% of each, w/v) (ECBT = 25 min) was used for desorption of phosphate. The desorbed ZAE was then rinsed solution of NaCl 1% and DI water until the pH of effluent solution downed to neutral pH, which was ready for next adsorption.

4.3. Results and discussions

4.3.1. Characteristics of the ZAE

Fig. 4-1 shows the characteristics of the ZAE fabricated by the molybdate intermediate method: (a) SEM image, (b) HR-TEM image and (c) change of equilibrium pH profile. As shown in Fig. 4-1a&b, the SEM and TEM images, HZO particles in nano-size were successfully dispersing within the spherical structure of the AE. In addition, the clear surface of the ZAE in the SEM image infers that HZO NPs was effectively precipitated onto the pore surface of the AE rather than deposited on the surface of AE. The HZO NPs was poor crystalline in nature (Fig. S4-1), be consistent with literature [17], presumed to be favorable to phosphate adsorption. Fig. 4-1c shows the change in the pH of the ZAE at equilibrium in comparison between two synthetic methods (the MIM and DM). As shown, both hybrid adsorbents exhibited almost the same property of surface charges, expressed by their coincidental graph of pH change and their similar pH_{pzc} values of ~7.6. This pH_{pzc} was found in similar value with previous report for HZO embedded AE [50]. In fact, the embedded HFO within AE has a higher value of pH_{pzc} compared with the bare zirconium oxide (average value for pH_{pzc} was reported about 6.5 [161]), inferring the highly referable interaction between HZO NPs with phosphate species at neutral pH value. These results indicate the successful fabrication of HZO embedded AE by the molybdate intermediate method, which showed almost the

same surface properties and crystalline structure with that of material from the previous method.

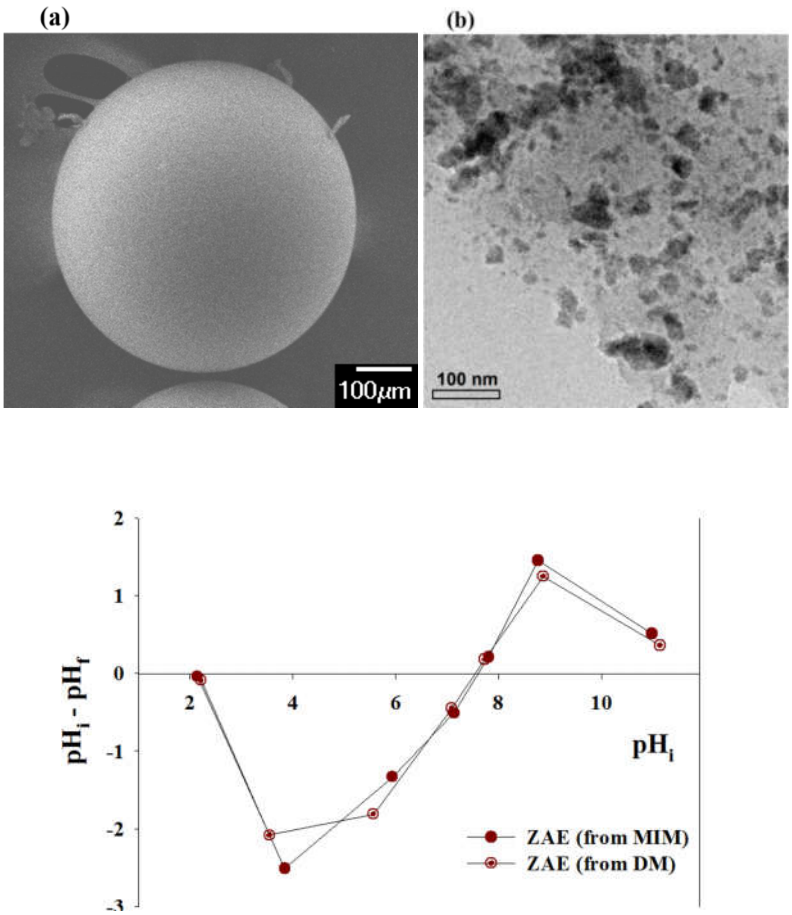

Fig. 4-1. (a) SEM and (b) HR-TEM images of the ZAE fabricated by the molybdate intermediate method (MIM); and (c) The change of equilibrium pH of the ZAE compared between by the MIM and the direct method (DM).

Enhanced Zr content in ZAE

Fig. 4-2 shows the Zr content found in the ZAE compared between the proposed method (MIM) and the conventional method (DM) with a certain number of repetitive cycles of the procedures. It is very interesting that the MIM showed much greater effective loading Zr than the DM. As shown, the weight% of Zr obtained from the MIM achieved up to ~18% only after two cycles of synthetic procedure and the further repetitive cycles of synthesis seemed not change the weight% of Zr in the ZAE, whereas the DM exhibited much lower weight% of Zr at every certain cycles of the synthetic process even up to four cycles of the process. The great performance of the MIM for effective loading Zr within the AE could be explained by that the molybdate-loaded resin was simultaneous desorbed, reacted and *in situ* precipitated as zirconium molybdate complexes onto pore surface of the AE. In addition, the charged coupling molybdate oxoanion with fixed positively charged quaternary ammonium groups of the resin might lead to enhance the permeability of zirconium into the polymeric phase of the resin due to partly compensating the electrostatic repulsion to zirconium ion (Donnan exclusion), a big challenge of the conventional method [19, 50]. Therefore, the development of the MIM is here of significance to both a potential of advanced method for effective preparation of the adsorbent in reducing time, cost and used chemicals as well and an improvement of efficient and selective removal of phosphate from water.

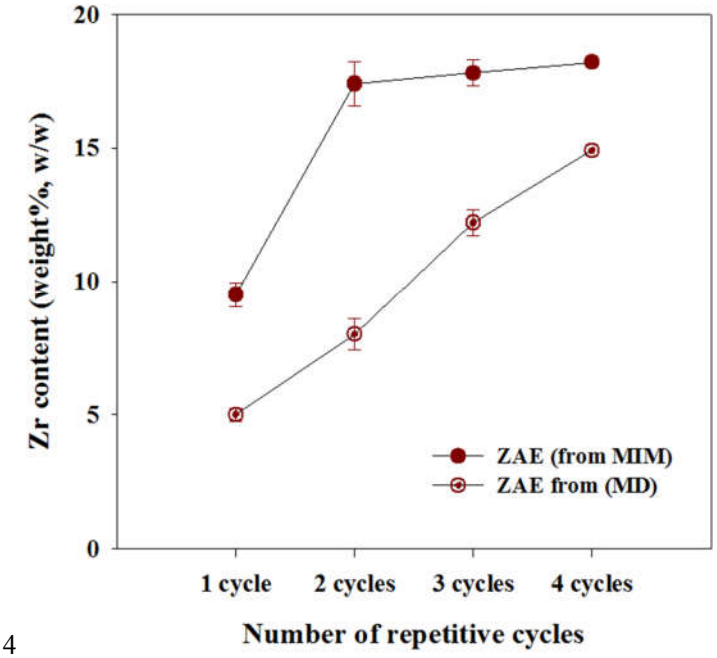

4

Fig. 4-2. Weight% of Zr found in the hybrid ZAE fabricated by the molybdate intermediate method (MIM) compared with that of the direct method (DM) after a certain cycles of synthetic process.

4.3.2. Phosphate adsorption: the role of Zr content

In order to access the effect of Zr content to the efficient and selective removal of phosphate of ZAE, there adsorbents with different Zr contents (ZAE-1 (4.9% Zr), ZAE-2 (11.8% Zr) and ZAE-3 (17.4% Zr)) were selected and studied for the adsorption. The pristine AE (0% Zr) was also involved for comparison.

4.3.2.1. Selective adsorption of phosphate

Fig. 4-3 shows the selective removal of phosphate among different hybrids (ZAE-1, ZAE-2 and ZAE-3) compared with pristine AE with: (a) effect of sulfate concentration, (b) selective phosphate removal in presence of mixed common ions (SO_4^{2-}, HCO_3^-, Cl^- and NO_3^-) modelled to Mekong river water [40] and (c) uptake of phosphate against with time in absence and presence of excessive sulfate ion (5 mM). As shown in Fig. 4-3a, the efficient removal of phosphate on ZAE increased with the increase of Zr content in order AE < ZAE-1 < ZAE-2 < ZAE-3 corresponding to their increasing of %Zr (0%, 4.9%, 11.8% and 17.4%, respectively). It is pointed that the tendency of change of the removal efficiency in the increasing sulfate concentration seemed to be similar among adsorbents (three hybrids and pristine AE) regardless of their different removal efficiencies due to the different Zr contents. Indeed, the phosphate removal of three hybrid adsorbents were dropped as increasing the molar ratio of $[SO_4]/[PO_4]$ and quickly stabilized at ratio of $[SO_4]/[PO_4]$ over

10/1, whereas that of the pristine AE was negligible at $[SO_4]/[PO_4]$ over 10/1. These results indicate that the ZAE possesses of two types of separated adsorption sites: (i) the non-selective sites from fixed positively charged quaternary ammonium groups of the supported resin and (ii) the selective sites from HZO NPs. At the ratio of $[SO_4]/[PO_4]$ over 10/1, sulfate ion can totally inhibit the adsorption of phosphate onto the supported resin, and thus, this selective adsorption of phosphate relies on the HZO NPs.

Similar to Fig. 4-3a, the results in Fig. 4-3b reflexed the role of loading HZO NPs for effective removal of phosphate in the effect of multi anions (Cl^-, NO_3^-, HCO_3^- and SO_4^{2-}) modelled to Mekong river water condition. As the results, the removal efficiency can be retained for three hybrids of ZAE (ZAE-3, ZAE-2 and ZAE-1, > 90% of removal) but not for the pristine AE (only ~10% removal). This result promises a high potential of the ZAE for selective removal of phosphate in real water.

Fig. 4-3c shows the phosphate uptake against with time contact in comparison among the hybrid adsorbents (ZAE-3, ZAE-2, ZAE-1) and pristine AE in the absence and presence of excessive sulfate ion (5mM). As the results, in the absence of sulfate ion, there was not much different phosphate adsorption behavior among adsorbents, besides there hybrids of the ZAE show higher adsorption efficiency than the pristine AE (95 – 99% removal for three hybrids and 64% removal for pristine AE at 8 h). In fact, the uptake of phosphate on three hybrid still occurred up to 8 h of investigated time, while that of the pristine AE was quickly approached

equilibrium at about 2 h. On the other hand, in the presence of excessive sulfate (5 mM), the pristine AE was powerless to adsorb phosphate ion, be consistent with the result of Fig. 4-3a [162]. Meanwhile, all the hybrids still adsorbed phosphate and the adsorption efficiency reflexed clearly the dependence to the Zr contents.

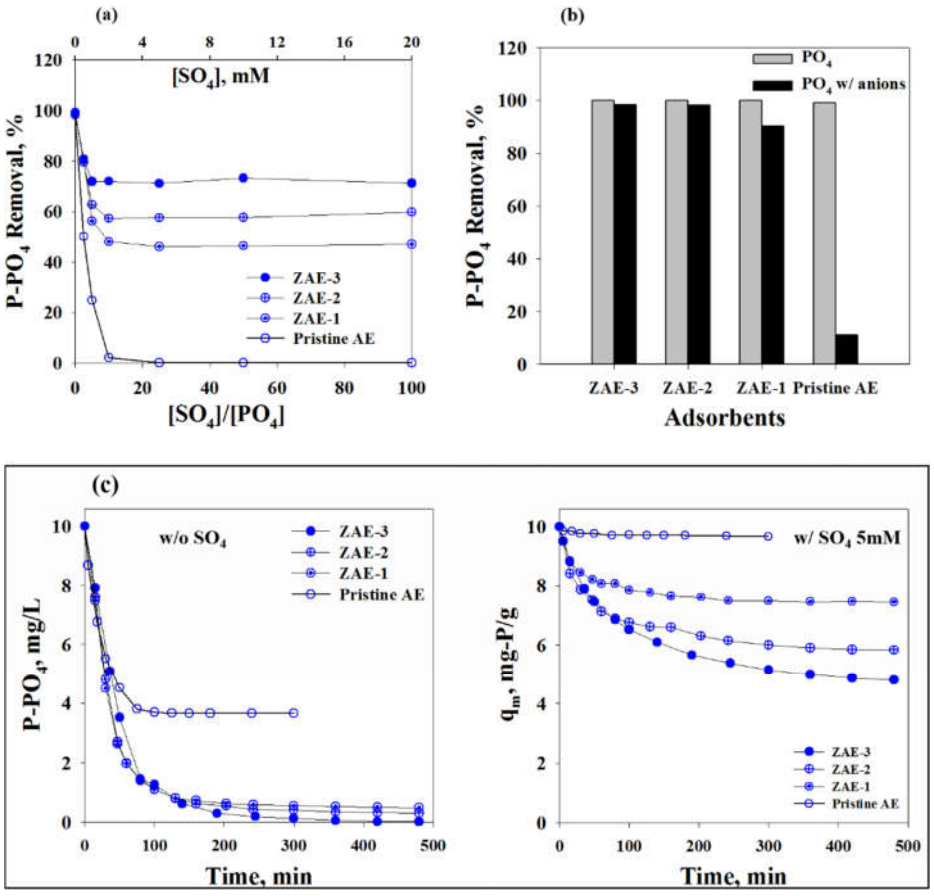

Fig. 4-3. Performance of phosphate adsorption among adsorbents (ZAE-1, ZAE-2 and ZAE-3) compared with pristine AE: (a) effect of sulfate concentration (adsorbent dose 0.5 g/L, P-PO_4 0.2 mM (6.2 mg/L), pH 7.0, 25°C, 24 h); (b) Effect of multi-anions modelled to Mekong river water (adsorbent dose 0.5 g/L, P-PO_4 2 mg/L, SO_4 120 mg/L, HCO_3^- 120 mg/L, Cl^- 100 mg/L, NO_3^- 12 mg/L, pH 7.0, 25°C, 24 h); and (c) Uptake of phosphate against with time contact in with and without sulfate ion (adsorbent dose 0.5 g/L, P-PO_4 10 mg/L, SO_4 5 mM, pH 7.0, 25°C).

4.3.2.2. Isotherm adsorption study

Fig. 4-4 depicts the comparison of phosphate adsorption at equilibrium among hybrids (ZAE-1, ZAE-2 and ZAE-3) and pristine AE and their fitting to Freundlich isotherm model in absence and presence of sulfate ion (5 mM). As shown in Fig. 4-4a, the phosphate adsorption in single phosphate solution of ZAE-1, ZAE-2 and ZAE-3 were not much difference but were higher than that of the pristine AE. It could be due to the HZO NPs inside the AE support enhanced phosphate adsorption efficiency.

On the other hand, the effective adsorption of phosphate at equilibrium under competing by sulfate ion (Fig. 4-4b) reflexed clearly the role of loaded HZO NPs to the selective adsorption of phosphate, which was consistent with the negligible adsorption of the pristine AE in this condition. As shown, the equilibrium adsorption capacity of phosphate was a function of Zr content. Indeed, the ZAE-3 exhibited the largest removal efficiency in the presence of excess sulfate ion and the efficiency was in order ZAE-3 > ZAE-2 > ZAE-1 >> pristine AE corresponding to their decreasing Zr content.

The equilibrium adsorption of all adsorbents were examined and fitted well to the non-linear Freundlich isotherm model and the results was summarized in Table 4-1, indicating the homogeneous adsorption process between phosphate and these adsorbents. The maximum adsorption capacities in excessive sulfate condition estimated from the Freundlich equation were found to be 16.2, 12.5 and 7.6 mg-P/g-

adsorbent for ZAE-3, ZAE-2 and ZAE-1, respectively. These adsorption capacities could be considered as the selective adsorption capacities of the hybrids because the phosphate adsorption on the pristine AE was neglected. In addition, the phosphate affinity K_F value of these hybrids in the presence of sulfate ion also increased with the increasing Zr content, be consistent with the increase adsorption selectivity.

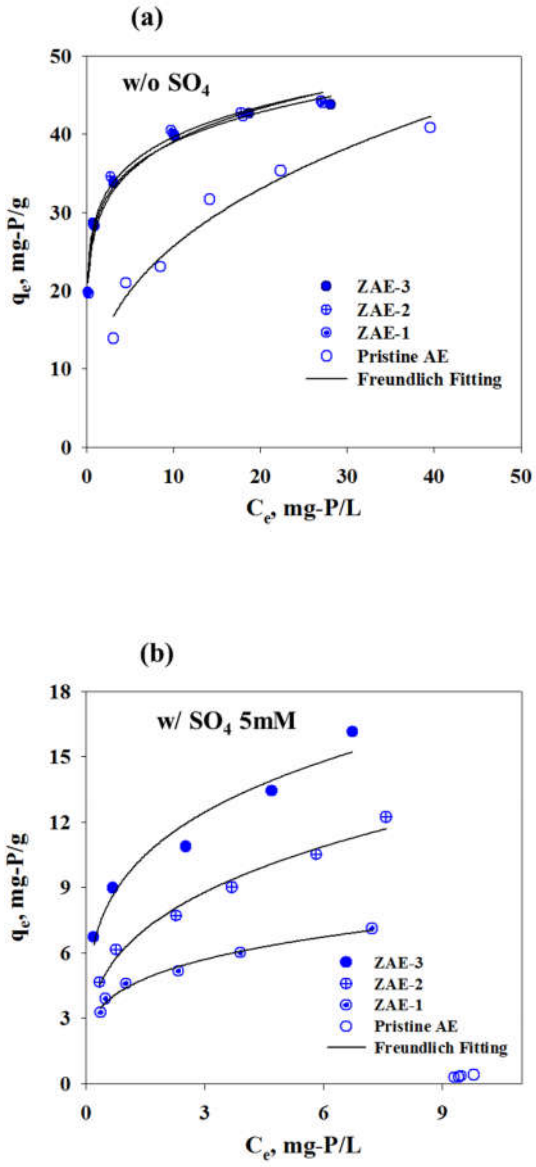

Fig. 4-4. Equilibrium adsorption of phosphate compared among the hybrids (ZAE-3, ZAE-2, ZAE-1) and pristine AE in absence and presence of sulfate ion (Adsorbent dose 0.1 – 2.5 g/L, P-PO_4 = 10 mg/L, SO_4 5 mM, pH 7.0, 25°C, 24 h.

Table 4-1. Freundlich isotherm parameters for phosphate adsorption of the hydrated zirconium oxide NPs embedded anion exchange resin (ZAE) compared with the pristine anion exchange resin (pristine AE).

	ZAE-3		**ZAE-2**		**ZAE-1**		**Pristine AE**	
	w/o SO_4	w/ SO_4	w/o SO_4	w/ SO_4	w/o SO_4	w/ SO_4	w/o SO_4	w/ SO_4
K_F (mg/g) $(mg/L)^{-1/n}$	28.59	9.49	29.18	6.26	27.81	4.37	11.17	–
1/n	0.135	0.248	0.133	0.309	0.148	0.240	0.362	–
R^2	0.992	0.955	0.986	0.981	0.977	0.984	0.957	–

4.3.2.3. Fixed-bed column test

Fig. 4-5 presents the breakthrough curve of column test for phosphate removal by those of ZAE hybrids compared with pristine AE using synthetic phosphate water containing other common anions in water/wastewater (Cl^-, NO_3^-, HCO_3^- and SO_4^{2-}) at pH about 7. As expected, the volume capacity of effective treatment for phosphate (below 0.5 mg-P/g-adsorbent, the maximum allowance of discharged phosphate) increased in order pristine AE << ZAE-1 < ZAE-2 < ZAE-3 corresponding to their increasing Zr content. Indeed, the effective volume treatment was found to be 440, 1980, 3980 and 5100 BVs for the pristine AE, ZAE-1, ZAE-2 and ZAE-3, respectively.

After adsorption process, the phosphate-adsorbed ZAE-3 was proceeded to be desorbed and regenerated at ambient air. The second run of phosphate removal by the ZAE-3 seemed to be retrieved up to about 4950 BVs. In addition, as shown in Fig. 4-6, phosphate desorption of the ZAE-3 after the 1st and 2nd adsorption processes was effective within 10 BVs of desorbate solution (> 90%) by using solution of NaOH-NaCl. The results of regeneration test indicates a high potential of long-term reusability of the hybrid ZAE for phosphate removal.

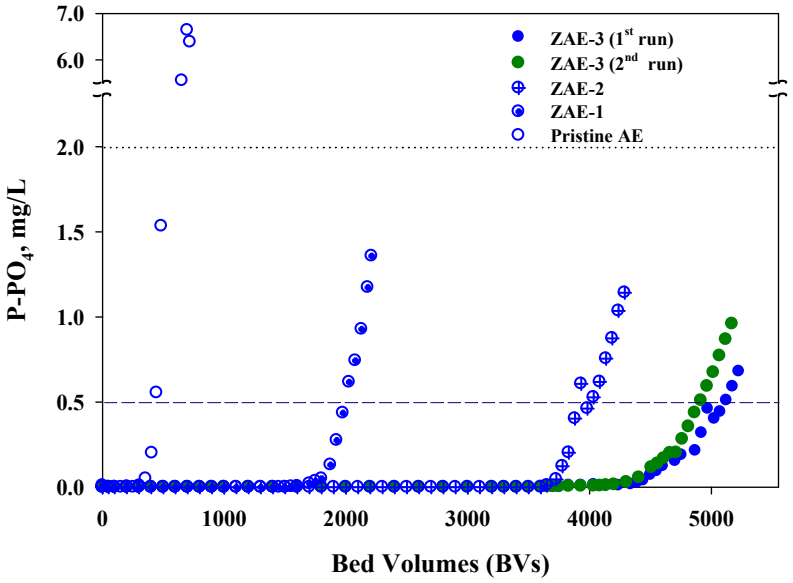

Fig. 4-5. Column adsorption for phosphate from synthetic water in comparison among the hybrids (ZAE-3, ZAE-2 and ZAE-1) and pristine AE. Experimental conditions (EBCT 4 min, 5 mL of adsorbent, P-PO_4 2 mg/L, Cl^- 100 mg/L, NO_3^- 12 mg/L, HCO_3^- 120 mg/L, SO_4^{2-} 120 mg/L, pH ~ 7 – 7.3).

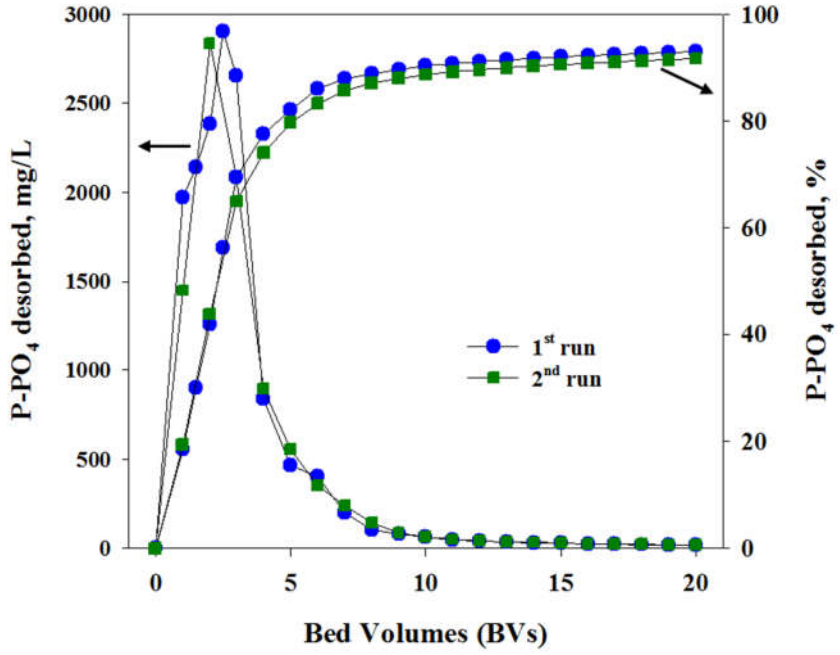

Fig. 4-6. Column phosphate desorption of the ZAE-3. Experimental conditions (EBCT 25 min, desorbate solution of NaOH–NaCl (5 wt % of each)).

4.3.3. Interpretation of selective removal of phosphate

Fig. 4-7 shows the correlation between the selective phosphate adsorption capacity of the ZAE and its Zr content for both case of the batch test (in presence of excessive sulfate ion) and column test (synthetic water). It is very interesting that the linear expressions with high coefficient value R^2 (~1.00) well demonstrated for both batch and column modes of the phosphate removal and expressed as follows:

Batch experiment: $y = 0.201x + 0.139$ ($R^2 = 0.999$) (1)

Column experiment: $y = 0.156x + 0.076$ ($R^2 = 0.998$) (2)

where, x (mmol·Zr/g·ZAE) is the amount of Zr in the ZAE and y (mmol·P/g·ZAE) is the corresponding phosphate adsorption of the ZAE.

The good linear expression (Eq. (1) & (2)) infers that the macroporous AE served as excellent nano-reactors for depositing and stabilizing of HZO NPs during their *in situ* precipitation process[127], which brings advantage in retaining the similar surface properties of the loaded HZO NPs at a wide range of Zr content. Thus, the selective adsorption performance for phosphate of the ZAE was proportional function with the Zr content. Indeed, Eq. (1) provides the strong relationship between the maximum capacity of selective phosphate adsorption on the ZAE (q_m, mmol·P/g) and its Zr content (mmol·Zr/g). Meanwhile, Eq. (2) demonstrates the strong dependence of effective adsorption capacity of the ZAE to its Zr content in column

mode application. As shown, the lower slope of Eq. (2) than Eq. (1) was expected, possibly due to the unfully-adsorbed phenomenon of non-equilibrium of column test. In addition, as shown in Fig. 4-7, the unparalleled degree of two linear expressions become more greater at high Zr content, which could be explained by that HFO NPs having the lower adsorption rate (than the quaternary ammonium functional groups) [82] may require more time to obtain higher capacity. Further evaluation of flow rate of synthetic water could provide better understanding for this explanation.

On the other hand, Eq. (1) could allow to predict the theoretical maximum capacity (theoretical q_m) for selective adsorption of phosphate based on the Zr content which was to be 72.6 mg-P/g-Zr (or 222.6 mg-PO_4/g-Zr). This result was higher than the capacity of bare ZrO_2 NPs as previously reported [9, 81, 157] possibly due to the support of Donnan membrane equilibrium from fixed charges of the supported AE. Also, the theoretical capacity for effective removal of phosphate by column test at experimental condition can be estimated by Eq. (2) to be 55.4 mg-P/g-Zr (or 169.7 mg-PO_4/g-Zr), which was about 75% theoretical q_m value.

In overall, the specific role of Zr content was experimentally explained in the Eq. (1) and (2), which was of significance not only in description of selective phosphate adsorption insights the ZAE but also in estimating the performance of the adsorbent based on the known amount of loaded Zr.

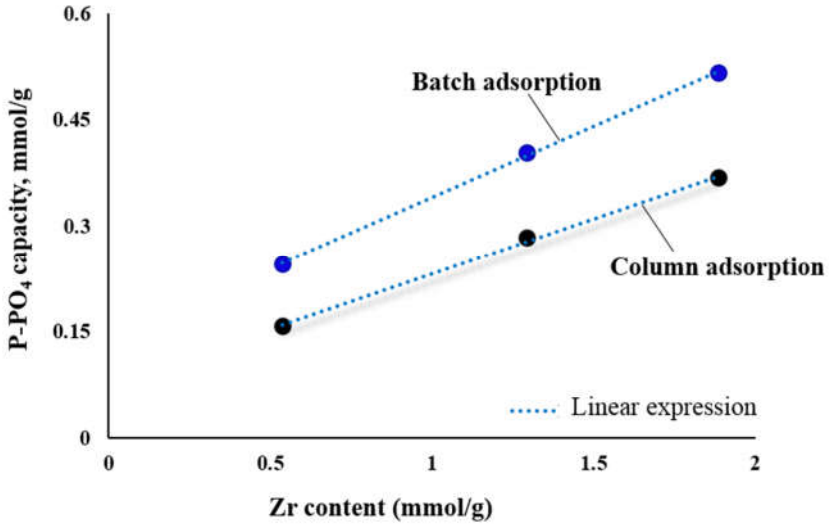

Fig. 4-7. Correlation between Zr content in the ZAE and the corresponding capacity of ZAE for effective adsorption of phosphate in batch mode (in presence of excessive sulfate ion) and column mode of synthetic water.

4.4. Conclusion

This study proposed a new synthetic method of the hybrid ZAE with effectively loading HZO NPs within the AE (~18 %Zr after two cycles of the synthesis). The structural and surface charges properties of the ZAE was characterized with high potential for phosphate adsorption, which was similar with that of the adsorbent fabricated by the conventional method. The loaded HZO NPs exhibited the enhancement of both adsorption efficiency and selectivity toward phosphate ion. The selective behavior of the ZAE toward phosphate ion (in the effect of sulfate ion) relied to the loaded HZO NPs and was in function of Zr content, which was well described by a good linear expression between the maximum capacity of effective adsorption and the Zr content (R^2 ~ 1.00) in presence of co-existing ions for either batch or column adsorption. Consequently, the theoretical q_m value could be estimated from the linear expression and found to be 72.6 mg·P/g·Zr (or 222.6 mg·PO_4/g·Zr). The successful column test of the ZAE provided the effective capacity of treatment was about 76% of theoretical q_m value. Finally, this study contributed not only an innovated synthesis of ZAE for effective removal of phosphate from water/wastewater in expectation of reducing time, cost and chemical wastes as well but also an understanding selectivity of phosphate adsorption insights of the ZAE for further research.

5. Conclusion

This dissertation reported the novel hybrid adsorbents of inorganic NPs embedded anion exchange resin, which are ZMAE and ZAE, for selective removal of phosphate and arsenic from water. The study of selective adsorption of the hybrid adsorbents toward phosphate and arsenic were placed in context of common co-existing anions of synthetic water.

(1) The first time the ZMAE was fabricated (with a single cycle of synthesis procedure) for selective removal of phosphate and arsenate, which showed much superior performance to the ZAE or pristine AE. There was about 62% of adsorption capacity of the ZMAE served the selectivity toward either phosphate ion or arsenate ion in the presence of excessive sulfate ion. The great selectivity of both phosphate and arsenate were given by the attribution of the ZM NPs, which not only exhibited excellent selectivity toward phosphate ion but also contributed to enhance the selective adsorption of the supported AE. The effect of pH to the adsorption showed that the adsorption of the ZMAE toward both phosphate and arsenate ions reveal the specific interaction which was less dependent to the surface charge of the adsorbent as usually reported in literature. Furthermore, the fixed-bed column adsorption of the ZMAE examined for phosphate and arsenic removal from synthetic water promise a high potential of field application of ZMAE for effective removal of arsenic and phosphate from water/wastewater.

(2) The molybdate intermediate method was proposed for fabricated of hybrid ZAE with a better effectiveness of dispersing HZO NPs within the resin and a better saving of time, cost and used chemicals than the previous method. The ZAE with high stability and regeneration performances showed its good candidate for removal of phosphate and arsenic at neutral pH water with long-term reusability. The linear expression between the maximum capacity of selective adsorption and the Zr content for either batch or column adsorption could allow to evaluate the adsorption performance of the ZAE toward phosphate/arsenic based on the Zr content. Therefore, this study could contribute an important understanding of selectivity of phosphate adsorption insights of the ZAE for further study.

The synthesis methods of both hybrids ZMAE and ZAE do not mean with endorsement of Zr, other metals can be extended to develop these methods as general and effective methods for propose a large-scale synthesis of high efficient and selective adsorbents. Furthermore, the understanding the role of Zr content in the ZAE to the selective adsorption of phosphate could play an important role for further study of adsorbent development and evaluation.

Supplementary data

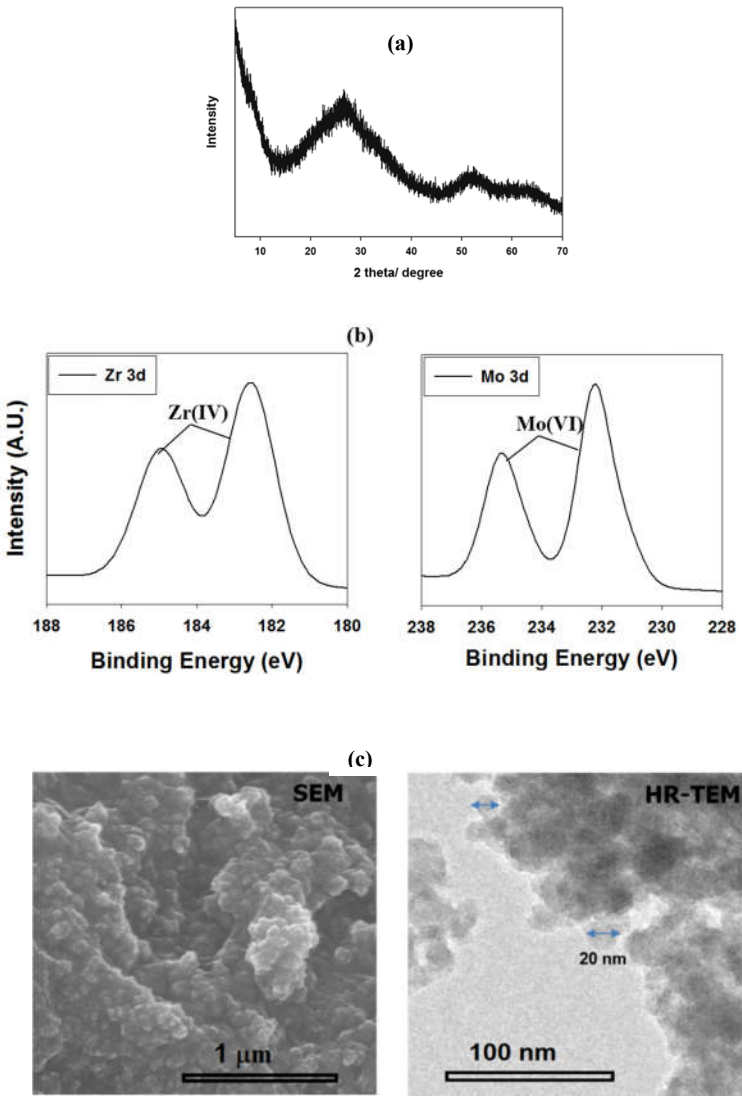

Fig. S3-1. (a) XPS spectra of the ZMAE (Zr 3d and Mo 3d core level of); (b) SEM and HR-TEM of ZM NPs, respectively.

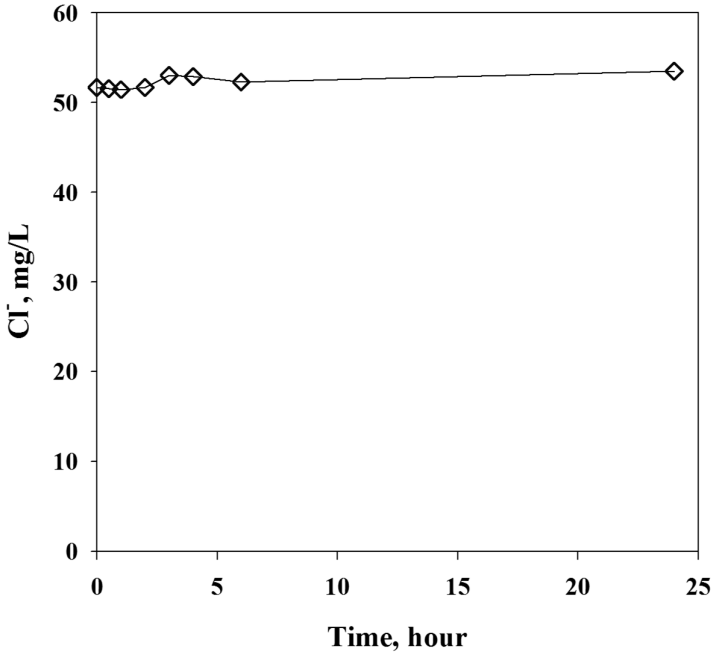

Fig. S3-2. Chloride adsorption of the bare ZM NPs with time ([ZM NPs] = 0.4 g/L, [Cl^-] = 51.7 mg/L, 25°C).

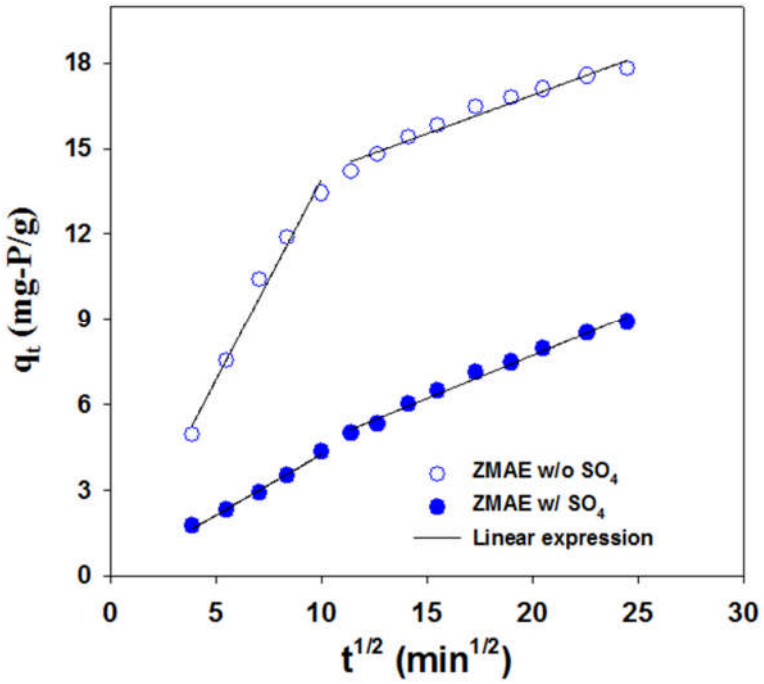

Fig. S3-3. Intra-particle diffusion model of phosphate adsorption on the ZMSA (adsorbent dose 0.5 g/L, [P-PO_4] = 10 mg/L, pH 5.5).

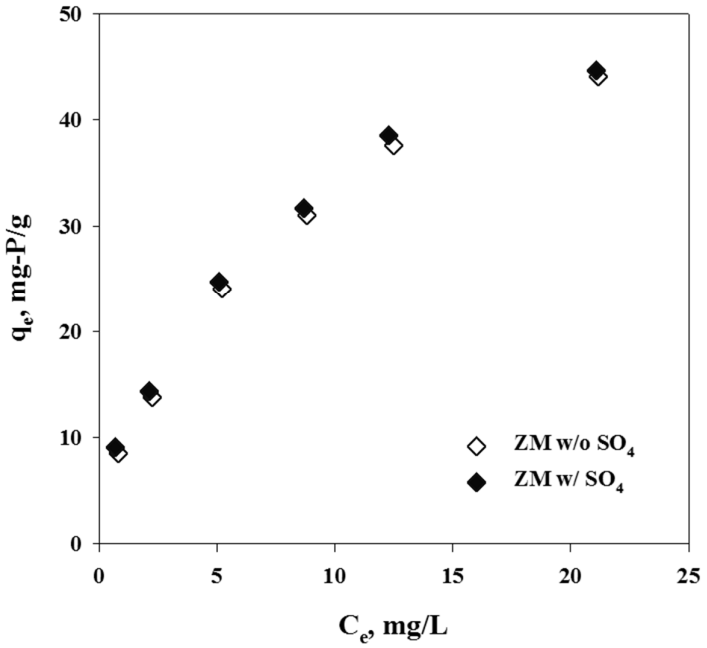

Fig. S3-4. Equilibrium adsorption of phosphate on the ZM NPs in in absence and presence of sulfate ([Adsorbent] = 0.2 g/L, [P-PO_4] = 2.5 – 30 mg/L, [SO_4] = 5 mM, pH 5.5, 25ºC, 24 h).

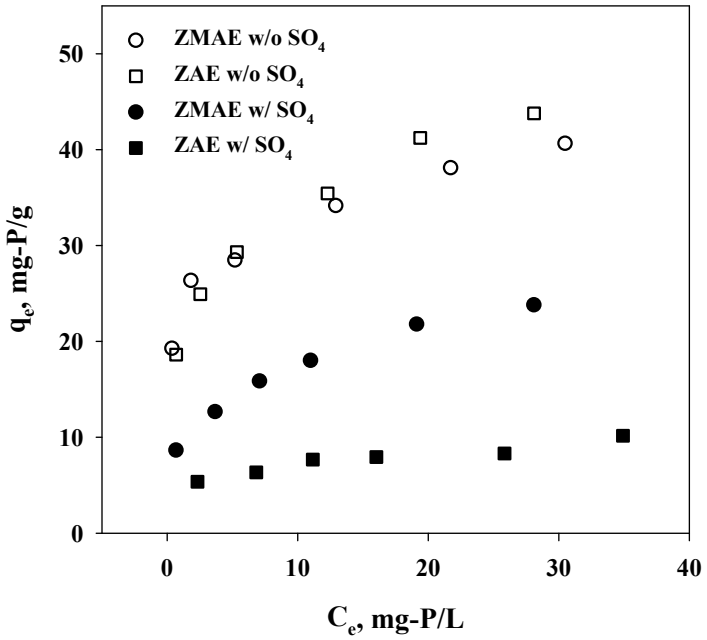

Fig. S3-5. Equilibrium adsorption of phosphate compared between the ZMAE and ZAE in absence and presence of sulfate ([Adsorbent] = 0.5 g/L, [P-PO_4] = 5 – 50 mg/L, [SO_4] = 5 mM, pH 5.5, 25°C, 24 h).

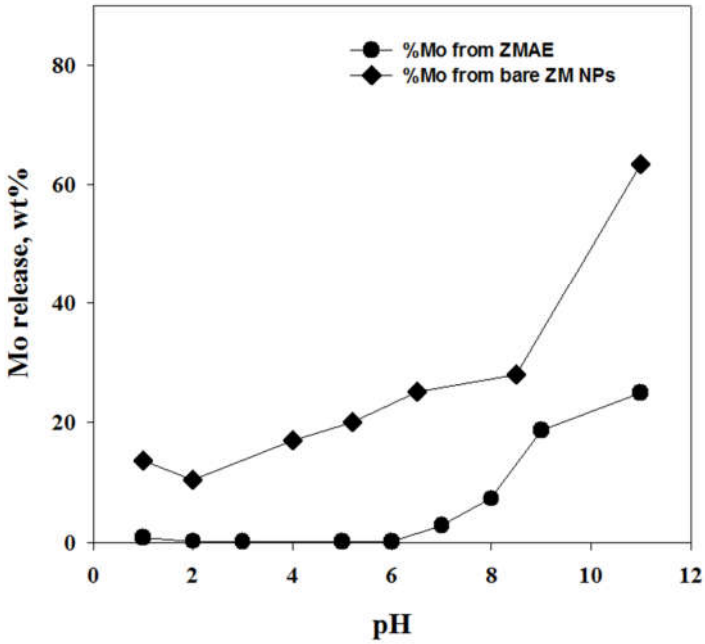

Fig. S3-6. Comparison of Mo released from the ZMAE and ZM particles (without supported resin) at different pH values (adsorbent dose 1g/L, 24 h).

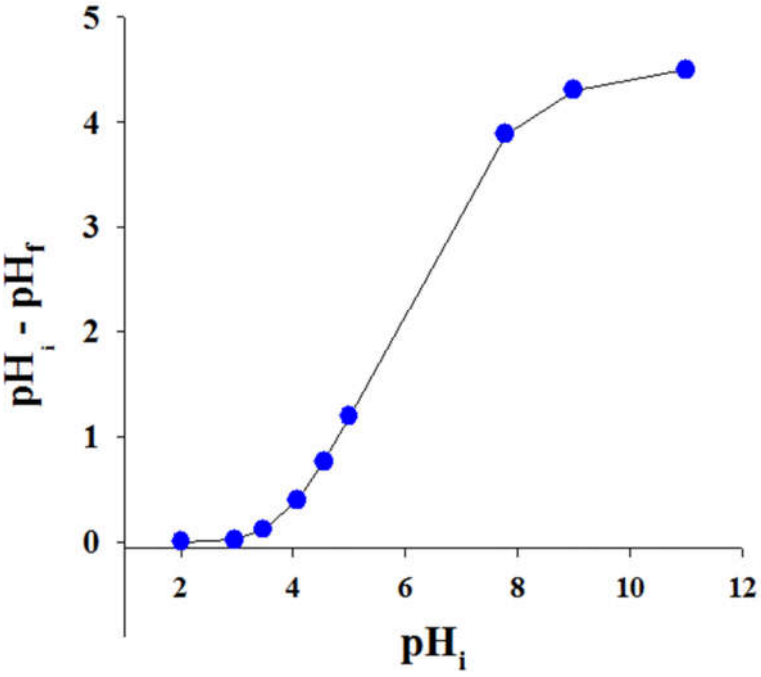

Fig. S3-7. Point of zero charge (pH_{pzc}) of the ZMAE was not determined (using drift method).

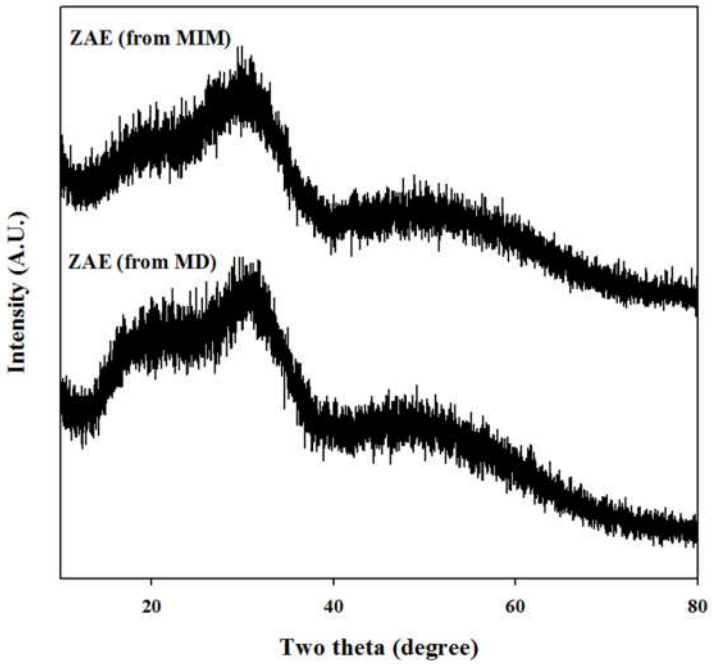

Fig. S4-1. XRD spectra of the ZAE fabricated by the molybdate intermediate method (MIM) compared with that of the previous method (DM).

Table S3-1. Adsorption kinetic parameters of phosphate on the ZMAE compared with the AE (calculated as P).

Adsorbents	q_e exp. (mg/g)	Pseudo-first-order			Pseudo-second-order			Intra-particle diffusion model			
		k_1, 10^{-2} (min^{-1})	q_e (mg/g)	R^2	k_2, 10^{-3} (min^{-1})	q_e (mg/g)	R^2	k_{1d} (mg/(g.$min^{1/2}$))	R_1^2	k_{2d} (mg/(g.$min^{1/2}$)	R_2^2
Pristine AE	12.9	5.27	16.4	0.987	5.61	13.5	0.997	-	-	-	-
ZMAE[a]	19.1	0.60	10.6	0.918	1.16	19.2	0.999	1.41	0.983	0.27	0.968
ZMAE[b]	12.0	0.21	9.8	0.983	0.48	10.9	0.994	0.42	0.992	0.30	0.989

[a]In the absence of sulfate

[b]In the presence of sulfate 5 mM

Table S3-2. Phosphate adsorption capacity compared between the ZMAE and pristine AE.

Adsorbents	**ZMAE**	**Pristine AE**
%Zr (w/w)	4.3	–
%Mo (w/w)	14.7	–
IEC, Cl^- form (dry, meq/g)	1.92	3.42
q_m, mg-P/g	42.2 ($q_{m\text{-}AE\ (inZMAE)}$ = 24.1, $q_{m\text{-}NPs\ (in\ ZMAE)}$ = 18.1)	43.1
q_m, mg-P/g in SO_4^{2-} 5 mM	26.1 (Case I: $q^*_{m\text{-}AE\ (inZMAE)}$ = 8.0 and $q^*_{m\text{-}NPs\ (in\ ZMAE)}$ = 18.1; Case II: $q^*_{m\text{-}AE\ (inZMAE)}$ = 1.0 and $q^*_{m\text{-}NPs\ (in\ ZMAE)}$ = 25.1)	1.8

Table S3-3. The solution pH changing before and after the adsorption on the ZMAE

		Initial pH	2.0	3.0	5.0	7.0	9.0	11.0
ZMAE	Phosphate adsorption	Final pH	2.0	2.9	4.3	4.4	5.7	7.8
	Sulfate adsorption	Final pH	2.0	2.9	4.1	4.2	5.8	7.7
Pristine AE	Phosphate adsorption	Final pH	2.0	3.1	4.9	6.7	8.8	11.0

References

[1] National Research Council, Report: Arsenic in Drinking Water. National Academy Press, Washington DC, 2001.

[2] T.S.Y. Choong, T.G. Chuah, Y. Robiah, F.L. Gregory Koay, I. Azni, Arsenic toxicity, health hazards and removal techniques from water: an overview, Desalination 217 (2007) 139-166.

[3] D. Mohan, C.U. Pittman Jr, Arsenic removal from water/wastewater using adsorbents—A critical review, J. Hazard. Mater. 142 (2007) 1-53.

[4] S. Bang, G.P. Korfiatis, X. Meng, Removal of arsenic from water by zero-valent iron, J. Hazard. Mater. 121 (2005) 61-67.

[5] G. Zhang, J. Qu, H. Liu, R. Liu, R. Wu, Preparation and evaluation of a novel Fe–Mn binary oxide adsorbent for effective arsenite removal, Water Res. 41 (2007) 1921-1928.

[6] X.-H. Guan, J. Wang, C.C. Chusuei, Removal of arsenic from water using granular ferric hydroxide: Macroscopic and microscopic studies, J. Hazard. Mater. 156 (2008) 178-185.

[7] N.P. Nikolaidis, G.M. Dobbs, J.A. Lackovic, Arsenic removal by zero-valent iron: field, laboratory and modeling studies, Water Res. 37 (2003) 1417-1425.

[8] M.R. Awual, M.A. Shenashen, T. Yaita, H. Shiwaku, A. Jyo, Efficient arsenic(V) removal from water by ligand exchange fibrous adsorbent, Water Res. 46 (2012) 5541-5550.

[9] Y. Su, H. Cui, Q. Li, S. Gao, J.K. Shang, Strong adsorption of phosphate by amorphous zirconium oxide nanoparticles, Water Res. 47 (2013) 5018-5026.

[10] G. Li, S. Gao, G. Zhang, X. Zhang, Enhanced adsorption of phosphate from aqueous solution by nanostructured iron(III)–copper(II) binary oxides, Chem. Eng. J. 235 (2014) 124-131.

[11] L. Chen, X. Zhao, B. Pan, W. Zhang, M. Hua, L. Lv, W. Zhang, Preferable removal of phosphate from water using hydrous zirconium oxide-based nanocomposite of high stability, J. Hazard. Mater. 284 (2015) 35-42.

[12] P. Loganathan, S. Vigneswaran, J. Kandasamy, N.S. Bolan, Removal and recovery of phosphate from water using sorption, Crit. Rev. Environ. Sci. Technol. 44 (2014) 847-907.

[13] R. Singh, S. Singh, P. Parihar, V.P. Singh, S.M. Prasad, Arsenic contamination, consequences and remediation techniques: A review, Ecotoxicol. Environ. Saf. 112 (2015) 247-270.

[14] Y.-h. Xu, T. Nakajima, A. Ohki, Adsorption and removal of arsenic(V) from drinking water by aluminum-loaded Shirasu-zeolite, J. Hazard. Mater. 92 (2002) 275-287.

[15] P. Delaney, C. McManamon, J.P. Hanrahan, M.P. Copley, J.D. Holmes, M.A. Morris, Development of chemically engineered porous metal oxides for phosphate removal, J. Hazard. Mater. 185 (2011) 382-391.

[16] L. Cumbal, A.K. SenGupta, Arsenic Removal Using Polymer-Supported Hydrated Iron(III) Oxide Nanoparticles: Role of Donnan Membrane Effect†, Environ. Sci. Technol. 39 (2005) 6508-6515.

[17] B. Pan, J. Xu, B. Wu, Z. Li, X. Liu, Enhanced removal of fluoride by polystyrene anion exchanger supported hydrous zirconium oxide nanoparticles, Environ. Sci. Technol. 47 (2013) 9347-9354.

[18] B. Pan, Z. Li, Y. Zhang, J. Xu, L. Chen, H. Dong, W. Zhang, Acid and organic resistant nano-hydrated zirconium oxide (HZO)/polystyrene hybrid adsorbent for arsenic removal from water, Chem. Eng. J. 248 (2014) 290-296.

[19] A.K. Sengupta, S. Padungthon, Hybrid anion exchanger impregnated with hydrated zirconium oxide for selective removal of contaminating ligand and methods of manufacture and use thereof, The United States Patent 9120093, 2015.

[20] Y. Huang, J.-K. Yang, A.A. Keller, Removal of Arsenic and Phosphate from Aqueous Solution by Metal (Hydr-)oxide Coated Sand, ACS Sustainable Chemistry & Engineering 2 (2014) 1128-1138.

[21] Y. Lee, I.-H. Um, J. Yoon, Arsenic(III) Oxidation by Iron(VI) (Ferrate) and Subsequent Removal of Arsenic(V) by Iron(III) Coagulation, Environ. Sci. Technol. 37 (2003) 5750-5756.

[22] M.E. Pena, G.P. Korfiatis, M. Patel, L. Lippincott, X. Meng, Adsorption of As(V) and As(III) by nanocrystalline titanium dioxide, Water Res. 39 (2005) 2327-2337.

[23] Y.Y. Chang, S.M. Lee, J.K. Yang, Removal of As(III) and As(V) by natural and synthetic metal oxides, Colloids Surf. Physicochem. Eng. Aspects 346 (2009) 202-207.

[24] F. Chang, J. Qu, R. Liu, X. Zhao, P. Lei, Practical performance and its efficiency of arsenic removal from groundwater using Fe-Mn binary oxide, Journal of Environmental Sciences 22 (2010) 1-6.

[25] Z. Xu, Q. Li, S. Gao, J.K. Shang, As(III) removal by hydrous titanium dioxide prepared from one-step hydrolysis of aqueous TiCl4 solution, Water Res. 44 (2010) 5713-5721.

[26] A. Sarkar, B. Paul, The global menace of arsenic and its conventional remediation - A critical review, Chemosphere 158 (2016) 37-49.

[27] W. Huang, Y. Zhang, D. Li, Adsorptive removal of phosphate from water using mesoporous materials: A review, J. Environ. Manage. 193 (2017) 470-482.

[28] X. Song, Y. Pan, Q. Wu, Z. Cheng, W. Ma, Phosphate removal from aqueous solutions by adsorption using ferric sludge, Desalination 280 (2011) 384-390.

[29] M. Zamparas, I. Zacharias, Restoration of eutrophic freshwater by managing internal nutrient loads. A review, Sci. Total Environ. 496 (2014) 551-562.

[30] N.R. Council, Clean Coastal Waters: Understanding and Reducing the Effects of Nutrient Pollution, The National Academies Press, Washington, DC, 2000.

[31] W. Xie, D. Zhao, Controlling phosphate releasing from poultry litter using stabilized Fe-Mn binary oxide nanoparticles, Sci. Total Environ. 542 (2016) 1020-1029.

[32] X. Zheng, J. Pan, F. Zhang, E. Liu, W. Shi, Y. Yan, Fabrication of free-standing bio-template mesoporous hybrid film for high and selective phosphate removal, Chem. Eng. J. 284 (2016) 879-887.

[33] S. Yeoman, T. Stephenson, J.N. Lester, R. Perry, The removal of phosphorus during wastewater treatment: A review, Environ. Pollut. 49 (1988) 183-233.

[34] M.N. Khan, F. Mohammad, Eutrophication: Challenges and Solutions, in: A.A. Ansari, S.S. Gill (Eds.) Eutrophication: Causes, Consequences and Control: Volume 2, Springer Netherlands, Dordrecht, 2014, pp. 1-15.

[35] A.A.L.S. Duarte, S.J.A. Cardoso, A.J. Alçada, Emerging and Innovative Techniques for Arsenic Removal Applied to a Small Water Supply System, Sustainability 1 (2009) 1288-1304.

[36] S. Olivera, H.B. Muralidhara, K. Venkatesh, V.K. Guna, K. Gopalakrishna, Y. Kumar K, Potential applications of cellulose and chitosan nanoparticles/composites in wastewater treatment: A review, Carbohydr. Polym. 153 (2016) 600-618.

[37] A.H. Nguyen, H.H. Ngo, W.S. Guo, T.Q. Pham, F.M. Li, T.V. Nguyen, X.T. Bui, Adsorption of phosphate from aqueous solutions and sewage using zirconium loaded okara (ZLO): Fixed-bed column study, Sci. Total Environ. 523 (2015) 40-49.

[38] Z. Veličković, G.D. Vuković, A.D. Marinković, M.-S. Moldovan, A.A. Perić-Grujić, P.S. Uskoković, M.Đ. Ristić, Adsorption of arsenate on iron(III) oxide coated ethylenediamine functionalized multiwall carbon nanotubes, Chem. Eng. J. 181–182 (2012) 174-181.

[39] Y. Zhao, Q. Yue, Q. Li, X. Xu, Z. Yang, X. Wang, B. Gao, H. Yu, Characterization of red mud granular adsorbent (RMGA) and its performance on phosphate removal from aqueous solution, Chem. Eng. J. 193–194 (2012) 161-168.

[40] X. Huang, M. Sillanpaa, E.T. Gjessing, R.D. Vogt, Water quality in the Tibetan Plateau: major ions and trace elements in the headwaters of four major Asian rivers, Sci. Total Environ. 407 (2009) 6242-6254.

[41] C. Su, R.W. Puls, Arsenate and Arsenite Removal by Zerovalent Iron: Effects of Phosphate, Silicate, Carbonate, Borate, Sulfate, Chromate, Molybdate, and Nitrate, Relative to Chloride, Environ. Sci. Technol. 35 (2001) 4562-4568.

[42] H. Zhu, Y. Jia, X. Wu, H. Wang, Removal of arsenic from water by supported nano zero-valent iron on activated carbon, J. Hazard. Mater. 172 (2009) 1591-1596.

[43] C. Novillo, D. Guaya, A. Allen-Perkins Avendano, C. Armijos, J.L. Cortina, I. Cota, Evaluation of phosphate removal capacity of Mg/Al layered double hydroxides from aqueous solutions, Fuel 138 (2014) 72-79.

[44] M.E. Morgada, I.K. Levy, V. Salomone, S.S. Farías, G. López, M.I. Litter, Arsenic (V) removal with nanoparticulate zerovalent iron: Effect of UV light and humic acids, Catal. Today 143 (2009) 261-268.

[45] I.A. Katsoyiannis, A.I. Zouboulis, Removal of arsenic from contaminated water sources by sorption onto iron-oxide-coated polymeric materials, Water Res. 36 (2002) 5141-5155.

[46] J. Wang, W. Xu, L. Chen, X. Huang, J. Liu, Preparation and evaluation of magnetic nanoparticles impregnated chitosan beads for arsenic removal from water, Chem. Eng. J. 251 (2014) 25-34.

[47] C. Shan, M. Tong, Efficient removal of trace arsenite through oxidation and adsorption by magnetic nanoparticles modified with Fe–Mn binary oxide, Water Res. 47 (2013) 3411-3421.

[48] B. Pan, J. Wu, B. Pan, L. Lv, W. Zhang, L. Xiao, X. Wang, X. Tao, S. Zheng, Development of polymer-based nanosized hydrated ferric oxides (HFOs) for enhanced phosphate removal from waste effluents, Water Res. 43 (2009) 4421-4429.

[49] M. Li, J. Liu, Y. Xu, G. Qian, Phosphate adsorption on metal oxides and metal hydroxides: A comparative review, Environ. Rev. 24 (2016) 319-332.

[50] S. Padungthon, M. German, S. Wiriyathamcharoen, A.K. SenGupta, Polymeric anion exchanger supported hydrated Zr(IV) oxide nanoparticles: A reusable hybrid sorbent for selective trace arsenic removal, Reactive & Functional Polymers 93 (2015) 84-94.

[51] A.A. Hekmatzadeh, A. Karimi-Jashni, N. Talebbeydokhti, B. Kløve, Adsorption kinetics of nitrate ions on ion exchange resin, Desalination 326 (2013) 125-134.

[52] H. Song, Y. Zhou, A. Li, S. Mueller, Selective removal of nitrate from water by a macroporous strong basic anion exchange resin, Desalination 296 (2012) 53-60.

[53] F. de Dardel, T.V. Arden, Ion Exchangers, Ullmann's Encyclopedia of Industrial Chemistry, Wiley-VCH Verlag GmbH & Co. KGaA2000.

[54] S. Sarkar, J.E. Greenleaf, A.K. SenGupta, Ion Exchange Technology, Encyclopedia of Polymer Science and Technology, John Wiley & Sons, Inc.2002.

[55] E. Korngold, N. Belayev, L. Aronov, Removal of arsenic from drinking water by anion exchangers, Desalination 141 (2001) 81-84.

[56] M.R. Awual, A. Jyo, Assessing of phosphorus removal by polymeric anion exchangers, Desalination 281 (2011) 111-117.

[57] W.Z. Sun, Q. Li, S. Gao, J.K. Shang, Exceptional arsenic adsorption performance of hydrous cerium oxide nanoparticles: Part B. Integration with silica monoliths and dynamic treatment, Chem. Eng. J. 185 (2012) 136-143.

[58] N. Kawasaki, F. Ogata, H. Tominaga, Selective adsorption behavior of phosphate onto aluminum hydroxide gel, J. Hazard. Mater. 181 (2010) 574-579.

[59] J. Mertens, J. Rose, R. Kagi, P. Chaurand, M. Plotze, B. Wehrli, G. Furrer, Adsorption of arsenic on polyaluminum granulate, Environ. Sci. Technol. 46 (2012) 7310-7317.

[60] M. Kartashevsky, R. Semiat, C.G. Dosoretz, Phosphate adsorption on granular ferric hydroxide to increase product water recovery in reverse osmosis-desalination of secondary effluents, Desalination 364 (2015) 53-61.

[61] H. Cui, Y. Su, Q. Li, S. Gao, J.K. Shang, Exceptional arsenic (III,V) removal performance of highly porous, nanostructured ZrO2 spheres for fixed bed reactors and the full-scale system modeling, Water Res. 47 (2013) 6258-6268.

[62] K.J. Reddy, T.R. Roth, Arsenic Removal from Natural Groundwater Using Cupric Oxide, Ground Water 51 (2013) 83-91.

[63] S. Ouvrard, M.-O. Simonnot, M. Sardin, Reactive Behavior of Natural Manganese Oxides toward the Adsorption of Phosphate and Arsenate, Ind. Eng. Chem. Res. 41 (2002) 2785-2791.

[64] L. Yan, Y. Huang, J. Cui, C. Jing, Simultaneous As(III) and Cd removal from copper smelting wastewater using granular TiO2 columns, Water Res. 68 (2015) 572-579.

[65] B. Manna, U.C. Ghosh, Adsorption of arsenic from aqueous solution on synthetic hydrous stannic oxide, J. Hazard. Mater. 144 (2007) 522-531.

[66] G. Zhang, H. Liu, R. Liu, J. Qu, Adsorption behavior and mechanism of arsenate at Fe–Mn binary oxide/water interface, J. Hazard. Mater. 168 (2009) 820-825.

[67] Z. Ren, L. Shao, G. Zhang, Adsorption of Phosphate from Aqueous Solution Using an Iron–Zirconium Binary Oxide Sorbent, Water, Air, Soil Pollut. 223 (2012) 4221-4231.

[68] K. Gupta, K. Biswas, U.C. Ghosh, Nanostructure iron(III)-zirconium(IV) binary mixed oxide: Synthesis, characterization, and physicochemical aspects of arsenic(III) sorption from the aqueous solution, Ind. Eng. Chem. Res. 47 (2008) 9903-9912.

[69] G. Zhang, Z. Ren, X. Zhang, J. Chen, Nanostructured iron(III)-copper(II) binary oxide: a novel adsorbent for enhanced arsenic removal from aqueous solutions, Water Res. 47 (2013) 4022-4031.

[70] U.C. Ghosh, D. Bandyopadhyay, B. Manna, M. Mandal, Hydrous Iron(III)-Tin(IV) Binary Mixed Oxide:

Arsenic Adsorption Behaviour from Aqueous Solution, Water Qual. Res. J. Canada 41 (2006) 198-209.

[71] F. Beduk, Superparamagnetic nanomaterial Fe3O4-TiO2 for the removal of As(V) and As(III) from aqueous solutions, Environmental Technology (United Kingdom) 37 (2016) 1790-1801.

[72] K. Wu, T. Liu, W. Xue, X.C. Wang, Arsenic(III) oxidation/adsorption behaviors on a new bimetal adsorbent of Mn-oxide-doped Al oxide, Chem. Eng. J. 192 (2012) 343-349.

[73] Y. Su, W. Yang, W. Sun, Q. Li, J.K. Shang, Synthesis of mesoporous cerium-zirconium binary oxide nanoadsorbents by a solvothermal process and their effective adsorption of phosphate from water, Chem. Eng. J. 268 (2015) 270-279.

[74] S.E. O'Reilly, D.G. Strawn, D.L. Sparks, Residence Time Effects on Arsenate dsorption/Desorption Mechanisms on Goethite, Soil Sci. Soc. Am. J. 65 (2001) 67-77.

[75] B. Nowack, A.T. Stone, Competitive adsorption of phosphate and phosphonates onto goethite, Water Res. 40 (2006) 2201-2209.

[76] W. Tang, Q. Li, S. Gao, J.K. Shang, Arsenic (III,V) removal from aqueous solution by ultrafine alpha-Fe2O3 nanoparticles synthesized from solvent thermal method, J. Hazard. Mater. 192 (2011) 131-138.

[77] S. Lunge, S. Singh, A. Sinha, Magnetic iron oxide (Fe3O4) nanoparticles from tea waste for arsenic removal, J. Magn. Magn. Mater. 356 (2014) 21-31.

[78] C.-H. Liu, Y.-H. Chuang, T.-Y. Chen, Y. Tian, H. Li, M.-K. Wang, W. Zhang, Mechanism of Arsenic Adsorption on Magnetite Nanoparticles from Water: Thermodynamic and Spectroscopic Studies, Environ. Sci. Technol. 49 (2015) 7726-7734.

[79] L.G. Yan, K. Yang, R.R. Shan, T. Yan, J. Wei, S.J. Yu, H.Q. Yu, B. Du, Kinetic, isotherm and thermodynamic investigations of phosphate adsorption onto core-shell Fe3O4@LDHs composites with easy magnetic separation assistance, J. Colloid Interface Sci. 448 (2015) 508-516.

[80] J. Pérez, L. Toledo, C.H. Campos, B.L. Rivas, J. Yañez, B.F. Urbano, Organic-inorganic interpenetrated hybrids based on cationic polymer and hydrous zirconium oxide for arsenate and arsenite removal, Chem. Eng. J. 287 (2016) 744-754.

[81] H. Liu, X. Sun, C. Yin, C. Hu, Removal of phosphate by mesoporous ZrO2, J. Hazard. Mater. 151 (2008) 616-622.

[82] K.D. Hristovski, P.K. Westerhoff, J.C. Crittenden, L.W. Olson, Arsenate Removal by Nanostructured ZrO2 Spheres, Environ. Sci. Technol. 42 (2008) 3786-3790.

[83] T.H. Bui, C. Kim, S.P. Hong, J. Yoon, Effective adsorbent for arsenic removal: core/shell structural nano zero-valent iron/manganese oxide, Environmental Science and Pollution Research 24 (2017) 24235-24242.

[84] L. Cumbal, J. Greenleaf, D. Leun, A.K. SenGupta, Polymer supported inorganic nanoparticles: characterization and environmental applications, Reactive & Functional Polymers 54 (2003) 167-180.

[85] J. Kim, W. Li, B.L. Philips, C.P. Grey, Phosphate adsorption on the iron oxyhydroxides goethite ([small alpha]-FeOOH), akaganeite ([small beta]-FeOOH), and lepidocrocite ([gamma]-FeOOH): a 31P NMR Study, Energy Environ. Sci. 4 (2011) 4298-4305.

[86] J. Gomez-Pastora, E. Bringas, I. Ortiz, Recent progress and future challenges on the use of high performance magnetic nano-adsorbents in environmental applications, Chem. Eng. J. 256 (2014) 187-204.

[87] Z. Wen, Y. Zhang, C. Dai, Removal of phosphate from aqueous solution using nanoscale zerovalent iron (nZVI), Colloids Surf. Physicochem. Eng. Aspects 457 (2014) 433-440.

[88] V. Tanboonchuy, J.C. Hsu, N. Grisdanurak, C.H. Liao, Gas-bubbled nano zero-valent iron process for high concentration arsenate removal, J. Hazard. Mater. 186 (2011) 2123-2128.

[89] F. Fu, D.D. Dionysiou, H. Liu, The use of zero-valent iron for groundwater remediation and wastewater treatment: A review, J. Hazard. Mater. 267 (2014) 194-205.

[90] S.R. Kanel, B. Manning, L. Charlet, H. Choi, Removal of arsenic(III) from groundwater by nanoscale zero-valent iron, Environ. Sci. Technol. 39 (2005) 1291-1298.

[91] M. Baikousi, Y. Georgiou, C. Daikopoulos, A.B. Bourlinos, J. Filip, R. Zbořil, Y. Deligiannakis, M.A. Karakassides, Synthesis and characterization of robust zero

valent iron/mesoporous carbon composites and their applications in arsenic removal, Carbon 93 (2015) 636-647.

[92] Y. Yao, B. Gao, J. Chen, L. Yang, Engineered biochar reclaiming phosphate from aqueous solutions: mechanisms and potential application as a slow-release fertilizer, Environ. Sci. Technol. 47 (2013) 8700-8708.

[93] L. Zhang, Y. Gao, M. Li, J. Liu, Expanded graphite loaded with lanthanum oxide used as a novel adsorbent for phosphate removal from water: performance and mechanism study, Environ. Technol. 36 (2015) 1016-1025.

[94] X. Xu, W. Song, D. Huang, B. Gao, Y. Sun, Q. Yue, K. Fu, Performance of novel biopolymer-based activated carbon and resin on phosphate elimination from stream, Colloids Surf. Physicochem. Eng. Aspects 476 (2015) 68-75.

[95] M.H. Mahaninia, L.D. Wilson, Cross-linked chitosan beads for phosphate removal from aqueous solution, J. Appl. Polym. Sci. 133 (2016).

[96] X. Liu, L. Zhang, Removal of phosphate anions using the modified chitosan beads: Adsorption kinetic, isotherm and mechanism studies, Powder Technol. 277 (2015) 112-119.

[97] J. Xie, L. Lai, L. Lin, D. Wu, Z. Zhang, H. Kong, Phosphate removal from water by a novel zeolite/lanthanum hydroxide hybrid material prepared from coal fly ash, Journal of Environmental Science and Health Part A: Toxic/Hazardous Substances & Environmental Engineering 50 (2015) 1298-1305.

[98] D. Guaya, C. Valderrama, A. Farran, C. Armijos, J. Luis Cortina, Simultaneous phosphate and ammonium removal from aqueous solution by a hydrated aluminum oxide modified natural zeolite, Chem. Eng. J. 271 (2015) 204-213.

[99] B. Pan, J. Wu, B. Pan, L. Lv, W. Zhang, L. Xiao, X. Wang, X. Tao, S. Zheng, Development of polymer-based nanosized hydrated ferric oxides (HFOs) for enhanced phosphate removal from waste effluents, Water Res. 43 (2009) 4421-4429.

[100] L.M. Blaney, S. Cinar, A.K. SenGupta, Hybrid anion exchanger for trace phosphate removal from water and wastewater, Water Res. 41 (2007) 1603-1613.

[101] X. You, A. Farran, D. Guaya, C. Valderrama, V. Soldatov, J.L. Cortina, Phosphate removal from aqueous solutions using a hybrid fibrous exchanger containing hydrated ferric oxide nanoparticles, Journal of Environmental Chemical Engineering 4 (2016) 388-397.

[102] L. Song, J. Huo, X. Wang, F. Yang, J. He, C. Li, Phosphate adsorption by a Cu(II)-loaded polyethersulfone-type metal affinity membrane with the presence of coexistent ions, Chem. Eng. J. 284 (2016) 182-193.

[103] W.A.C. Campen, A.M.J. Sledsens, An investigation of the quinoline phosphomolybdate method for determining phosphate: its applicability in international trade, Analyst 86 (1961) 467-471.

[104] M. Bobtelsky, I. Barzily, A rapid and precise heterometric method for the determination of traces of phosphoric or arsenic acid with nitron and molybdate, Anal. Chim. Acta 28 (1963) 118-126.

[105] J. Ma, M.K. Sengupta, D. Yuan, P.K. Dasgupta, Speciation and detection of arsenic in aqueous samples: A review of recent progress in non-atomic spectrometric methods, Anal. Chim. Acta 831 (2014) 1-23.

[106] P. Su-Cheng, Y. Chung-Cheng, J.P. Riley, Effects of acidity and molybdate concentration on the kinetics of the formation of the phosphoantimonylmolybdenum blue complex, Anal. Chim. Acta 229 (1990) 115-120.

[107] Y.C. Zhao, A.I. Zouboulis, K.A. Matis, Flotation of molybdate oxyanions from dilute solutions Part II. Selective separation from phosphates, arsenates and silicates, Hydrometallurgy 43 (1996) 155-167.

[108] L. Dambies, T. Vincent, E. Guibal, Treatment of arsenic-containing solutions using chitosan derivatives: uptake mechanism and sorption performances, Water Res. 36 (2002) 3699-3710.

[109] C.Y. Chen, T.H. Chang, J.T. Kuo, Y.F. Chen, Y.C. Chung, Characteristics of molybdate-impregnated chitosan beads (MICB) in terms of arsenic removal from water and the application of a MICB-packed column to remove arsenic from wastewater, Bioresour. Technol. 99 (2008) 7487-7494.

[110] Q. Du, S. Zhang, B. Pan, L. Lv, W. Zhang, Q. Zhang, Bifunctional resin-ZVI composites for effective removal of arsenite through simultaneous adsorption and oxidation, Water Res. 47 (2013) 6064-6074.

[111] F.G. Donnan, Theory of membrane equilibria and membrane potentials in the presence of non-dialysing electrolytes. A contribution to physical-chemical physiology, J. Membr. Sci. 100 (1995) 45-55.

[112] S. Sarkar, A.K. SenGupta, P. Prakash, The Donnan Membrane Principle: Opportunities for Sustainable Engineered Processes and Materials, Environ. Sci. Technol. 44 (2010) 1161-1166.

[113] B.P. Tripathi, V.K. Shahi, Organic–inorganic nanocomposite polymer electrolyte membranes for fuel cell applications, Prog. Polym. Sci. 36 (2011) 945-979.

[114] J. Gi Hong, Y. Chen, Synthesis of Novel Nanocomposite Reverse Electrodialysis (RED) Ion-exchange Membranes for Salinity Gradient Power Generation, J. Membr. Sci.

[115] H. Lu, J. Wang, Z. Du, Y. Liu, M. Li, P. Chen, L. Zhang, In-situ anion-exchange synthesis AgCl/AgVO3 hybrid nanoribbons with highly photocatalytic activity, Mater. Lett. 157 (2015) 231-234.

[116] A.A. Khan, U. Baig, Electrical and thermal studies on poly(3-methyl thiophene) and in situ polymerized poly(3-methyl thiophene)cerium(IV)phosphate cation exchange nanocomposite, Composites Part B: Engineering 56 (2014) 862-868.

[117] O. Shepelev, S. Kenig, H. Dodiuk, 16 - Nanotechnology Based Thermosets, in: H. Dodiuk, S.H. Goodman (Eds.) Handbook of Thermoset Plastics (Third Edition), William Andrew Publishing, Boston, 2014, pp. 623-695.

[118] K.-L. Wu, S.-C. Chou, Y.-Y. Cheng, Comparison of polyimide/multiwalled carbon nanotube (MWNT) nanocomposites by in situ polymerization and blending, J. Appl. Polym. Sci. 116 (2010) 3111-3117.

[119] Y. Pang, G. Zeng, L. Tang, Y. Zhang, Y. Liu, X. Lei, Z. Li, J. Zhang, G. Xie, PEI-grafted magnetic porous powder for highly effective adsorption of heavy metal ions, Desalination 281 (2011) 278-284.

[120] A.A. Khan, S. Shaheen, Preparation, characterization of polyacrylonitrile–aluminum hydroxide composite anion exchanger and its analytical application as selective membrane electrode, Composites Part B: Engineering 58 (2014) 312-317.

[121] S.A. Nabi, A. Akhtar, M.D.A. Khan, M.A. Khan, Synthesis, characterization and electrical conductivity of Polyaniline-Sn(IV)tungstophosphate hybrid cation exchanger: Analytical application for removal of heavy metal ions from wastewater, Desalination 340 (2014) 73-83.

[122] P.T. Nonjola, M.K. Mathe, R.M. Modibedi, Chemical modification of polysulfone: Composite anionic exchange membrane with TiO2 nano-particles, Int. J. Hydrogen Energy 38 (2013) 5115-5121.

[123] M. Islam, P.C. Mishra, R. Patel, Microwave assisted synthesis of polycinnamamide Mg/Al mixed oxide nanocomposite and its application towards the removal of arsenate from aqueous medium, Chem. Eng. J. 230 (2013) 48-58.

[124] A.E. Chávez-Guajardo, J.C. Medina-Llamas, L. Maqueira, C.A.S. Andrade, K.G.B. Alves, C.P. de Melo, Efficient removal of Cr (VI) and Cu (II) ions from aqueous media by use of polypyrrole/maghemite and polyaniline/maghemite magnetic nanocomposites, Chem. Eng. J. 281 (2015) 826-836.

[125] X. Li, D. Wang, G. Cheng, Q. Luo, J. An, Y. Wang, Preparation of polyaniline-modified TiO2 nanoparticles and their photocatalytic activity under visible light illumination, Applied Catalysis B: Environmental 81 (2008) 267-273.

[126] C.-W. Chiu, T.-K. Huang, Y.-C. Wang, B.G. Alamani, J.-J. Lin, Intercalation strategies in clay/polymer hybrids, Prog. Polym. Sci. 39 (2014) 443-485.

[127] S. Sarkar, E. Guibal, F. Quignard, A.K. SenGupta, Polymer-supported metals and metal oxide nanoparticles: synthesis, characterization, and applications, J. Nanopart. Res. 14 (2012).

[128] X. Zhao, L. Lv, B. Pan, W. Zhang, S. Zhang, Q. Zhang, Polymer-supported nanocomposites for environmental application: A review, Chem. Eng. J. 170 (2011) 381-394.

[129] A.K. SenGupta, L.H. Cumbal, Hybrid Anion Exchanger for Selective Removal of Contaminating Ligands from Fluids and Method of Manufacture Thereof. Patent No.: US 7,291,578 B2, United States Patent (2007).

[130] E. Kociolek-Balawejder, E. Stanislawska, I. Jacukowicz-Sobala, Synthesis and characterization of CuO-loaded macroreticular anion exchange hybrid polymer, Reactive & Functional Polymers 100 (2016) 107-115.

[131] C.H. Campos, B.F. Urbano, B.L. Rivas, Hybrid composites from poly[(4-vinylbenzyl)trimethylammonium chloride]–metal oxide using simultaneous radical polymerization/sol–gel synthesis, Mater. Lett. 131 (2014) 198-202.

[132] S. Singh, A. Jasti, M. Kumar, V.K. Shahi, A green method for the preparation of highly stable organic-inorganic hybrid anion-exchange membranes in aqueous media for electrochemical processes, Polymer Chemistry 1 (2010) 1302-1312.

[133] Y.H. Wu, C.M. Wu, T.W. Xu, Y.X. Fu, Novel anion-exchange organic-inorganic hybrid membranes prepared through sol-gel reaction of multi-alkoxy precursors, J. Membr. Sci. 329 (2009) 236-245.

[134] Q. Du, S.J. Zhang, B.C. Pan, L. Lv, W.M. Zhang, Q.X. Zhang, Effect of spatial distribution and aging of ZVI on the reactivity of resin-ZVI composites for arsenite removal, Journal of Materials Science 49 (2014) 7073-7079.

[135] Z.M. Jiang, S.J. Zhang, B.C. Pan, W.F. Wang, X.S. Wang, L. Lv, W.M. Zhang, Q.X. Zhang, A fabrication strategy for nanosized zero valent iron (nZVI)-polymeric anion exchanger composites with tunable structure for nitrate reduction, J. Hazard. Mater. 233 (2012) 1-6.

[136] X. Li, K. He, B. Pan, S. Zhang, L. Lu, W. Zhang, Efficient As(III) removal by macroporous anion exchanger-supported Fe–Mn binary oxide: Behavior and mechanism, Chem. Eng. J. 193–194 (2012) 131-138.

[137] S. Sengupta, A. Pandit, Selective removal of phosphorus from wastewater combined with its recovery as a solid-phase fertilizer, Water Res. 45 (2011) 3318-3330.

[138] W. Yang, Z. Yu, B. Pan, L. Lv, W. Zhang, Simultaneous organic/inorganic removal from water using a new nanocomposite adsorbent: A case study of p-nitrophenol and phosphate, Chem. Eng. J. 268 (2015) 399-407.

[139] X. You, D. Guaya, A. Farran, C. Valderrama, J.L. Cortina, Phosphate removal from aqueous solution using a hybrid impregnated polymeric sorbent containing hydrated ferric oxide (HFO), J. Chem. Technol. Biotechnol. 91 (2016) 693-704.

[140] A. Sendrowski, T.H. Boyer, Phosphate removal from urine using hybrid anion exchange resin, Desalination 322 (2013) 104-112.

[141] J. Ren, N. Li, L. Zhao, Adsorptive Removal of Cr(VI) from Water by Anion Exchanger Based Nanosized Ferric Oxyhydroxide Hybrid Adsorbent, Chem. Biochem. Eng. Q. 26 (2012) 111-118.

[142] N.Y. Acelas, B.D. Martin, D. Lopez, B. Jefferson, Selective removal of phosphate from wastewater using hydrated metal oxides dispersed within anionic exchange media, Chemosphere 119 (2015) 1353-1360.

[143] Y. Miao, F. Han, B. Pan, Y. Niu, G. Nie, L. Lv, Antimony(V) removal from water by hydrated ferric oxides supported by calcite sand and polymeric anion exchanger, Journal of Environmental Sciences 26 (2014) 307-314.

[144] S.A. Nabi, R. Bushra, M. Naushad, A.M. Khan, Synthesis, characterization and analytical applications of a new composite cation exchange material poly-o-toluidine stannic molybdate for the separation of toxic metal ions, Chem. Eng. J. 165 (2010) 529-536.

[145] H.T. Fan, T. Sun, H.B. Xu, Y.J. Yang, Q. Tang, Y. Sun, Removal of arsenic(V) from aqueous solutions using 3- 2-(2-aminoethylamino)ethylamino propyl-trimethoxysilane functionalized silica gel adsorbent, Desalination 278 (2011) 238-243.

[146] Inamuddin, Y.A. Ismail, Synthesis and characterization of electrically conducting poly-*o*-methoxyaniline Zr(1V) molybdate Cd(II) selective composite cation-exchanger, Desalination 250 (2010) 523-529.

[147] J.J. Uhlrich, J. Sainio, Y. Lei, D. Edwards, R. Davies, M. Bowker, S. Shaikhutdinov, H.J. Freund, Preparation and characterization of iron–molybdate thin films, Surf. Sci. 605 (2011) 1550-1555.

[148] B. Shah, U. Chudasama, Synthesis and characterization of a novel hybrid material as amphoteric ion exchanger for simultaneous removal of cations and anions, J. Hazard. Mater. 276 (2014) 138-148.

[149] J. Murphy, J.P. Riley, A modified single solution method for the determination of phosphate in natural waters, Anal. Chim. Acta 27 (1962) 31-36.

[150] S. Tsang, F. Phu, M.M. Baum, G.A. Poskrebyshev, Determination of phosphate/arsenate by a modified molybdenum blue method and reduction of arsenate by $S_2O_4^{2}$, Talanta 71 (2007) 1560-1568.

[151] B. Liu, X. Lv, X. Meng, G. Yu, D. Wang, Removal of Pb(II) from aqueous solution using dithiocarbamate modified chitosan beads with Pb(II) as imprinted ions, Chem. Eng. J. 220 (2013) 412-419.

[152] Y.S. Petrova, A.V. Pestov, M.K. Usoltseva, L.K. Neudachina, Selective adsorption of silver(I) ions over copper(II) ions on a sulfoethyl derivative of chitosan, J. Hazard. Mater. 299 (2015) 696-701.

[153] F. Karas, J. Hnát, M. Paidar, J. Schauer, K. Bouzek, Determination of the ion-exchange capacity of anion-selective membranes, Int. J. Hydrogen Energy 39 (2014) 5054-5062.

[154] Z. Bai, C. Zhou, N. Gao, H. Pang, H. Ma, A chitosan–Pt nanoparticles/carbon nanotubesdoped phosphomolybdate nanocomposite as a platform for the sensitive detection of nitrite in tap water, RSC Advances 6 (2016) 937-946.

[155] S. Berchmans, R. Karthikeyan, S. Gupta, G.E.J. Poinern, T.B. Issa, P. Singh, Glassy carbon electrode modified with hybrid films containing inorganic molybdate anions trapped in organic matrices of chitosan and ionic liquid for the amperometric sensing of phosphate at neutral pH, Sensors Actuators B: Chem. 160 (2011) 1224-1231.

[156] T.R.C. Zezza, M.d.S. Castilho, N.R. Stradiotto, Determination of phosphorus in biodiesel using 1:12 phosphomolybdic modified electrode by cyclic voltammetry, Fuel 95 (2012) 15-18.

[157] R. Chitrakar, S. Tezuka, A. Sonoda, K. Sakane, K. Ooi, T. Hirotsu, Selective adsorption of phosphate from seawater and wastewater by amorphous zirconium hydroxide, J. Colloid Interface Sci. 297 (2006) 426-433.

[158] T. Hori, Formation of colourless molybdate complexes of phosphorus compounds in aqueous solution, J. Inorg. Nucl. Chem. 39 (1977) 2173-2177.

[159] S. Padungthon, M. German, S. Wiriyathamcharoen, A.K. SenGupta, Polymeric anion exchanger supported hydrated Zr(IV) oxide nanoparticles: A reusable hybrid sorbent for selective trace arsenic removal, React. Funct. Polym. 93 (2015) 84-94.

[160] I.I. Salame, T.J. Bandosz, Surface Chemistry of Activated Carbons: Combining the Results of Temperature-Programmed Desorption, Boehm, and Potentiometric Titrations, J. Colloid Interface Sci. 240 (2001) 252-258.

[161] M. Kosmulski, The Significance of the Points of Zero Charge of Zirconium (Hydr)Oxide Reported in the Literature, J. Dispersion Sci. Technol. 23 (2002) 529-538.

[162] T. Sata, Studies on anion exchange membranes having permselectivity for specific anions in electrodialysis — effect of hydrophilicity of anion exchange membranes on permselectivity of anions, J. Membr. Sci. 167 (2000) 1-31.